Stability Analysis of Fully Power Converter-based Microgrids

Vishnukumar Murugesan

School of Electrical Engineering

Thesis submitted for examination for the degree of Master of Science in Technology.

Espoo 29.08.2019

Thesis supervisor:

Prof. Edris Pouresmaeil

Thesis advisor:

D.Sc. (Tech.) Mikko Qvintus

Aalto University
School of Electrical
Engineering

AALTO UNIVERSITY
SCHOOL OF ELECTRICAL ENGINEERING

ABSTRACT OF THE
MASTER'S THESIS

Author: Vishnukumar Murugesan

Title: Stability Analysis of Fully Power Converter-based Microgrids

Date: 29.08.2019 Language: English Number of pages: 12+81

Department of Electrical Engineering and Automation

Major: Electrical Power and Energy Engineering Code: ELEC3024

Supervisor: Prof. Edris Pouresmaeil

Advisor: D.Sc. (Tech.) Mikko Qvintus

Due to rising energy demand and climate crisis, distributed energy generation utilizing the renewable energy resource is constantly evolving. Generation near the electrical loads within a defined boundary forms a microgrid. It can be operated by connecting with utility-grid or as a stand-alone system. Solar and wind energy resources use a power-electronic converter to interface with the load or grid. The fast dynamics of the converter is very different from the inertial dynamics of the grid with large synchronous machines. Furthermore, low short-circuit capacity, more resistive network and unbalanced loading are few inherent characteristics concerning the operational reliability of the microgrid.

This thesis aims to present the various issues with fully power converter-based microgrids in terms of stability and protection. High-power converters with LCL-filter are simulated under various operating conditions in typhoon real-time simulator. A relay function is used to detect the unstable operating points. High resistance-to-reactance ratio in the low-voltage line forms active-reactive power coupling, making the conventional droop control inaccurate. For a disturbance, droop control allows a steep voltage or frequency deviations which lead to unnecessary protection tripping. Use of virtual inertia control avoids the steep change in the system variables and preserves the stability. Parallel droop-based converters with non-identical parameters or output impedance induce circulating current or reactive power oscillations. Use of virtual impedance control minimizes the circulating current and enhances power-sharing. Phase-locked loop synchronized with a weak grid (high-impedance grid) is unstable on large-signal disturbances. Current-reference saturation limits the converter current for a three-phase balanced fault condition. For higher fault-impedance, the fault current is nearly equal to the load current, which possibly blinds the microgrid protection.

Keywords: Power converter-based microgrid, Grid-forming, Weak grid, Droop control, Virtual inertia emulation

Preface

The research work was done at ABB Oy - Solar, as a Master's thesis to Aalto University, School of Electrical Engineering, Finland.

I would like to express my gratitude to my advisor from ABB, Dr.Mikko Qvintus for giving me this interesting topic and supporting me with his valuable suggestions throughout the thesis. I would like to thank my supervisor from Aalto University, Prof. Edris Pouresmaeil for his untiring guidance and suggestions in structuring and improving the quality of the thesis.

I'm very grateful to my ex-manager Mrs. Kaija Salonen for giving me an opportunity to be a part of ABB. I would like to thank my team members (Antti, Leng, Lucas, Jukka, Jere, Jakov, Jaakko) at ABB for giving me a fruitful ambience throughout my journey. I would like to thank my manager Mr. Janne Hellberg for being very kind and supportive.

I'm very grateful to my friend Subha for being my prominent support, throughout my studies. I would like to thank my sisters Divya, Abitha and my brother Irfan for their care, support and guidance.

Finally, I'm forever indebted to my parents Mr.Murugesan, Mrs.Anusuya, my brother Vasanth and Bad boys for their unconditional love, endless support and encouragement throughout my life.

Otaniemi, 29.08.2019 Vishnukumar Murugesan

Contents

Symbols and Abbreviations

Symbols - Constants

α_{c}	current-controller bandwidth
α_{PLL}	phase-locked loop controller bandwidth
α_{v}	voltage-controller bandwidth
A_{f}	cross-sectional area of the feeder (cable/bus-bar)
C_{b}	base capacitance
C_{dc}	DC-bus capacitance
C_{f}	LCL-filter capacitance
d	d-axis component
D	damping constant in synchronous machine model
D_{p}	frequency droop gain
D_{q}	voltage droop gain
H	inertia constant
H_{f}	feed-forward current gain
J	moment of inertia
κ	peak current factor
k	duty-ratio of the switching device
K_{a}	desired attenuation factor for filter inductance
K_{f}	feed-forward voltage gain
K_{ic}	current-controller integral gain
$K_{\mathrm{i,PLL}}$	phase-locked loop controller integral gain
K_{iv}	voltage-controller integral gain
K_{pc}	current-controller proportional gain
$K_{\mathrm{p,PLL}}$	phase-locked loop controller proportional gain
K_{pv}	voltage-controller proportional gain
l_{f}	length of the feeder (cable/bus bar)
L	inductance
L_{fc}	converter-side filter inductance
L_{fg}	grid-side filter inductance
L_{s}	synchronous machine stator inductance
m	milli/10^{-3}
m	meter
$M_{\mathrm{f}}.i_{\mathrm{f}}$	synchronous machine field voltage constant
n	rated or nominal value
N	numbers (quantity)
η	efficiency
$p.u$	per-unit
ρ_{f}	resisitivity
P1	point of three-phase bolted fault
q	q-axis component
r	active resistance used in the current-controller

r_{sc}	resistance as a percentage of rated short-circuit impedance
R	resistance
R_{c}	converter-side filter resistance
R_{d}	passive damping resistor for LCL-filter
R_{f}	resistance of the feeder (cable/bus-bar)
R_{g}	grid-side filter resistance
R_{s}	synchronous machine stator resistance
R_{T}	resistance of the transformer in ohms
R_{v}	virtual resistance
RLC	resistor-inductor-capacitor connected in series
s	laplace operator
s	seconds
T_{d}	control-induced time delay
T_{s}	sampling time
τ	time-constant of the synchronous machine
τ_{i}	time-constant of the current-controller
u	voltage
u_{base}	selected base voltage for per-unit calculation
u_{n}	nominal line-line voltage
ω_{n}	nominal frequency of the system
ω_{PM}	gain crossover frequency for the desired phase margin
ω_{v}	cut-off frequency of low-pass filter used for virtual impedance compensation
x_{j}	design factor for j^{th} parallel converters to share active power equally
X	reactance
$X_{\mathrm{bus,m}}$	reactance of bus-bar per meter
$X_{\mathrm{cab,m}}$	reactance of underground cable per meter
X_{f}	reactance of the feeder (cable/bus-bar)
$X_{\mathrm{f,m}}$	reactance of the feeder (cable/bus-bar) per meter
X_{M}	reactance of electrical motor
X_{PD}	reactance of circuit breaker
X_{T}	reactance of transformer in ohms
X_{v}	virtual reactance
y_{j}	design factor of j^{th} parallel converters to share reactive power equally
Z	impedance
Z_{b}	base impedance
Z_{bus}	impedance of the bus-bar
Z_{cab}	impedance of underground cable
Z_{f}	impedance of the feeder (cable/bus-bar)
Z_{M}	impedance of the electrical motor
Z_{Mk}	fault-impedance from the electrical motor to the point of fault

Z_{PD}	impedance of the protection device
Z_{T}	impedance of the transformer
Z_{x}	impedance of a device (x) in the network
ζ	damping ratio of the second-order system

Symbols - Variables

δ	phase angle between two voltages
$\cos\,\varphi$	power factor
ϕ	synchronous machine flux
θ	impedance angle
θ_{PLL}	grid voltage phase angle tracked by phase locked loop
θ_{ref}	reference phase angle of the output voltage generated for the power converter control
ω	angular frequency
ω_{g}	measured grid frequency
ω_{m}	virtual angular frequency of the virtual synchronous machine
ω_{min}	minimum frequency/threshold in droop control
ω_{o}	natural frequency of second-order system
ω_{ref}	reference frequency of the output voltage generated for the power converter control
ω_{res}	resonance frequency of the LCL-filter
ω_{s}	synchronous speed in mechanical radians
e_{s}	voltage-source or generated voltage of synchronous machine
E	energy
E_{c}	energy stored in the DC-bus capacitor
f	frequency
f_{sw}	switching frequency
i_{c}	current flowing from the power converter to the point of fault
$i_{\mathrm{c,abc}}$	three-phase converter current measured after the converter-side inductor of LCL-filter
$i_{\mathrm{c,max}}$	maximum current rating of the power converters
i_{ck}	short-circuit current flowing from the power converters to the point of fault
$i_{\mathrm{cd}}, i_{\mathrm{cq}}$	d-axis and q-axis converter-side current measured before filter capacitor
$i_{\mathrm{d,ref}}, i_{\mathrm{q,ref}}$	d-axis and q-axis current reference for the current control
$i_{\mathrm{g,abc}}$	three-phase grid current measured after the grid-side inductor of LCL-filter
i_{gk}	short-circuit current flowing from the utility grid to the point of fault

i_{gkp}	maximum short-circuit current flowing from the utility grid to the point of fault
$i_{\mathrm{gd}}, i_{\mathrm{gq}}$	d-axis and q-axis grid-side current measured after filter
i_{k}	short-circuit current flowing from the source to the point of fault
i_{kp}	maximum short-circuit current flowing from the source to the point of fault
$i_{\mathrm{kp,gc}}$	maximum short-circuit current in grid-connected mode
$i_{\mathrm{kp,is}}$	maximum short-circuit current in islanded mode
i_{Mk}	short-circuit current flowing from the electrical motor to the point of fault
i_{Mkp}	maximum short-circuit current flowing from the electrical motor to the point of fault
i_{oT}	no-load current of the transformer
i_{s}	stator current of a synchronous machine
L_{grid}	inductance of the utility power grid
P	active power
P_{j}	active power of j^{th} parallel converter
P_{ref}	active power reference
P_{elec}	electrical power of the synchronous machine
P_{m}	output power of electrical motor
P_{max}	maximum active power of the converter
P_{mech}	mechanical power of the synchronous machine
P_{o}	active power consumption of the converter at no-load
P_{oT}	no-load losses of the transformer
P_{s}	active power of the given power source
P_{VSM}	output power of a virtual synchronous machine
Q	reactive power
Q_{j}	reactive power of j^{th} parallel converter
Q_{max}	maximum reactive power of the converter
Q_{o}	reactive power consumption of the converter at no-load
Q_{ref}	reactive power reference
Q_{s}	reactive power of the given power source
r_{k}	short-circuit resistance
S	apparent power
S_{c}	apparent power of the power converter
S_{g}	apparent power of the grid-source
S_{n}	nominal apparent power
S_{T}	rated power of the transformer
S_{x}	apparent power of a device (x) in the network
$u_{\mathrm{c,abc}}$	three-phase converter voltage measured across the capacitor of LCL-filter
$u_{\mathrm{c}}^{\mathrm{s}}, u_{\mathrm{g}}^{\mathrm{s}}$	converter and grid voltage in stationary coordinates
$u_{\mathrm{cd}}, u_{\mathrm{cq}}$	d-axis and q-axis converter voltage
$u_{\mathrm{d,ref}}, u_{\mathrm{q,ref}}$	d-axis and q-axis voltage reference for voltage control

u_{droop}	voltage reference from the droop control
u_{dc}	DC-bus voltage
u_{field}	field voltage of synchronous machine
u_{g}	utility grid voltage
$u_{\mathrm{gd}}, u_{\mathrm{gq}}$	d-axis and q-axis utility grid voltage
u_{sc}	voltage drop on full load expressed as a percentage of the rated voltage
u_{m}	terminal voltage of the electrical motor
u_{min}	minimum/threshold voltage in droop control
u_{mg}	microgrid voltage
u_{o}	output voltage
u_{ref}	reference voltage for the control pulse generation
u_{sc}	short-circuit reactance in terms of voltage
$u_{\mathrm{T,LV}}$	voltage of the transformer referred to low voltage side
u_{v}	voltage drop across virtual impedance
$U_{\mathrm{d}}, U_{\mathrm{q}}$	d-axis and q-axis voltage controller output
X_{g}	reactance of utility grid
x_{k}	short-circuit reactance
Z_{g}	impedance of the utility power grid
Z_{gk}	impedance of the network from the utility grid to the point of fault
Z_{k}	impedance of the network for a three-phase fault

Operators

$\Delta E_{\mathrm{stored}}$	stored energy in the system
Δf	desired frequency deviation
$\Delta i_{\mathrm{L,max}}$	maximum peak-to-peak ripple current across the inductor
ΔP	desired active power deviation
ΔQ	desired reactive power deviation
ΔT	desired torque deviation
Δu	desired voltage deviation
$\frac{\mathrm{d}}{\mathrm{d}t}$	derivative with respect to time

Transfer functions

$G_{\mathrm{ol,PLL}}(s)$	open-loop transfer function of phase-locked loop
$G_{\mathrm{cl,PLL}}(s)$	closed-loop transfer function of phase-locked loop
$G_{\mathrm{pc}}(s)$	plant transfer function considered for current-controller
$G_{\mathrm{pv}}(s)$	plant transfer function considered for voltage-controller
$G_{\mathrm{cl,f}}(s)$	desired closed-loop system
$G_{\mathrm{cc}}(s)$	closed-loop transfer function of current-controller
$G_{\mathrm{cv}}(s)$	closed-loop transfer function of voltage-controller

Abbreviations

AC	Alternating Current
AGC	Automatic Generation Control
ANSI	American National Standards Institute
AVR	Automatic Voltage Regulator
DC	Direct Current
DER	Distributed Energy Resource
DG	Distributed Generation
DSOGI-FLL	Dual-Second Order Generalized Integrator-Frequency Locked Loop
DVOC	Dispatchable Virtual Oscillator Control
ESR	Equivalent Series Resistance
HV	High Voltage
IEC	International Electro-technical Commission
LV	Low Voltage
MV	Medium Voltage
PCC	Point of Common Coupling
PLL	Phase Locked Loop
PM	Phase Margin
PV	Photovoltaics
PWM	Pulse Width Modulation
RoCoF	Rate of Change of Frequency
SCR	Short Circuit Ratio
SCADA	Supervisory Control and Data Acquisition
SM	Synchronous Machine
SoC	State of Charge
SPC	Synchronous Power Control
STATCOM	Static Synchronous Compensator
THD	Total Harmonic Distortion
VHiL	Virtual Hardware-in-Loop
VSC	Voltage Source Converter
VSM	Virtual Synchronous Machine
VOC	Virtual Oscillator Control

1 Introduction

1.1 Background and Motivation

In conventional power system, use of resources, efficiency and reliability highly impact the economy and environment of the stakeholders. Low efficiency in fuel-electrical energy conversion, transmission losses, cascading outages, increased pricing on peak demands, carbon emission from the fossil fuels and rising energy demand are the main issues which necessitate a development in the power system [1]. This led to the concept of Distributed Generation (DG) utilizing the eco-friendly, economical and vastly available renewable energy. DG is a small-scale generation using Distributed Energy Resources (DERs) at the distribution level or near the electric loads to reduce the cost of electricity, interruptions and transmission losses. The generated power, energy storages and electrical loads, connected in a network with a defined boundary form a Microgrid [2]. Microgrid can be operated as an islanded grid or by connecting with the central grid. Grid-connected microgrids have a point of interconnection or Point of Common Coupling (PCC) with the utility grid. Grid-connected operation can economically benefit the owner by intelligently managing DERs and loads, for exporting energy to the utility grid or store the energy for peak-shaving. Either of the two economically benefits the customer. In standalone operation, microgrids supply the network of loads with regulated voltage, frequency and power by itself. As the generation is nearby loads, transmission structure is removed, the line losses are reduced. As most of the electrical home appliances use rectified power, DC power can be directly fed to them, avoiding AC-DC conversion losses. Proper planning and operation of microgrids deliver uninterrupted power to critical facilities like healthcare, water, transportation [2, 3].

In grid-connected mode, microgrid follows the frequency and voltage of the central grid. The high inertial characteristics of the large interconnected synchronous machines act as energy (kinetic) storage to compensate the smaller disturbances or the faster transmission line dynamics [3, 4]. Further, the generator control system compensates the larger disturbances within their rated capacity. For a short-circuit fault, voltage-source operation of the grid allows higher current contribution based on the fault-impedance. Thus, the protection devices easily detect and isolate the faulty

system from the network. For reliable operation, protection devices are designed to allow only stable operating points considering the slower system dynamics [4].

However, in case of stand-alone microgrids, reliability is of huge concern due to their drastic change in the network structure and the characteristics of the connected equipment. Due to the benefits offered and their vast availability, DERs like solar and wind energy are commonly used. The grid injection of the power generated from these DERs is of varying nature. Thus, they use partial or full power-electronic converter coupling to adapt the power to standard values before injecting it to the grid. Fast converter dynamics is dominant in the islanded systems as the inertia is very low or zero [3, 4], leading to unstable coupling with line dynamics. Unlike conventional grid, which is more inductive, low voltage lines are more resistive. Also, power converters can operate as voltage-source, only within their rated capacity. Thus their fault-current contribution is low. Furthermore, stochastic nature of the renewable energy sources, unbalanced operation shows a different system behavior when compared to the conventional power system [3].

Absence of inertia, synchronizing torque and high current carrying capability are the main drawbacks of power converters, which are often needed to preserve the network stability. Added to these, the converter control system has few concerns. Droop control is the earliest control technique for power converters, which uses the voltage and speed droop characteristics of synchronous machines. Since the microgrids are more resistive, droop control derived for inductive grid becomes inaccurate, due to the active and reactive power coupling. For a disturbance in the network, droop control has fast Rate of Change of Frequency (RoCoF) and overshoot/undershoots in voltage and frequency. This results in frequent tripping of protection device [2–4]. For parallel droop-based converters, circulating current or reactive power oscillations due to non-identical system parameters are main issues. At some point, due to poor synchronization, one converter acts as a load to the other converter. Due to the current limitation of converters, post-fault stability is often compromised. Phase-Locked Loop (PLL) used for the synchronization of parallel converters is not stable in the weak grid (grid with low short-circuit power). Also, the protection of the microgrid is different from the central grid by various aspects in terms of current rating, RoCoF setting, bidirectional flow and trip coordination.

Standalone microgrids are rapidly increasing in remote communities of developing countries, distribution networks and many individual business organizations. The need for reliability in terms of energy balance, stability and power quality standards becomes prominence. Thus, the unique characteristics of microgrid and its associated operational concerns demand a clear understanding for planning and designing a reliable 100% power-electronic converter-based microgrids [3].

1.2 Objective

The main objective of this thesis is to study the various stability and protection issues in implementing fully power converter-based microgrids. This suggests the study of

operating points of the converter equipped with LCL-filter under different control techniques, control parameters, line impedance, load conditions, parallel operation and short-circuit faults. The microgrid model is simulated in Typhoon real-time simulator.

1.3 Thesis Structure

The remaining chapters of the thesis are structured as follows, Chapter 2 gives an insight about the microgrid and its unique characteristics. Chapter 3 presents the main issues with power converter-based microgrid in terms of protection and causes for the different instabilities. Chapter 4 describes the design of the microgrid simulation model in Typhoon real-time simulator and the various operating conditions to which it is subjected. Chapter 5 discusses the simulation results and the findings from each test cases relative to Chapter 3. Chapter 6 presents the conclusion from the results and suggestions for the future work.

2 Microgrid

This chapter aims to present a general overview of microgrid, and its associated components relative to the conventional grid.

2.1 Components

Microgrid comprises energy sources, energy/power conversion devices, energy storages and loads in a connected network as shown in figure 2.1. Photovoltaics (PV), Wind energy, Internal Combustion Engine, Micro-turbines, Hydro-power, Fuel cells are the commonly used DERs. They use different interfacing devices like a direct generator coupling (synchronous/asynchronous machines) to transform the actual form of energy into electrical energy, termed as energy converter or use a power-electronic converter to attain the desired electrical output, termed as power converter.

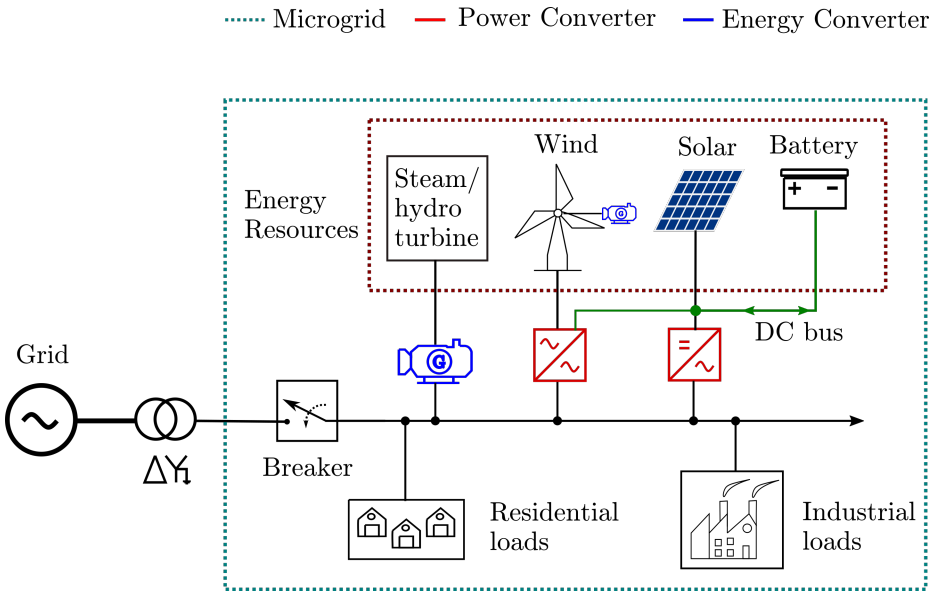

Figure 2.1: Microgrid and its components

For instance, diesel engine, wind, hydropower, micro-turbines use rotating generators to convert respective energies to electrical energy. PV and fuel cells produce DC electrical output and so the power converter (static generator) is used to convert and regulate the output. Depending upon on the resource availability, DGs with wind energy sometimes need both energy and power converters to generate standard output. Distributed energy resource with added conversion device is termed as DG

unit. Microgrids can be of Alternating Current (AC), Direct Current (DC) and hybrid type based on the type of DG units used [2–5]. Renewables like solar and wind are stochastic in nature, making it non-dispatchable. Use of energy storages like batteries, supercapacitors or flywheel stabilizes stochastic energy generation.

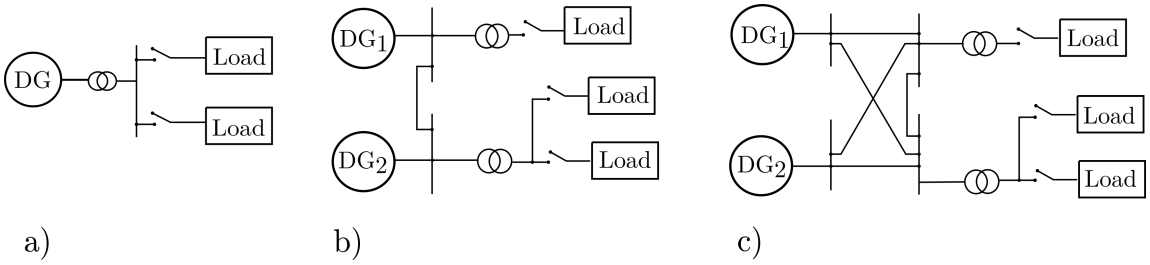

Figure 2.2: Network structure of microgrid a) radial type b) loop type c) mesh type

Microgrid networks are normally radial, loop or mesh type structures which depends on the number of DG units, voltage level and the critical loads requirements. Radial is the cheapest option to build and it has one source with a group of customers connected to it (figure 2.2). A fault could interrupt the service to the customer, and it prolongs until the fault is cleared. A loop structure has sources and customers connected in a loop such that, the event of failure won't interrupt the service of the customer offering more reliability. However, this structure is often expensive due to the increased switches and conductors. Mesh type structure has interconnected networks, where many sources are connected to a customer (critical loads) for high reliability. It is commonly used in the distribution networks and densely populated areas [5].

2.2 Grid-forming Source

Energy/power converter capable of operating as a voltage-source, supplying standard electrical quantities to a group of electrical loads in a network, is referred to grid-forming source. A grid-forming source should also deliver synchronized operation of parallel sources and black-starting capability. Black-starting is the ability to form the grid to restore its operation after a complete system collapse without importing any external power [5]. Characteristics of both the rotating and static grid-forming sources used in the microgrid are briefly discussed hereafter.

2.2.1 Synchronous Machines

Synchronous Machines (SM) inherently includes three units, rotor to couple an energy source (turbine), electromagnetic energy conversion unit, rotor inertia as energy (kinetic) storage unit. It converts the mechanical energy to electrical energy by the magnetic coupling between its stator and rotor. The kinetic energy stored in the rotating mass directly compensates the power imbalance and avoids reacting to small load or source disturbances. SMs have Automatic Voltage Regulator (AVR) for voltage support by rotor excitation voltage adjustments, Automatic Generation

Control (AGC) for adjusting the mechanical input to act on limited disturbances. Synchronous machine fault current is asymmetrical with DC offset (50-60% of the AC component). Figure 2.3 shows the asymmetrical current resulting from a step load-change and slow dynamics of SM.

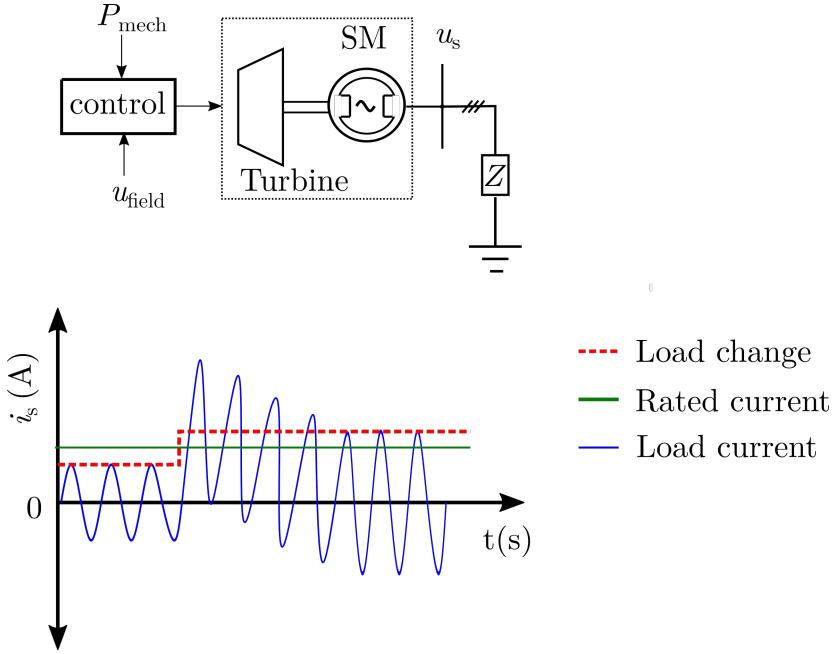

Figure 2.3: Voltage-source representation and over-loading characteristics of synchronous machine

Upon overloading, SM acts as a constant-power source until the control system responds to maintain its standard operating point. It can handle high currents in the order of 5-10 p.u owing to high thermal inertia. When connected to the grid, it remains intact with the use of synchronizing torque and inherent frequency-locked loop enabled by swing equation to balance the power [1].

2.2.2 Power-Electronic Converters

Power converters are the conversion units without any energy storage or energy resource embedded in it. Decoupled energy source and conversion unit limit the power balance. Power converters are two-level or multi-level voltage source converters based on their operating voltage. It is a controlled bidirectional DC-AC transformer. High-frequency switching pulses modulated with a sine wave is used to operate the semiconductor switches. Output voltage is the switching-cycle-averaged value controlled by the switch-on time. Output filter is used to synthesize the sine wave output from the high-frequency pulses. System output variables are measured or estimated to control within the limits. Power converters can be represented as controlled voltage-source with low output impedance or controlled current source with high output impedance, as shown in the figure 2.4 (a, b). During voltage-source operation, the frequency and amplitude of the converter voltage are kept

constant for grid-forming. Power converters are controlled in current-source mode (also termed as grid-feeding) for injecting active/reactive power to the grid, by following a grid-forming source.

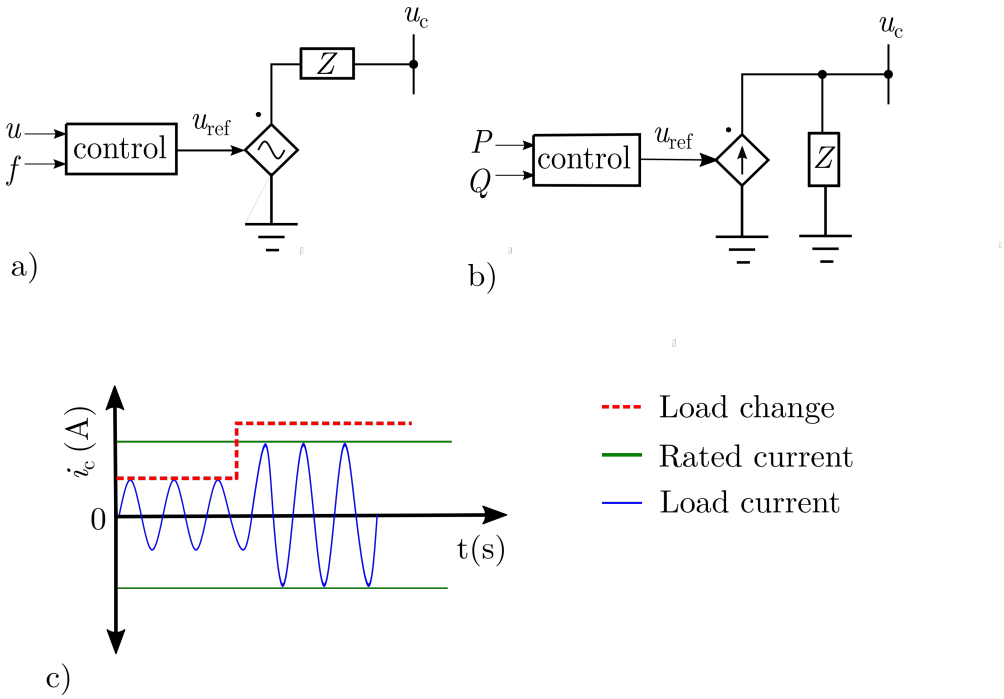

Figure 2.4: Power converter represented as a) voltage-source b) current-source c) over-loading characteristics

However, when operating as voltage-source, on overloading condition, the current is not a function of impedance. Thus, power converter is made to act as a current source providing constant current (rated maximum) which is shown in figure 2.4c. For a given rating, the low thermal inertia of switching devices requires current limiting control strategies. This limits the voltage support and the black starting capability under extreme network conditions. Parallel synchronized operation of converters needs external communication to follow common voltage and frequency references [4].

2.3 Types of Microgrids

Microgrids are classified as utility, remote and facility microgrids, based on their functionalities [2].

- Utility microgrid can be operated in island and grid-connected mode. It spans over a relatively large area with different types of loads and DERs.
- Remote microgrid is a limited capacity microgrid, operated only in islanded mode with relatively less power quality than others.

- Facility microgrid is connected to a host utility and restricted to a single organizational entity (hospitals, industry and military) for cost-effective reliable operation of critical loads. It can operate continuously in an intentional or unintentional island mode.

2.4 Unique Characteristics

Microgrids are small-scale version of utility grid with different system components. Microgrid, operating in grid-connected mode, acts like a positive/negative load connected to the grid. It follows the voltage and frequency imposed by the strong utility grid. Grid formed with the large synchronous machines has slower dynamics due to their rotor inertia (stored kinetic energy) which compensates the smaller disturbances approximately within 5 seconds. Thus, small disturbances have lesser impact on microgrid stability.

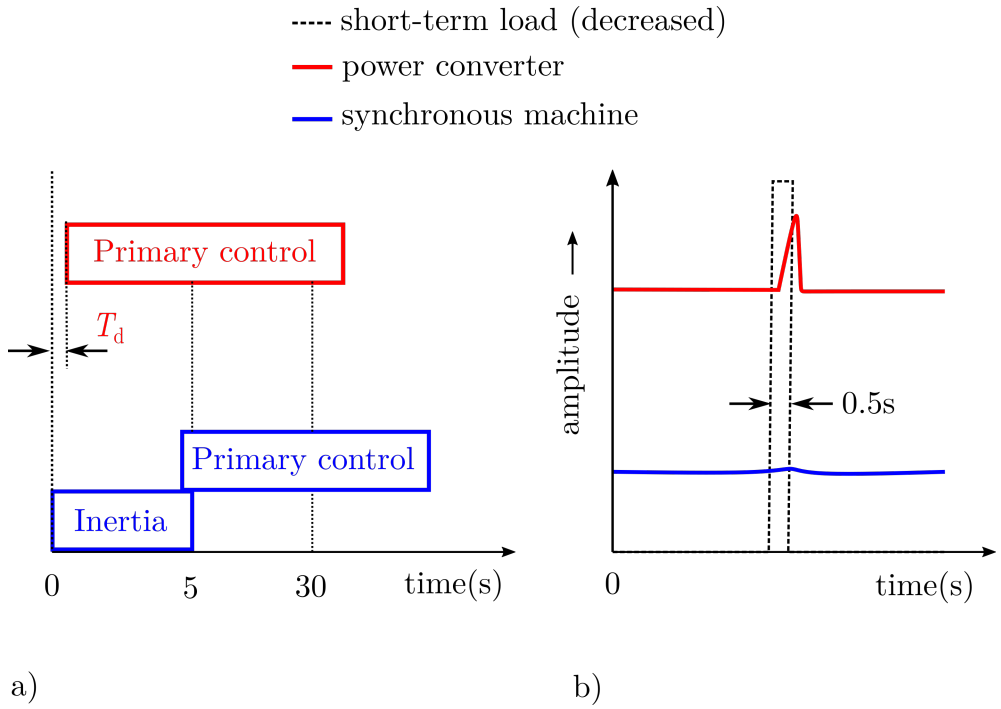

Figure 2.5: Comparison of synchronous machine and power converter a) controller time-scale b) disturbance response

However, in standalone mode, faster dynamics make the system prone to instabilities. This is because the inertia possessed by the standalone grid-forming sources is low or zero. Small SMs have very low inertia. Power converters do not have inertia or inherent energy storage to compensate for the disturbances instantly. Though their controller has faster actuation (within a fraction of seconds), the processing delay ($T_d \approx 0.2s$) limits the instant disturbance rejection capabilities like the SM inertia [4]. It is explained using figure 2.5, for a short-time load change, the output supplied by the power converter has fluctuations, due to the fast reference tracking by the

controller. Fast dynamics upon interaction with the line/load dynamics could result in unstable conditions. However, large synchronous machines resist the change in the output due to their large inertia. The excess energy required for the short-term load change is compensated by the stored kinetic energy in the SM rotor. Microgrid lines are shorter and operated at medium voltage (MV) or low voltage (LV) levels, the resistance-reactance ratio (R/X) is high when compared to conventional power systems [3–6]. Microgrid loads are typically unbalanced between the phases. For grid-connected microgrid, stiffness can be measured from the term Short-circuit Ratio (SCR) at PCC. It is the ratio of short-circuit power at the PCC to the rated power of the generator. Any grid with SCR less than 3 is termed as weak grid [3, 6]. Islanded microgrids have the short-circuit capacity equal to the rated power of the generator. Thus, for a fault in grid-connected mode, utility grid with large SMs deliver a fault current magnitude of approximately 10 p.u. Fault current from power converter based DGs are limited within their rated capacity ($\approx$ 2 p.u). Impact of these characteristics in continuous system operation will be discussed in the following chapter.

3 Issues with Power Converter-based Microgrid

This chapter discusses the operational challenges imposed by the characteristics of the microgrid in terms of stability and protection. Protection issues are discussed with a fault-current calculation. Then, the causes for different types of stability issues are explained.

3.1 Power System Reliability

Power system reliability is defined by system adequacy (resource availability) and system security (operational security). System security comprises two interdependent aspects namely system stability and hardware protection. System should maintain its parameters within their limits during and after the disturbance for preserving the stable operating points and thereby hardware. System security mainly depends upon the stiffness or the strength of the grid. As mentioned earlier, islanded microgrid is less stiff in terms of SCR and inertia.

Thus, system security (stability and protection) issues with the microgrid operating in islanded condition will be focused in the following sections.

3.2 Protection Issues

Conventional power grid is very prone to short-circuit due to various environmental and location factors. Thus, to ensure reliable operation for a fault-free network, protection devices are used to isolate the faulty part. Selection of protection devices mainly depends on the operational speed, voltage and the availability of the fault current. Operational speed is selected in a way to preserve the stability of a healthy network and sensitive customers.

Microgrids are subjected to same safety requirements as the conventional grid. It is necessary to protect the microgrid on both modes of operation. Protection system should isolate the microgrid from the faults on the utility network. For faults inside the microgrid, the protection system may isolate the smallest possible fault zone from the network. The use of traditional protection schemes normally fails to work effectively in the islanded mode as their characteristics change drastically [8]. Choice of the grid-forming source directly affects the fault current. As mentioned earlier, the maximum current rating of DG units using power converter is limited. Also, the R/X ratio of the network is high compared to that of the conventional power grid. Hence, the short-circuit current is low. The reduced difference between

short-circuit current and full-load current affects the time-current characteristics of the protection device resulting in delayed tripping. Thus, device heating effects or power imbalance would arise, leading to unstable oscillations [8]. Microgrids demand more directional protection schemes than the conventional grid protection, as the former have DG units at different locations rather being central, resulting in fault current contributions from different directions. Loss of neutral grounding while transferring to islanding mode must be taken care, as it affects the earth-fault protection. Furthermore, on intentional islanding, change in relay coordination affects selectivity. These differences lead to unusual selectivity (false or unnecessary tripping), sensitivity (undetected faults) and speed (slower tripping) [8]. To understand these characteristics, short-circuit calculation for a sample microgrid is studied.

3.2.1 Short-circuit Current Calculation of Microgrid

Traditional short-circuit calculation method can be used for power converter based microgrid but with few additional assumptions as per standard IEC 60909 which is compatible with all the networks up to 550kV [9]. It is used to calculate the fault-current of the sample microgrid network shown in figure 3.1, for both the modes of operation.

Few assumptions considered in this calculation method [9].

- Three-phase bolted fault is considered, as it provokes the maximum short-circuit current in the network
- Selected network is radial
- Number of phases involved in the fault doesn't change
- Voltage responsible for the short-circuit current is constant
- Load currents and line capacitance are neglected
- Single line to ground fault possesses maximum short-circuit current than the three-phase bolted fault, if zero sequence impedance at the point of fault is lower than the positive sequence impedance. In that case calculation of symmetrical components is needed.
- For circuit components without essential data, impedance (Z_{x}) can be calculated using,
$$Z_{\mathrm{x}} = \frac{u_{\mathrm{base}}^2}{S_{\mathrm{x}}}$$
- R/X ratio of the component is 0.1 for MV networks and 0.2 for LV networks and X/Z ratio of 0.995 are normally considered

Short-circuit impedance (Z_k) is the sum of all the resistance (r_k) and reactance (x_k) from voltage-source to the fault location. It is the positive-sequence impedance per phase. i_k, is the short-circuit current in the network.

$$Z_\mathrm{k} = \sqrt{\Sigma r_\mathrm{k}^2 + \Sigma x_\mathrm{k}^2} \tag{3.1}$$

$$i_\mathrm{k} = \frac{u_\mathrm{base}}{\sqrt{3} Z_\mathrm{k}} \tag{3.2}$$

For grid, the downstream source impedance (Z_g) can be calculated using grid voltages (u_g) and apparent power(S_g),

$$Z_\mathrm{g} = \frac{u_\mathrm{g}^2}{S_\mathrm{g}} * \left(\frac{u_\mathrm{base}}{u_\mathrm{g}} \right)^2 \tag{3.3}$$

For transformer, the reactance is calculated using short-circuit voltage (u_sc) expressed as percentage of the impedance, and resistance is derived from the no-load losses (P_oT) or its specification as in equation (3.4). For N identically-rated transformers connected in parallel, the resistance and reactance are divided by N.

$$R_\mathrm{T} = \frac{r_\mathrm{sc}}{100} * \left(\frac{u_\mathrm{T,LV}^2}{S_\mathrm{T}} \right) = \frac{P_\mathrm{oT}}{3 I_\mathrm{oT}} \tag{3.4}$$

$$Z_\mathrm{T} = \frac{u_\mathrm{sc}}{100} * \left(\frac{u_\mathrm{T,LV}^2}{S_\mathrm{T}} \right) \tag{3.5}$$

$$X_\mathrm{T} = \sqrt{Z_\mathrm{T}^2 - R_\mathrm{T}^2} \tag{3.6}$$

Overhead lines connecting grid and transformer are considered here but normally they are negligible. Bus bars and cables are commonly referred to feeders. The typical values of reactance per meter ($X_\mathrm{cab,m}$) and resistivity (ρ_f) [9, 10] with their length (l_f) and cross sectional area (A_f) are used to calculate its resistance (R_f) and reactance (X_f) values. The impedance of the feeder can change with the alignment of conductors inside the cable. Temperature of the cable is assumed as 20°C.

$$X_\mathrm{f} = X_\mathrm{f,m} * l_\mathrm{f} \tag{3.7}$$

$$R_\mathrm{f} = \rho_\mathrm{f} * \left(\frac{l_\mathrm{f}}{A_\mathrm{f}} \right) \tag{3.8}$$

Protection device or static switch near PCC has a reactance of $15 m\Omega$ typical value [9]. Short-circuit contribution of motors is much like a generator (equation (3.9)). When the motor is isolated from the network, it maintains a voltage across the terminal due to the stored magnetic field lasting few hundredths of cycles (4-8 cycles). When their terminals are short-circuited energy decays even faster according to R/X ratio

of the system. During the fault, motor attributes 20-25% of impedance (only sub-transient). Thus, the current contribution can be almost equal to the starting current of the motor. ANSI standard C37.010 gives the guidance of assuming the current contribution as four times the rated/full-load current. R/X ratio is considered as 0.2. For simplification, current from the single motor and their cables are calculated and multiplied by N.

$$X_{\mathrm{M}} = \frac{u_{\mathrm{sc}}}{100} * \left(\frac{u_{\mathrm{M}}^2}{S_{\mathrm{M}}}\right) \tag{3.9}$$

A shunt capacitor bank near the fault location contributes to the fault increasing the short-circuit current. It is not necessarily considered in the fault current calculation. But depending on the instance of the fault, fault-current may be symmetrical or asymmetrical, thereby increasing the peak short-circuit current. Grid and motor act as a voltage-source. On the other hand, power converter on short-circuit gives away constant current output, thereby acting as a current source. Short-circuit current at the point of fault is calculated for both grid-connected and islanded modes. While calculating the short-circuit impedance of the HV and MV networks, moreover resistance value is neglected and only the reactance values are considered. Typical value of R/X ratio is 0.2 [9,10]. But in LV networks, R value is non-negligible. Peak current or prospective current calculation (equation (3.11)) is also influenced by R/X ratio. Peak current factor, κ is,

$$\kappa = 1.02 + 0.98e^{-\left(\frac{3\mathrm{R}}{\mathrm{X}}\right)} \tag{3.10}$$

$$i_{\mathrm{kp}} = \kappa.\sqrt{2}.i_{\mathrm{k}} \tag{3.11}$$

The microgrid shown in figure 3.1 is considered for short-circuit calculations. The specification of the microgrid components is given in the Table 3.1. Considering three-phase bolted fault at P1, fault-impedance and fault current at P1 is to be calculated.

Table 3.1: Microgrid circuit specification and calculated impedance values

Section	**Parameters**	$\boldsymbol{R(m\Omega)}$	$\boldsymbol{X(m\Omega)}$	$\boldsymbol{Z(m\Omega)}$
Grid (g)	$u_{\mathrm{g}} = 20$ kV $S_{\mathrm{g}} = 100$MVA	0.344	1.71	1.72
Transformer (T)	20kV/415V $S_{\mathrm{T}} = 5$MVA $u_{\mathrm{sc}} = 5\%$, $r_{\mathrm{sc}} = 0.1\%$	0.174	1.73	1.74
Protection-device (PD)	circuit breakers	0	0.15	0.15
Bus-bars (bus)	$400m\mathrm{m}^2$, 10m, $X_{\mathrm{bus,m}} = 0.15m\Omega/\mathrm{m}$, $\rho = 0.023$	0.57	1.5	1.604
Cable1 (cab1)	$400m\mathrm{m}^2$, 100m, $X_{\mathrm{cab1,m}} = 0.15m\Omega/\mathrm{m}$, $\rho = 0.036$	9	15	17.49
Cable2 (cab2)	$70m\mathrm{m}^2$, 30m, $X_{\mathrm{cab2,m}} = 0.15m\Omega/\mathrm{m}$, $\rho = 0.023$	9.9	2.7	10.26
Power converter (c)	$N = 2$, $S_{\mathrm{c}} = 2.2$MVA, $i_{\mathrm{c,max}} = 3000$A	-	-	-
Motors (M)	$N = 12$, $S_{\mathrm{M}} = 50$ kW, $\eta = 0.9$, $\cos\varphi = 0.8$, $u_{\mathrm{sc}} = 25\%$	121	605	616.98

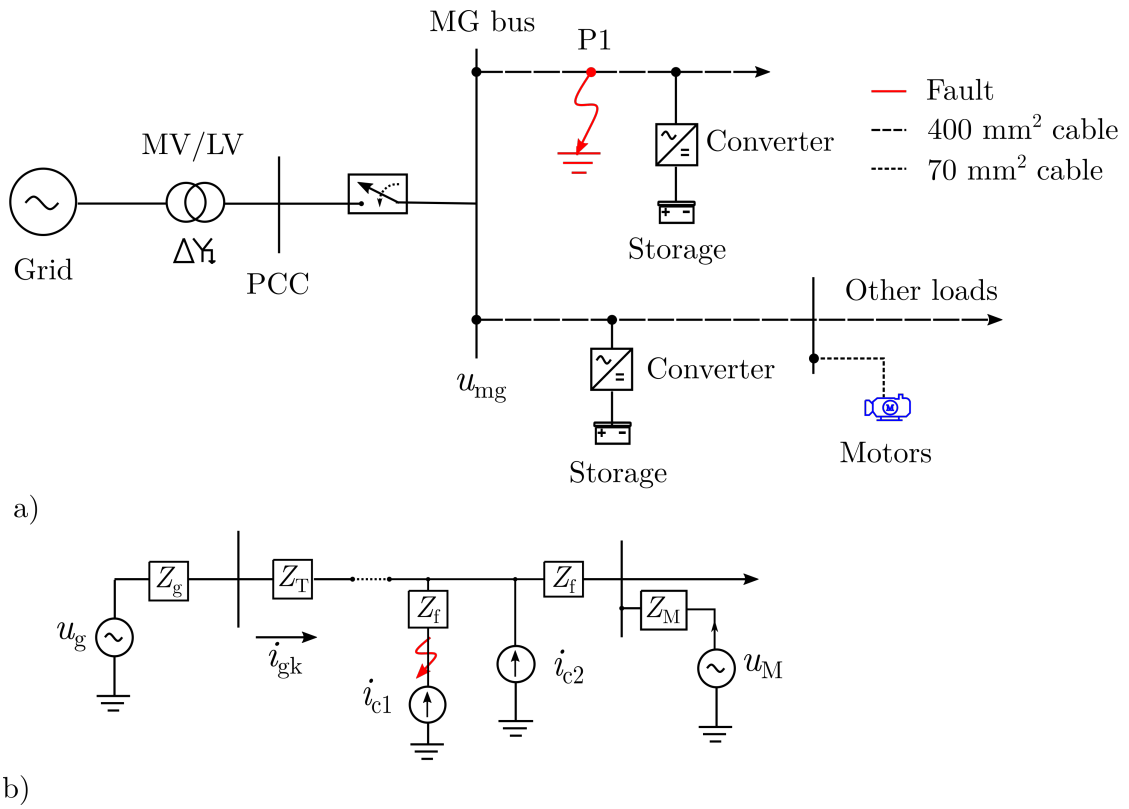

Figure 3.1: Microgrid on short-circuit a) schematic circuit b) simplified equivalent circuit

Impedance for the grid-source (Z_{gk}) is the sum of impedances of grid (Z_g), transformer (Z_T), protection device (Z_{PD}) and feeder (Z_f). Here, Z_f is the sum of bus bar (Z_{bus}) and cable1 (Z_{cab1}).

$$Z_{gk} = Z_g + Z_T + Z_{PD} + Z_f = 1.72 + 1.74 + 0.15 + 19.094 = 22.704\ m\Omega$$

Substituting in equation (3.1),

$$i_{gk} = \frac{415}{\sqrt{3} * 22.7 * 10^{-3}} = 10553.4\ \text{A}$$

R/X ratio of $Z_{gk} = 0.51$ and applying in equation (3.10), gives $\kappa = 1.2$. Using κ in equation (3.11),

$$i_{gkp} = 1.2 * 10553.4 = 12664.08\ \text{A}$$

Impedance for motor-source is sum of impedance of motor (Z_M) and feeder (Z_f). Here, Z_f is the sum of bus bar (Z_{bus}), cable1 (Z_{cab1}) and cable2 (Z_{cab2}).

$$Z_{Mk} = Z_M + Z_f = 616.98 + 29.354 = 637.4\ m\Omega$$

Substituting in equation (3.2),

$$i_{Mk} = \frac{415}{\sqrt{3} * 637.4 * 10^{-3}} = 375.9\ \text{A}$$

For 6 motors the total current contribution,

$$i_{\mathrm{MkT}} = i_{\mathrm{Mk}} * 6 = 2256.8 \text{ A}$$

R/X ratio of $Z_{\mathrm{Mk}} = 0.225$ and applying in equation (3.9), gives $\kappa = 1.02$. Using in equation (3.11),

$$i_{\mathrm{Mkp}} = 1.02 * 2256 = 2301 \text{ A}$$

For the fault-current calculation, power converter is modelled as a positive sequence current-source. Source current varies with short-circuit impedance when the current is under rated value. Maximum allowable current rating ($i_{\mathrm{c,max}}$) of the converter is assumed as 3000A.

$$i_{\mathrm{ck}} = i_{\mathrm{c1,max}} + i_{\mathrm{c2,max}} = 6000 \text{ A}$$

The maximum current of the converter should be considered from the manufacturer specification [9]. For unbalanced faults, the negative-sequence impedance depends on the design and control schemes used by the manufacturer.

Table 3.2: Fault-current of power converter-based microgrid

Microgrid condition	**Fault contribution**	**Fault current,** i_{k}	
		(A)	**(p.u)**
Grid-connected mode with motor loads	$i_{\mathrm{kp,gc}} = i_{\mathrm{Mkp}} + i_{\mathrm{gkp}} + i_{\mathrm{ck}}$	20965	7
Islanded mode with motor loads	$i_{\mathrm{kp,is}} = i_{\mathrm{Mkp}} + i_{\mathrm{ck}}$	8301	2.8
Islanded mode without motor loads	$i_{\mathrm{kp,is}} = i_{\mathrm{ck}}$	6000	2

The fault current calculated for both the modes of the operation are given in Table 3.2. The short-circuit capacity of the microgrid is 6000A (2 p.u). Assume the over-current protection limit is 2.2 p.u. For higher fault-impedance, the fault current can be around 2 p.u which is nearly same as the maximum current output of the converter. In that case, there will be a selectivity problem leading to delayed tripping or no tripping at all. This is not the case in grid-connected mode, where protection device clearly distinguishes between the fault current (7 p.u) and the load current (2 p.u) and isolates the converter from the grid. As the converter acts as a current-source after reaching the rated current value, protection based on under-voltage instead of over-current would be effective.

3.3 Stability Classifications

Stability definitions are same as the conventional power system, but the system-level difference introduces different classifications. A stable microgrid should be able to damp down the oscillations, for the continued system operation with system parameters such as voltage, current and frequency under desired limits. Load shedding scenarios to isolate the system from the faulty network or intentional load tripping to limit the system parameters are considered stable for this classification. But, the load tripping during or after disturbances like device failures, load changes and operation mode changes is considered as unstable states.

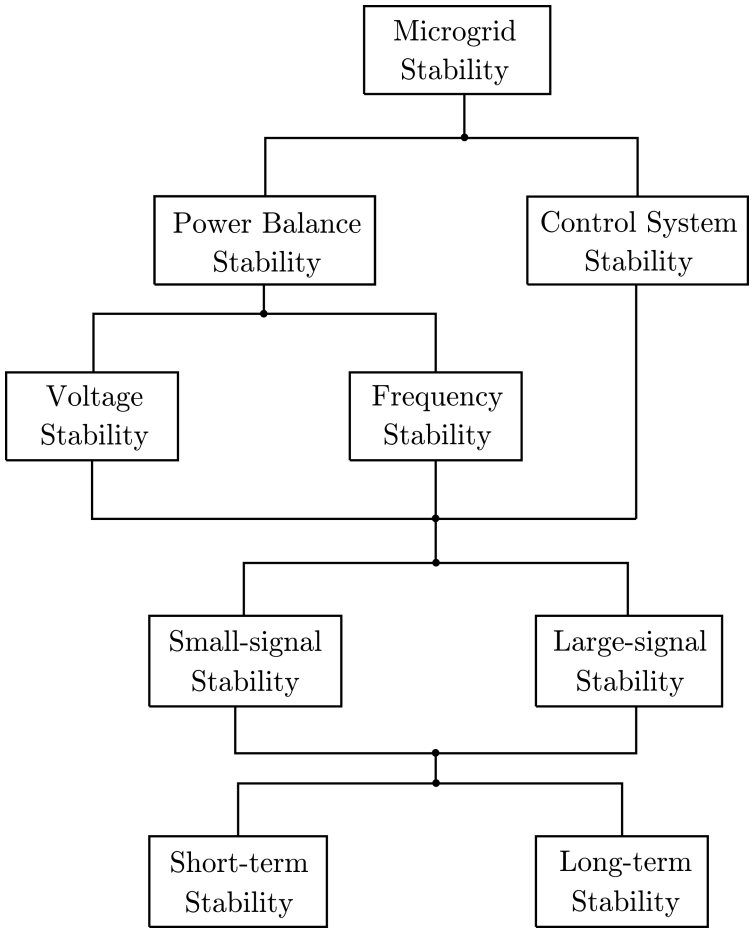

Figure 3.2: Stability classification of power converter based-islanded microgrid

Unlike conventional power system where the transient and voltage stability problems occur often, islanded microgrid suffers from frequency instability due to the lack of inertial dynamics of large synchronous machines in the microgrid. In the distribution networks, higher line resistance forms the active-reactive power coupling resulting in instability, but the type of instability is unclear. Identification of causes for instability and improvement factors are greatly facilitated by categorizing the issues. Figure 3.2 shows the microgrid stability classifications [3]. Microgrid stability comprises device control system and power balancing stabilities. Power balance stability includes both

voltage and frequency stabilities. This type of instability is mainly due to power imbalances, inertia and poor power-sharing between parallel DERs. They are further classified as frequency and voltage instability. Voltage and frequency ride-through is difficult under weak grid conditions [3, 4]. Rotor-angle stability in power system is replaced with control system stability since it is vital for the stability of power converters.

3.3.1 Frequency Stability

Frequency instability is caused by the large frequency excursions resulting from source or load disturbances. Frequency deviations are faster in islanded microgrids due to their low inertia. As mentioned in figure 3.3, large synchronous machines have very slow inertial-dynamics, but the time-scale of converters are very fast: in the range of milliseconds. This difference is introduced by the inertia. Inertia of the synchronous machine is nothing but a resistance in the form of stored kinetic energy, to counteract the power imbalance. It compensates the disturbance lasting for a time span of few seconds. On larger/longer disturbance, the primary and secondary control responds to restore the system operating point [4]. Equation (3.12) represents the swing equation where, H is the inertia constant and P_{mech} and P_{elec} are the mechanical and electrical power and ω_{s} is the system frequency.

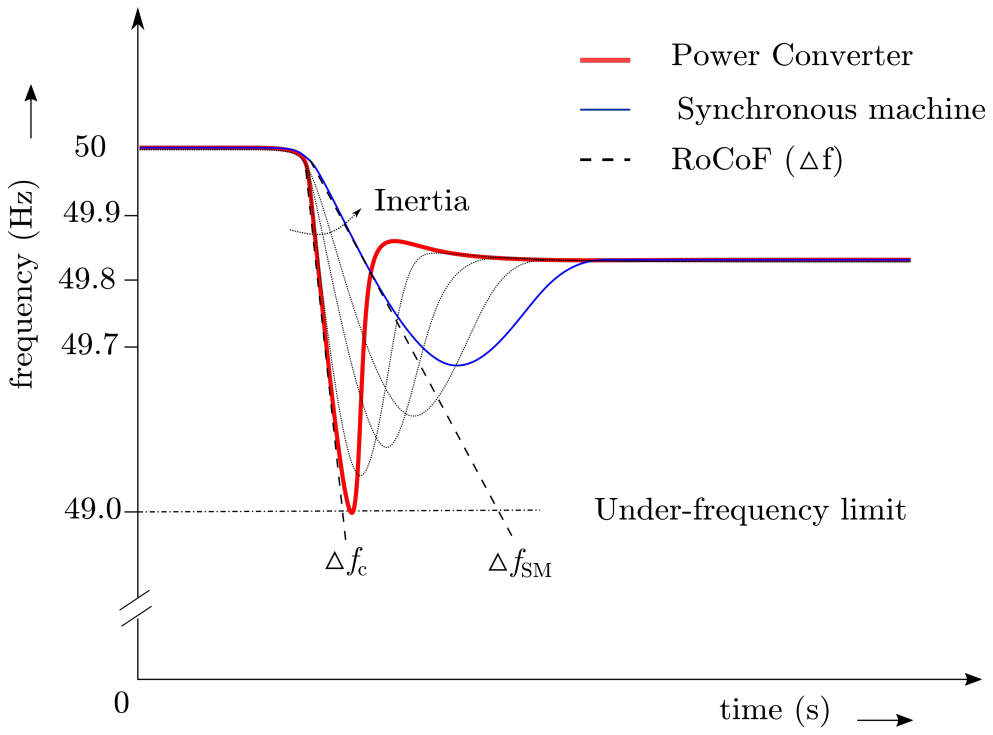

Figure 3.3: RoCoF comparison of synchronous machine and power converter

$$\frac{2H}{\omega_{\text{s}}}\left(\frac{\text{d}\omega_{\text{s}}}{\text{dt}}\right) = P_{\text{mech}} - P_{\text{elec}} \tag{3.12}$$

The relation between speed of the generator, system frequency and the power are not valid in power converter-based generator, as there is no mechanical power connected to the converter DC-bus. They do not possess rotating inertia or any energy buffers as like the conventional generators. Substituting, inertia constant $H = 0$, eliminates the frequency and power relation in power converters results in equation (3.13).

$$0 = P_{\text{mech}} - P_{\text{elec}} \tag{3.13}$$

As mentioned earlier, power converters do not effectively respond for the first instants of the contingency due to the delay in detection or measurement [4]. Since inertia is an inherent part of the synchronous machine, it reacts to disturbances immediately. Sudden change or dip is not allowed in the system. This inertial property is related to a term called Rate of Change of Frequency (RoCoF). Sudden loss of large load or source leads to fast frequency changes in power systems. Power imbalance between the load and the active power generated leads to instability in the power system. Thus, based on the detected RoCoF, either generator control is actuated to restore the nominal frequency value or load shedding is initiated. On using the converter-based systems, due to the absence of inertia, frequency change is faster even in the normal operating conditions resulting in RoCoF detection/tripping. Figure 3.3 shows the frequency output of a synchronous machine and a power converter for an increase in active power. For the same load change, power converters have faster RoCoF and steep magnitude than the SM. This could also result in unnecessary under-frequency tripping. Inertia constant of the synchronous machine is typically 5 seconds [1]. Substituting in equation (3.14) gives 0.1s^{-1} RoCoF for a per-unit power change of synchronous machines. For power converters, assuming it as $10ms$ and RoCoF will be 50s^{-1}.

$$\text{RoCoF} = \frac{\Delta P}{2H} \tag{3.14}$$

Thus, energy storage linked with the power converter could compensate the imbalance between generated power and load power, as given in equation (3.15).

$$\Delta E_{\text{stored}} = P_{\text{mech}} - P_{\text{elec}} \tag{3.15}$$

Stored energy in the converter's DC capacitor is very negligible when compared to the system inertia, a DC side energy storage like battery physically compensate for the lack of inertia and imbalance. Though, it could provide a certain amount of ΔE_{stored} to the system, their dynamics are still faster than the rotating inertia [4].

3.3.2 Voltage Stability

In microgrids, voltage instabilities are caused mainly due to the reactive power oscillations, fast controller interaction, voltage drop and converter current limits. Due to low inertia and SCR voltage dip is severe during faults [11].

For parallel converters, unequal power sharing affects the voltage stability due to reactive power oscillations. To ensure proper system operation and control, the load

should be equally shared among the DGs. In the steady state, the active (P) and reactive power (Q) ratios should be equal among the converters as mentioned in equation (3.16).

$$\left(\frac{P_1}{x_1} = \frac{P_2}{x_2} = \frac{P_\mathrm{i}}{x_\mathrm{i}}\right)\left(\frac{Q_1}{y_1} = \frac{Q_2}{y_2} = \frac{Q_\mathrm{i}}{y_\mathrm{i}}\right) \tag{3.16}$$

x and y are the design factors which drives the power-sharing. In case of proportional power sharing, x and y are considered equal to the apparent power (S). There exist a few problems in achieving the desired power-sharing in microgrids. When converters of different ratings are operated in parallel, the system induces reactive power oscillations for a step change/disturbance. Output impedance of the converter depends on the cables connecting the parallel converters, which varies the output voltage. Small difference in the output voltage might introduce circulating current [3]. This is because of the poor synchronization between the converters resulting in loading of one converter by the other. The control techniques used for converters influence the system variables. For instance, droop control setpoints move as per the reactive power change. Lack of inertia in droop control allows fast-changing voltage references. Thus, the dips are severe which might trip the under-voltage relay. Due to the shorter network, any change in voltage is instantly reflected on the load side leading to under-voltage tripping which is not safer for critical loads.

Islanded microgrids suffer from unbalanced loads. Unbalanced voltage dips produce current harmonics due to double-frequency oscillations from negative sequence component. Normal synchronous frame PI-controllers have a poor tracking with unbalanced load and so, a dedicated negative sequence control is additionally needed to maintain voltage stability [3, 14]. Limited overloading capability of the power converters limits the fault current in islanded microgrid. Thus, low voltage-ride-through function is limited unless there is an adequate power source to support the voltage [3]. Limited overloading can cause instability during transformer energizing and starting of induction motor. Their high inrush currents could result in the activation of current limiting function, deteriorating the voltage stability. Limited overloading is mainly a problem during black-starting the islanded microgrid. As microgrids are more resistive than the conventional grid, the voltage drop across the network is high.

3.3.3 Control System Stability

Poor tuning of control system parameters is the main reason for this type of instabilities. Harmonic resonance of parallel power converters, PLL instability, filter design, line-impedance and controller tuning are some of the issues.

Harmonic distortion is more in islanded microgrids due to the limited capacity of the DGs and higher line-impedance. Use of passive components in the feeder further triggers the low-order harmonic resonances [3]. Hence, the line currents are severely distorted even when the controllers and filters are tuned properly. To reduce losses

in high-power converters for lower switching frequency is generally preferred. L-filters with low switching frequency increases the Total Harmonic Distortion (THD) value [3]. When using LCL-filter, poor controller tuning induces high-frequency harmonic oscillation on the resonance condition. The grid impedance increases with the increasing number of converters operating in parallel. And so, the resonance frequency moves towards lower frequencies [15] as shown in the equation (3.17) and figure 3.4.

$$f_{\text{res}} = \frac{1}{2\pi}\sqrt{\frac{1}{C_{\text{f}}}\left(\frac{1}{L_{\text{fc}}} + \frac{1}{L_{\text{fg}} + N.L_{\text{grid}}}\right)} \tag{3.17}$$

$L_{\text{fc}}, C_{\text{f}}$ and L_{fg} are the LCL-filter components. L_{grid} is the network inductance. The resonance frequency (f_{res}) shift should be considered for the controller design for stable operation of the parallel converters.

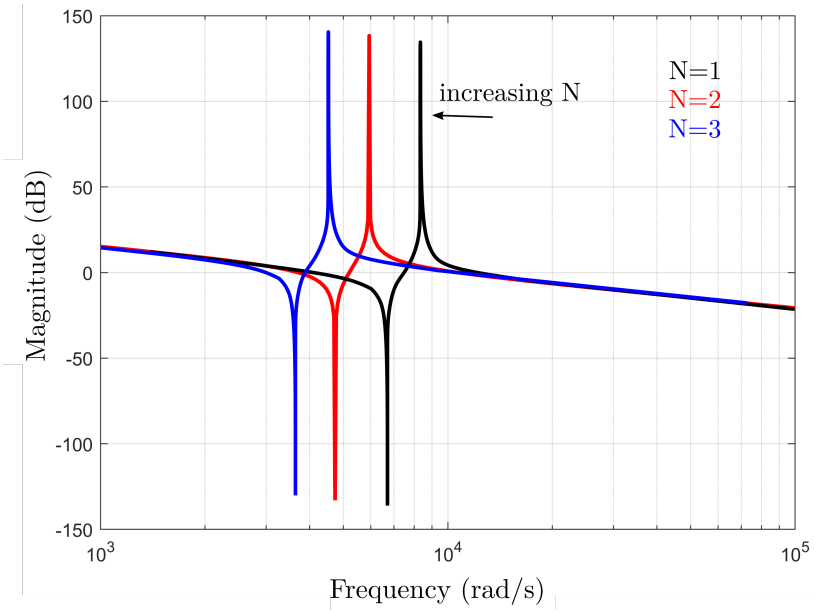

Figure 3.4: Resonance frequency shift for the increasing number of parallel converters

Grid-feeding converter normally uses PLL for synchronizing with the grid-forming voltage source. Measured grid voltage is transformed to the synchronous reference (dq) frame, shown in figure 3.5. At steady state, $\theta = \theta_{\text{PLL}}$ and u_{gd} is aligned with d-axis resulting in $u_{\text{gd}} = u_{\text{g}}$ and $u_{\text{gq}} = 0$ for perfect synchronization. For a large angle change during transients, the angle error ($\theta - \theta_{\text{PLL}}$) is significant. Fast PLL tracking gives oscillatory response/overshoots resulting in loss of phase-lock with the grid. This is severe for high reactance network. Change in angle also increases the voltage drop. Thus, the active power transfer is limited in a weak grid condition. Post-fault or under unbalanced loads, PLL performance is deteriorated, due to distorted input signal [7].

It can be limited by reducing the PLL bandwidth, since the oscillations higher than

the controller bandwidth are attenuated [11, 14, 16, 17]. Slow response of the control system reduces power flow accuracy during transient conditions. A reactive power source in the microgrid or increased converter rating can reduce these limitations.

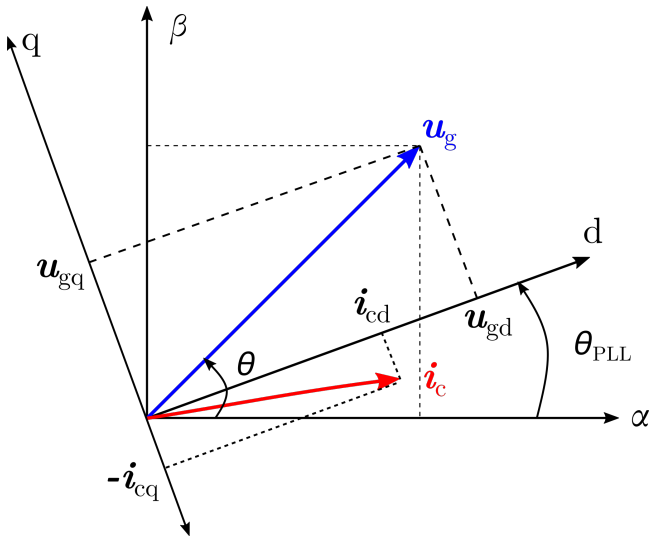

Figure 3.5: PLL phasor diagram at transient state

Few considerations/limitations for the existing grid-forming converter control techniques are discussed briefly.

Droop control

Traditional droop control used in SM is typically used to control the power converters. Unequal output impedance between the converters, droop gains D_p, D_q and parameter mismatch introduces circulating currents into the system contributing to unequal power-sharing and small-signal instability [2, 3, 10]. The dominance of reactance or resistance in the network forms a coupling between active and reactive powers based on the equations (3.17) and (3.18).

$$P_s = \frac{e_s}{Z} R(e_s - u_g cos\ \delta) + X(u_g sin\ \delta) \tag{3.18}$$

$$Q_s = \frac{e_s}{Z} X(e_s - u_g cos\ \delta) - R(u_g sin\ \delta) \tag{3.19}$$

P_s, Q_s represents the active and reactive powers flowing between the power converter and bus, e_s and u_g are their voltage values, $Z = R + jX$ is the line impedance between source and load, θ is the impedance angle. δ is the phase difference between the voltage-source and grid. Considering δ is small, $\sin\ \delta \approx \delta$ and $\cos\ \delta \approx 1$. From equations (3.18) and (3.19) considering $X >> R$ for conventional grid, R is neglected results in equations (3.20) and (3.21),

$$\delta = \frac{P_s X}{u_g e_s} \tag{3.20}$$

$$e_s - u_g = \frac{Q_s X}{e_s} \tag{3.21}$$

For the conventional grid, the active power and power angle are proportional, reactive power and voltage difference are proportional. Normally, microgrids in the distribution networks are more resistive $R >> X$, thus neglecting X gives a relation as in equations (3.22) and (3.23). The change in active power influences the output voltage, reactive power is proportional to the power angle.

$$e_s - u_g = \frac{P_s R}{e_s} \tag{3.22}$$

$$\delta = -\frac{Q_s R}{u_g e_s} \tag{3.23}$$

$$\theta = tan^{-1}\left(\frac{X}{R}\right) \tag{3.24}$$

Operating the conventional droop control is not effective in microgrid and/or resistive grid, which is also explained in the figure 3.6. The active-reactive power coupling of the microgrid when the resistive part is non-negligible is shown in figure 3.6(b,c).

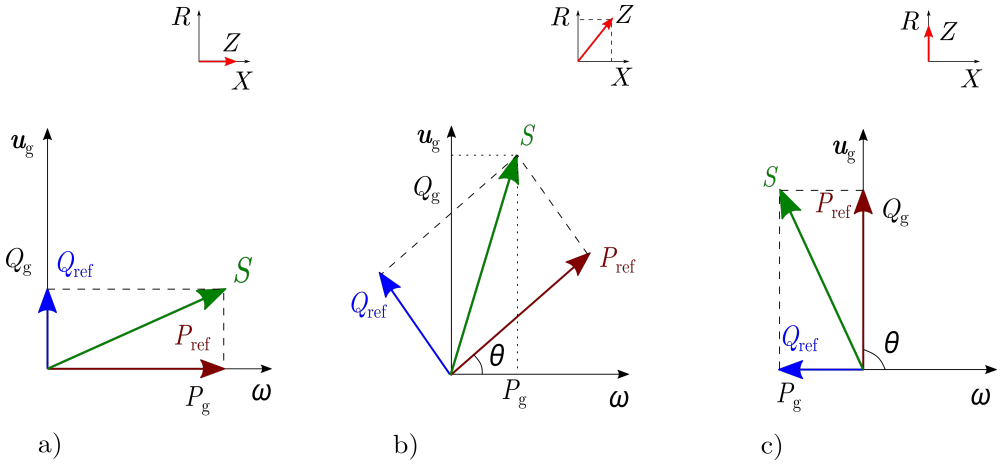

Figure 3.6: Effect of R/X ratio on active and reactive power equations a) $R/X = 0$ b) $R/X = 1$ c) $R/X = \infty$

As shown in figure 3.6b, the delivered power is P_g but the frequency value changes for the reference P_{ref} which is not desired. The active power from the converter is reduced due to the voltage drop across series resistance and increased impedance angle increases the grid reactive power more than the reference. Thus, the traditional droop control given below cannot control the system parameters effectively.

$$\Delta\omega = -D_p \Delta P \tag{3.25}$$

$$\Delta u = -D_{\mathrm{q}} \Delta Q \tag{3.26}$$

Δ refers to desired deviation of system parameters allowed. ω is the frequency, u is the voltage. When the grid resistance is not negligible, droop control should consider the combined effect of both R and X, then the control equations becomes,

$$\Delta \omega = -D_{\mathrm{p}} (\Delta P - \Delta Q) \tag{3.27}$$

$$\Delta u = -D_{\mathrm{q}} (\Delta P + \Delta Q) \tag{3.28}$$

In case of purely resistive grid, the reverse droop must be deployed for controlling the system parameters. The frequency is related to positive reactive power deviation. Voltage is related to active power. Droop gains cannot be the same and should be selected based on the desired deviation allowed.

$$\Delta \omega = D_{\mathrm{q}} \Delta Q \tag{3.29}$$

$$\Delta u = -D_{\mathrm{p}} \Delta P \tag{3.30}$$

To use the conventional droop even in the resistive grid, a reactance can be added to improve the R/X ratio thereby impedance angle, θ [7, 10]. By adding the reactance outside the converter, the losses will be high. Thus, the impedance is added in the control loop virtually as a signal [18]. The voltage drop from the virtual impedance is reduced from the converter voltage-reference before given to the controller.

$$u_{\mathrm{ref}} = u_{\mathrm{droop}} - i_{\mathrm{g}} * (R_{\mathrm{v}} + \left(\frac{\omega_{\mathrm{v}}}{s + \omega_{\mathrm{v}}} \right) s L_{\mathrm{v}}) \tag{3.31}$$

u_{ref} is the reference given to the voltage controller, u_{droop} is the voltage from the reactive power droop. To avoid high-frequency noise, amplified by the time derivative of the output grid current, a low-pass filter with a cut-off frequency of ω_{v} is used. It removes the cross-coupling exists between active-reactive power leading to better power-sharing.

Stability analysis of parallel converters in [3, 19–21] shows that length of distribution lines is directly proportional to the limits for the droop coefficient selection. Increasing the SCR of the network moves the poles away from the unstable region. Strong grid makes better stability in parallel grid-forming. In other words, the higher grid impedance affects the stability due to excess reactive power consumption or voltage drop across the network. Also, for non-identical droop gains in parallel converters, the system poles are in unstable region [21].

The problems with the basic converter control (droop) have been studied so far. The main stability limitation is imposed by the inertial difference between converters and synchronous machines. Droop-controlled converters have no embedded inertia. To

emulate inertia and damping properties of conventional synchronous machines in power converters, the concept of virtual inertia has been developed. Inertia can be added to power converters with a proper control mechanism and a short-term energy storage [21]. This concept is generally referred to Virtual Synchronous Machine (VSM) in this work. With proper energy management, converters can use their DC-link energy storage much like a kinetic energy reservoir in the rotating mass of SM. Unlike SM having the damper winding to absorb power fluctuations, VSM absorbs and releases the energy using the storage. Few commonly used control techniques allowing both voltage-source and current-source operation of the converter are discussed here, most of the available techniques are discussed elaborately in [22]. Virtual inertia techniques use the swing equation for deriving the phase angle reference, θ from equation (3.32). The output power of VSM can be given as,

$$P_{\mathrm{VSM}} = P_{\mathrm{elec}} + J\frac{\mathrm{d}\omega_{\mathrm{m}}}{\mathrm{dt}} + D(\omega_{\mathrm{m}} - \omega_{\mathrm{g}}) \tag{3.32}$$

P_{VSM} and P_{elec} are the input and output power of the converter, ω_{m} and ω_{g} are the angular frequency of virtual machine and measured angular frequency of grid. J, inertia emulating constant, selected such that VSG exchanges its rated active power on desired RoCoF. D emulates the damper winding effect in SM. J and D are chosen so that input and output power are equal at maximum frequency deviation. If J and D equals zero, VSM reduces to droop control. The electrical power output P_{elec} for each control varies as defined below.

VISMA

To emulate the inertial dynamics with the power converter, synchronous machine model is used in Virtual Synchronous Machine (VISMA). VISMA uses the output variables of the synchronous machine model to generate the current or voltage references for controlling the converter. A balanced three-phase voltage is used as the generated voltage e_{s} of the SM model. A hysteresis current controller is employed in regulating the reference. These techniques include complete SM model, thus higher processor capacity for solving the differential equation [22]. The current measurement noise amplified by the derivative term in equation (3.33) could lead to transient peaks/discontinuities in voltage reference calculation, causing numerical instability [21].

$$u_{\mathrm{s}}(s) = e_{\mathrm{s}}(s) - i_{\mathrm{s}}(s)(R_{\mathrm{s}} + sL_{\mathrm{s}}) \tag{3.33}$$

u_{s} and i_{s} are the output voltage and current of SM which can be used to generate current or voltage reference for grid-feeding/grid-forming operation. e_{s} is the generated voltage. R_{s} and L_{s} are the resistance and inductance of SM windings. The product of output voltage and current defines the electrical power.

Synchronverter

Synchronverter uses a similar approach but more detailed model of synchronous machine, exciter, voltage droop parameters to generate output references [23]. Generated voltage is the result of change in flux associated with stator and field windings. Synchronverter topology has comparatively less computation burden but still the numerical stability is a problem with the derivative term [22].

$$\varphi = i_{\mathrm{s}} R_{\mathrm{s}} + L_{\mathrm{s}} \frac{\mathrm{d}i_{\mathrm{s}}}{\mathrm{dt}} + M_{\mathrm{f}}.i_{\mathrm{f}} \cos\theta \tag{3.34}$$

$$e_{\mathrm{s}} = -\frac{\mathrm{d}\varphi}{\mathrm{dt}} \tag{3.35}$$

Synchronous Power Controller

Synchronous Power Controller (SPC) uses the swing equation to emulate the SM dynamics with an intrinsic droop control in its structure. It avoids current derivative term in its implementation and optimize the oscillatory response with an over-damped second-order response to the system [22]. Different second order transfer functions can be used to achieve different damping response. The implementation of equation (3.36) gives a current reference. With the voltage reference (from droop/PLL) and frequency reference (from swing equation), converter is controlled. Swing equation can be used to adjust the system response. It is reported as numerically stable [24].

$$i_{\mathrm{s}}(s) = \frac{e_{\mathrm{s}}(s) - u_{\mathrm{s}}(s)}{R_{\mathrm{s}} + sL_{\mathrm{s}}} \tag{3.36}$$

However, the tuning of the control system parameter is complex. As it has zeroes in active power transfer functions, possible non-minimum phase behavior (output response has under-shoot initially) exists.

Virtual Oscillator Control

A completely different control scheme from VSM which mimics the synchronizing behavior of oscillators is proposed in [25]. It is a faster synchronizing control scheme using only the available local variables and termed as Virtual Oscillator Control (VOC). It uses a nonlinear dead-zone oscillator much like a Van der Pol oscillator to generate the voltage reference. The differential equations emulating the dynamics of the oscillator are programmed in the digital controller, thus realizing the oscillator virtually. As the oscillations result from the energy exchange between the RLC circuit and a nonlinear voltage-controlled current source, the larger oscillations are damped. Dispatchable VOC is tested in [25] for the black starting capability, synchronization, non-uniform power-sharing and dispatchability of the parallel converters. Though it satisfies the synchronization, frequency and voltage sensitivity problems, it needs further study in implementation, and it is not yet widely used [4]. VOC reduces to droop control in quasi-steady state, but it has more robustness and faster synchronization properties than droop control [25, 26].

All these VSM emulations typically possess control-induced delay due to their computation. All VSMs parameters are tuned to recreate slower dynamics of SM, but not to expand stability limits for the connected network. Post-contingency response is very prone to transient peaks. It should be limited within the capacity (instantaneous) to maintain stability. DC-link voltage signal represents the power imbalance. However, it is not considered in the above-mentioned grid-forming techniques. A current-control technique emulating the inertia from the DC-bus dynamics (storage) is proposed in [27]. Grid-forming technique using this topology is not yet studied. Another new control technique called matching control is being developed considering the DC-link signal and less computational delay, but not yet widely used [26].

3.3.4 Other Classifications

All the above-mentioned stabilities are further classified based on the disturbance magnitude as small-signal and large-signal disturbance stabilities. In islanded microgrids, converter control loops are the major cause for small-signal instabilities. Large load change, fault and loss of generation are some of the causes for large-signal instabilities [2]. Depending on the disturbance duration they are further classified as short-term and long-term stabilities. Short-term instability can be caused by poor control, fast dynamic power changes and its mismatch. Long-term instability can be from the limited output of DERs and gradually increasing demands.

4 Simulation Model

This chapter mainly deals with the design and modeling of power converters in Typhoon real-time simulator. Also, it briefly describes the test cases under which the power converters is subjected to operate.

4.1 Typhoon

Typhoon real-time simulator is the simulation tool used in this work. The tool has different variants, the one used in this work is Virtual Hardware-in-Loop (VHiL). It has two interface windows namely Schematic editor and the SCADA. The schematic model is compiled and uploaded in the VHiL. SCADA is used to simulate the model in VHiL, control the input and access the output variables through different displays. It has time-step ranging from 0.5 µs. To have faster execution and smaller time step, the simulation model is partitioned, and each sub-part of the model is computed in parallel processors. The partition is based on the maximum number of converter switches, contactors and memory utilization per processor core. This partition is done by a coupling element which is an ideal transformer with 1:1 ratio and 1 time-step delay. The coupling element has two sides, one is current source side (red) which should be coupled to the capacitor and the other is voltage source side (green) which should be coupled to the inductor. In case of using the coupling element in some other parts of the model, the snubber circuit must be enabled to avoid the direct-source degenerations like voltage-source connected in parallel or current-source connected in series which generate erroneous results. Coupling stability should be verified during model compilation. A macro is programmed with different operating conditions for testing the model in SCADA. Simulation time-step is selected as 2 µs based on the computational load of this work.

4.2 Design of Power Converters

The microgrid considered in this work is utility-scale LV microgrid. Thus, the Two-level Voltage Source Converters (2L-VSC) is selected which is a common choice for low voltage levels (< 1 kV) [19]. The main components of the power converters are AC side filter and DC-link capacitor. The design of these components used in the simulation is given in following subsections.

4.2.1 DC-link Capacitor Sizing

Selection of DC-link Capacitor involves the voltage ripple due to high-frequency switching and the desired DC-link time-constant. The energy stored in the DC-link capacitor has a significant impact on the stability of DC-link during the transients [19]. The energy stored in the capacitor is,

$$E_{\mathrm{c}} = \frac{1}{2} C_{\mathrm{dc}} u_{\mathrm{dc}}^2 \tag{4.1}$$

DC input power across the capacitor is P_{dc} which is rated converter power with losses. τ_{i} is the time-constant of the capacitor to hold the energy.

$$E_{\mathrm{c}} = P_{\mathrm{dc}} \tau_{\mathrm{i}} \tag{4.2}$$

Then, τ_{i} is selected as 5 switching cycles. Equating both the equations (4.1) and (4.2),

$$C_{\mathrm{dc}} = \frac{10 P_{\mathrm{dc}}}{f_{\mathrm{sw}} u_{\mathrm{dc}}^2} \tag{4.3}$$

C_{dc} is the selected DC-link capacitor. u_{dc} is the DC-link voltage. As grid-forming operation or black-starting with stochastic DC-source is an issue, DG source is selected as battery in this work. For the converter having the DG-source as battery, DC-link capacitor has no impact and therefore it is not needed in this work. Since DC-link capacitor is an inherent part of the power converter, design procedure is explained here.

4.2.2 LCL-filter Design

Most common choice of AC-side filter is L-type. Since the converter is rated for high power, lower switching frequency is selected for reducing losses, making the L-filter bulkier and expensive. Thus, LCL-filter is common in modern VSCs due to their better attenuation characteristics and smaller inductance size when compared to L-filter. The design procedure for the LCL-filter is taken from [28]. Base impedance and base capacitance are calculated using the equations (4.4) and (4.5).

$$Z_{\mathrm{b}} = \frac{u_{\mathrm{n}}^2}{S_{\mathrm{n}}} \tag{4.4}$$

$$C_{\mathrm{b}} = \frac{1}{\omega_{\mathrm{n}} Z_{\mathrm{b}}} \tag{4.5}$$

ω_{n} is the nominal frequency and u_{n} is the nominal line-line voltage. Filter capacitance, C_{f} can be chosen to be maximum of 5% of the base capacitance, C_{b}. The maximum current ripple at output of the converter is,

$$\Delta i_{\mathrm{L,max}} = \frac{2 u_{\mathrm{dc}}}{3 L_{\mathrm{fc}}} (1 - k) k \frac{1}{f_{\mathrm{sw}}} \tag{4.6}$$

Considering maximum peak to peak ripple at duty ratio $k = 0.5$

$$\Delta i_{\mathrm{L,max}} = \frac{u_{\mathrm{dc}}}{6 f_{\mathrm{sw}} L_{\mathrm{fc}}} \tag{4.7}$$

A 10-25% of the rated current is selected as the maximum allowable current ripple by the output converter-side inductor.

$$\Delta i_{\mathrm{L,max}} = \left(\frac{20}{100}\right) * i_{\mathrm{c,max}} \tag{4.8}$$

Maximum current is calculated from the converter power rating,

$$i_{\mathrm{c,max}} = \frac{S_{\mathrm{n}}\sqrt{2}}{u_{\mathrm{n}}\sqrt{3}} \tag{4.9}$$

So, the converter-side inductance can be calculated by,

$$L_{\mathrm{fc}} = \frac{u_{\mathrm{dc}}}{6 f_{\mathrm{sw}} \Delta i_{\mathrm{L,max}}} \tag{4.10}$$

The allowable current ripple for the second level of attenuation by grid-side inductor is selected as 10%, thereby the output of the converter has 2% ripple. The grid side inductance can be calculated as given in equation (4.11), K_{a} is desired attenuation (0.1 or 10%).

$$L_{\mathrm{fg}} = \frac{\sqrt{\frac{1}{K_{\mathrm{a}}^2}} + 1}{\omega_{\mathrm{sw}}^2 C_{\mathrm{f}}} \tag{4.11}$$

The resonance frequency of the selected LCL-filter components is given by,

$$\omega_{\mathrm{res}} = \frac{L_{\mathrm{fc}} + L_{\mathrm{fg}}}{L_{\mathrm{fc}} L_{\mathrm{fg}} C_{\mathrm{f}}} \tag{4.12}$$

The resonance peak must be damped to avoid amplifying the high-frequency components. Commonly used resonance damping techniques are active damping, passive damping and notch filter. Passive damping is the simplest of all the available techniques which is adding a resistance in series or parallel with filter components, normally with the filter capacitor. Filter capacitor with series resistance have low losses and commonly used in practice [28]. Increasing resistance improves the attenuation but also the cost and losses. Damping resistance should introduce the impedance at the resonant frequency, R_{d} should be selected equal to the impedance of the capacitor. To reduce the losses, it is adjusted to one-third of the impedance by the capacitor in this work.

$$R_{\mathrm{d}} = \frac{1}{3\omega_{\mathrm{res}} C_{\mathrm{f}}} \tag{4.13}$$

It is necessary to check a few conditions after calculating the filter component values.

- The total filter inductance should be less than 0.1 p.u to reduce the voltage drop across the filter
- The resonant frequency should be at least 10 times the nominal line frequency and one half of the switching frequency to avoid resonance in the lower and upper parts of the harmonic spectrum

If these conditions are not true, then the procedure is iterated again with different capacitance value. The designed filter is used in both grid-forming and grid-feeding converter models.

4.3 Control of Grid-forming Converters

Power converters controlled as AC voltage-source with regulated electrical quantities in islanded systems are termed as grid-forming power converters. In grid-forming control, u$\angle\theta$ reference is self-generated based on the calculated active power and reactive power output of the converter. The grid-forming control block diagram is shown in the figure 4.1.

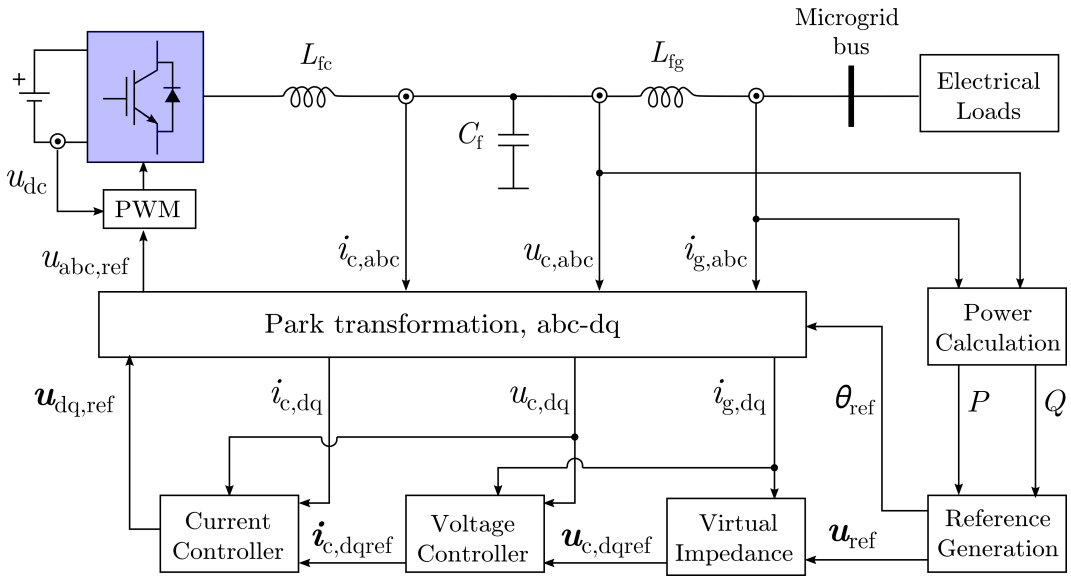

Figure 4.1: Grid-forming converter control block diagram

Each block will be explained in the following subsections. A simple PI-controller is generally used to control the system variables. As the control of AC signals using PI-controller is prone to poor tracking and steady-state error, the output variables are controlled in the synchronous reference frame. Park transformation ($abc-dq0$) allows the variables to control as DC signals. The three-phase variables are transformed to dq-frame by means of park transformation given in the matrix below.

$$\begin{bmatrix} d \\ q \\ 0 \end{bmatrix} = \frac{2}{3} \begin{bmatrix} \sin\theta & \sin(\theta - 120°) & \sin(\theta - 240°) \\ \cos\theta & \cos(\theta - 120°) & \cos(\theta - 240°) \\ 0.5 & 0.5 & 0.5 \end{bmatrix} \begin{bmatrix} a \\ b \\ c \end{bmatrix} \tag{4.14}$$

Zero sequence component is not used in this work. Thus, the park transformation is referred with $abc - dq$ in the figure 4.1.

4.3.1 Reference Generation

As the scope of the work is to study the stability of converter-based microgrids, only two commonly used reference generation techniques are modelled and used in the simulation namely, Droop control and Synchronverter.

Droop Control

It is the direct replication of SM's speed droop and voltage droop property in the power converters, where the frequency-active power and voltage-reactive power of the power source is related (figure 4.2).

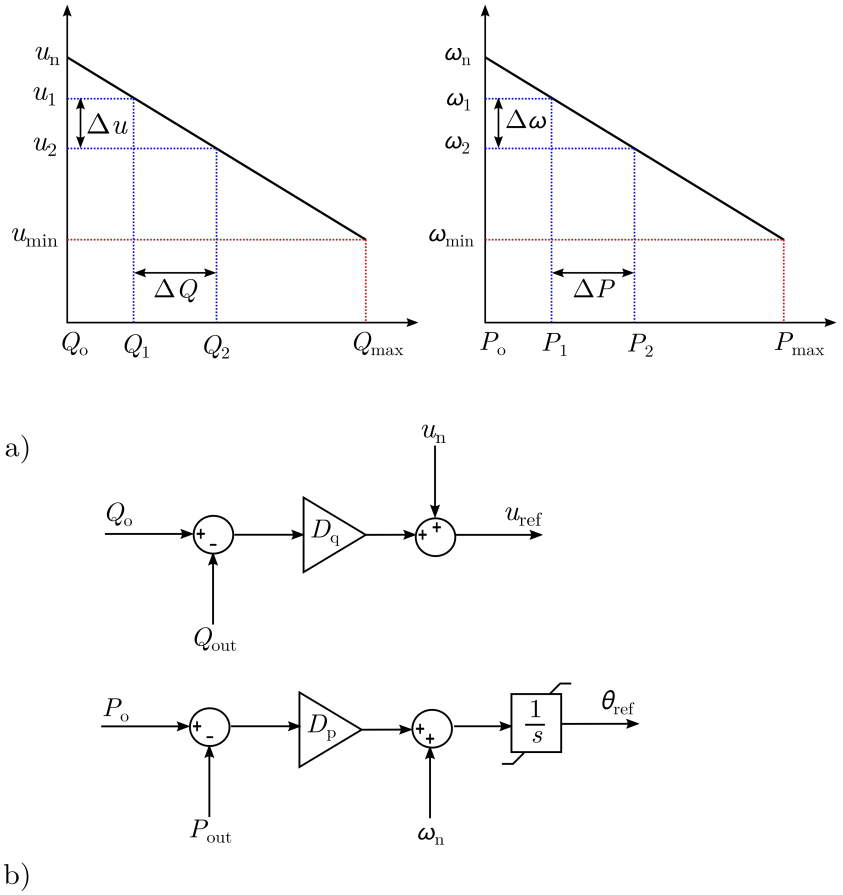

Figure 4.2: Conventional droop a) P-f and Q-u characteristics b) control structure

P_o and Q_o are the active and reactive power consumption of the converter at no-load. P_{out} and Q_{out} are the active and reactive power output of the converter. u_{ref} is the converter reference voltage. θ_{ref} is the angle of the converter reference voltage. s is the Laplace operator. D_p and D_q are the voltage and frequency droop gains which are selected from the equations (4.15) and (4.16).

$$D_p = \frac{\omega_n - \omega_{min}}{P_{max} - P_o} = \frac{15.7}{0.9e^6} = 17\,\mu Hz/W \tag{4.15}$$

$$D_q = \frac{u_n - u_{min}}{Q_{max} - Q_o} = \frac{10}{0.42e^6} = 24\,\mu V/VAr \tag{4.16}$$

u_{min} selected as 390 V and ω_{min} selected as $2\pi(47.5)$ rad/s. P_{max} be selected as 900 kW and Q_{max} be selected as 420 kW for 1 MW converter rating. Choice of droop gains influences stability and limited by the network impedance.

Synchronverter

This topology uses more detailed model of synchronous machines with machine parameters considered in the reference generation unit [23, 26]. The swing equation is used to generate the phase angle reference (θ_{ref}) and voltage reference (u_{ref}) is generated as per the reactive power consumed and the field voltage applied (figure 4.3). $M_f.i_f$ is the field mutual inductance and the field current. ω_m is the mechanical frequency of the VSM.

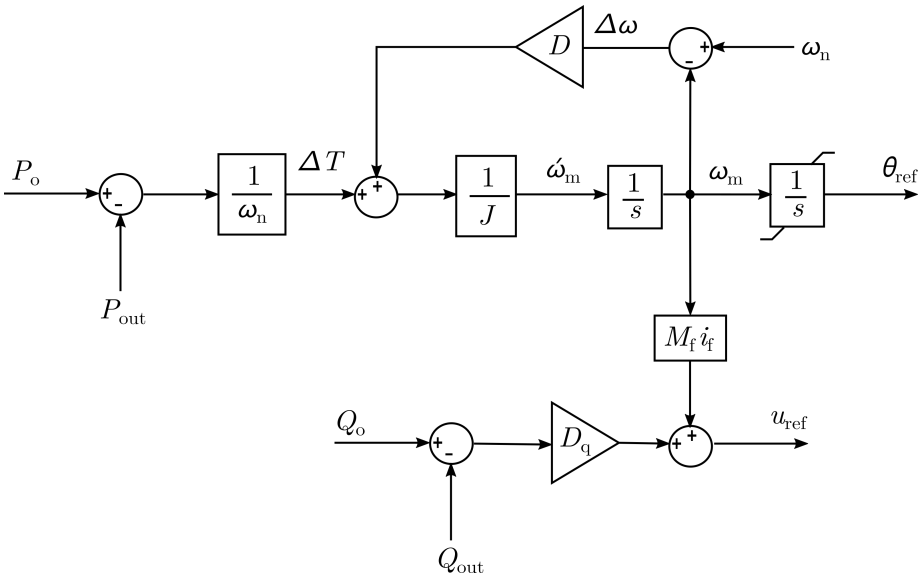

Figure 4.3: Synchronverter control structure

Inertia (J) and Damper (D) of the swing equation, introduced in the control loop, emulates the synchronous machine behavior. They can be selected using the equations (4.17) and (4.18).

$$D = -\frac{\Delta T}{\Delta \omega} = -\frac{\Delta P}{\omega_{\mathrm{n}} \Delta \omega} = \frac{900000}{314.16 * 2\pi 50 * 0.05} = 182 \tag{4.17}$$

$$J = D\tau = 182 * 1 = 182 \tag{4.18}$$

ΔT and ΔP are the torque and active power deviation of the synchronverter. $M_{\mathrm{f}}.i_{\mathrm{f}}$ value can be selected as a constant value(1.04) which derives the voltage reference equal to the nominal value (400 V). J is selected as the maximum frequency deviation for desired power change. D is selected such that input power and output power in the swing equation are equal. Hence, $J = D$ is suggested [23, 26] which implies $\tau = 1$. The effect of these parameters will be discussed in the next chapter.

4.3.2 Virtual Impedance

To increase the system damping and enhance the effectiveness of droop control in the resistance dominant network, addition of virtual impedance is suggested in [7, 18]. The virtual impedance can be inner or outer virtual impedance. Power flow control can be realized by outer impedance control. Thus, virtual impedance is added between reference generation and voltage controller. It reduces the coupling between active and reactive power to increase the power sharing accuracy. It can also enhance the dynamic performance of the controller upon proper design based on root locus or impedance-based stability analysis [18]. The voltage drop from the virtual impedance is reduced from the converter voltage reference from droop/synchronverter before given to voltage controller. Virtual impedance representation in dq-frame be,

$$u_{\mathrm{v,d}} = i_{\mathrm{gd}} \left(R_{\mathrm{v}} + sL_{\mathrm{v}}\right) - i_{\mathrm{gq}} \, \omega_{\mathrm{g}} L_{\mathrm{v}} \tag{4.19}$$

$$u_{\mathrm{v,q}} = i_{\mathrm{gq}} \left(R_{\mathrm{v}} + sL_{\mathrm{v}}\right) + i_{\mathrm{gd}} \, \omega_{\mathrm{g}} L_{\mathrm{v}} \tag{4.20}$$

R_{v} and L_{v} are the resistance and inductance of the virtual impedance. It is selected more than the output impedance for its effectiveness as suggested in [7].

4.3.3 AC-Voltage Controller

AC-Voltage controller is added for tracking the voltage reference derived from virtual impedance block, as shown in figure 4.1. Voltage is controlled in synchronous reference frame. This control derivation is taken from [26–30]. The dynamics of voltage from the capacitor current in dq-frame be,

$$C_{\mathrm{f}} \frac{\mathrm{d}u_{\mathrm{cd}}}{\mathrm{dt}} = i_{\mathrm{cd}} - i_{\mathrm{gd}} + j\omega_{\mathrm{g}} C_{\mathrm{f}} u_{\mathrm{cq}} \tag{4.21}$$

$$C_{\mathrm{f}} \frac{\mathrm{d}u_{\mathrm{cq}}}{\mathrm{dt}} = i_{\mathrm{cq}} - i_{\mathrm{gq}} - j\omega_{\mathrm{g}} C_{\mathrm{f}} u_{\mathrm{cd}} \tag{4.22}$$

i_{gd} and i_{gq} are the output current out of the filter. $\omega_{\mathrm{g}} C_{\mathrm{f}} u_{\mathrm{c}}$ is the cross-coupling term which should be cancelled to control d and q axis voltages separately. $u_{\mathrm{cq,ref}}$ is

normally set to zero. $u_{\mathrm{cd,ref}}$ is the voltage output of virtual impedance block. The control strategy to deliver the current reference be,

$$i_{\mathrm{cd,ref}} = G_{\mathrm{cv}}(u_{\mathrm{cd,ref}} - u_{\mathrm{cd}}) - j\omega_{\mathrm{g}} C_{\mathrm{f}} u_{\mathrm{cq}} + K_{\mathrm{f}} i_{\mathrm{gd}} \tag{4.23}$$

$$i_{\mathrm{cq,ref}} = G_{\mathrm{cv}}(u_{\mathrm{cq,ref}} - u_{\mathrm{cq}}) + j\omega_{\mathrm{g}} C_{\mathrm{f}} u_{\mathrm{cd}} + K_{\mathrm{f}} i_{\mathrm{gq}} \tag{4.24}$$

This control strategy is explained in figure 4.4.

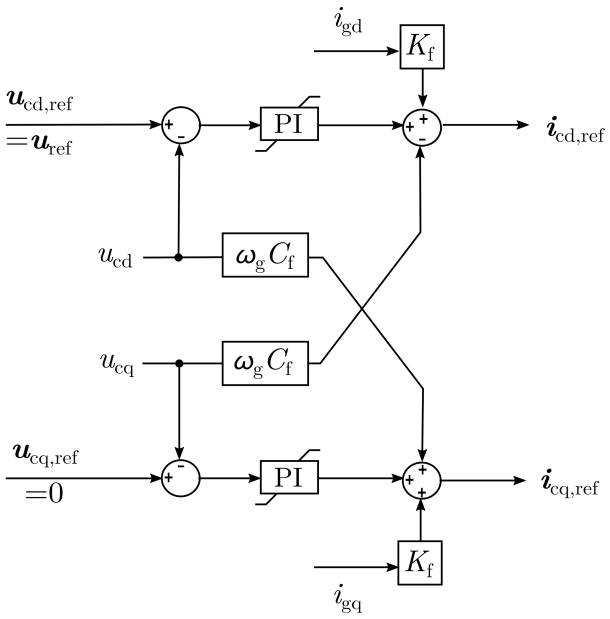

Figure 4.4: AC-voltage controller block

To reduce the effect of load disturbance on the controller output, a feed-forward compensation of output current (with a gain term, $K_{\mathrm{f}} = 1$) is added to controller output which ensures proper damping across all the load changes [26–30]. Substituting control output U to $G_{\mathrm{cv}}(u_{\mathrm{c,ref}} - u_{\mathrm{c}})$ in the above equations (4.23) and (4.24) and substituting them in equations (4.21) and (4.22) cancels the coupling and disturbance term to zero resulting in,

$$C_{\mathrm{f}} \frac{\mathrm{d}u_{\mathrm{cd}}}{\mathrm{dt}} = U_{\mathrm{d}} \tag{4.25}$$

$$C_{\mathrm{f}} \frac{\mathrm{d}u_{\mathrm{cq}}}{\mathrm{dt}} = U_{\mathrm{q}} \tag{4.26}$$

On Laplace transform and representing in per-phase,

$$sC_{\mathrm{f}} u_{\mathrm{c}}(s) = U(s) \tag{4.27}$$

$$\frac{u_{\mathrm{c}}(s)}{U(s)} = \frac{1}{C_{\mathrm{f}} s} \tag{4.28}$$

The plant model to be controlled is,

$$G_{\mathrm{pv}}(s) = \frac{1}{C_{\mathrm{f}} s} \tag{4.29}$$

The closed-loop system is a cascaded loop of voltage-controller (G_{cv}), current-controller (G_{cc}) and the plant model (G_{pv}). The desired closed-loop transfer function be,

$$G_{\mathrm{cl,f}}(s) = \frac{G_{\mathrm{pv}} G_{\mathrm{cc}} G_{\mathrm{cv}}}{1 + G_{\mathrm{pv}} G_{\mathrm{cc}} G_{\mathrm{cv}}} \tag{4.30}$$

G_{cc} can be approximated with the first order transfer function as given in equation (4.30). τ_{i} is the closed-loop time constant of the current-controller, ($\tau_{\mathrm{i}} = \frac{1}{\alpha_{\mathrm{c}}}$). α_{c}, current-controller bandwidth should be selected prior to this voltage controller design, since outer loop controller is normally designed to respond slower than the inner loop controller.

$$G_{\mathrm{cc}}(s) = \frac{1}{\tau_{\mathrm{i}} s + 1} \tag{4.31}$$

$$G_{\mathrm{cv}}(s) = \frac{K_{\mathrm{pv}} s + K_{\mathrm{iv}}}{s} \tag{4.32}$$

$G_{\mathrm{cl,f}}$ has double pole at $s = 0$, thus phase margin is -180° for low frequencies. Symmetrical optimum principle is used to control the closed-loop system ($G_{\mathrm{cl,f}}$) having two poles at origin. Selecting the desired phase margin gives the gain crossover frequency of the voltage controller.

$$z = \tau_{\mathrm{i}}^{-1} \left(\frac{1 - \sin \varphi_{\mathrm{PM}}}{1 + \sin \varphi_{\mathrm{PM}}} \right) \tag{4.33}$$

$$\omega_{\mathrm{PM}} = \sqrt{\frac{z}{\tau_{\mathrm{i}}}} \tag{4.34}$$

z is the pole location of the voltage controller. If the gain crossover frequency, ω_{PM} is selected equal to the voltage-controller bandwidth α_{v}, the φ_{PM} becomes the phase margin of the controller. To have the unity loop gain with the α_{v}, gain has to be selected to $K_{\mathrm{pv}} = \alpha_{\mathrm{v}} C_{\mathrm{f}}$. Based on symmetrical optimum principle, the resultant closed-loop system is third order system with one real pole at α_{v}. The location of remaining two poles depends on the selected phase margin. The phase margin is typically selected to be between 30°-75°. Selecting the phase margin to be 53° directly places the two poles at α_{v}, thus making three poles at α_{v} [29]. The voltage controller gains are calculated as shown in equation equations (4.35) and (4.36).

$$K_{\mathrm{pv}} = \alpha_{\mathrm{v}} C_{\mathrm{f}} \tag{4.35}$$

$$K_{\mathrm{iv}} = z \alpha_{\mathrm{v}} C_{\mathrm{f}} \tag{4.36}$$

The saturation symbol in PI-controller blocks represents back-calculation anti-windup method for limiting the control variable. Anti-windup function used in the PI-controller is shown in figure 4.5. The controller output is limited only when the input and output of the saturation block is equal.

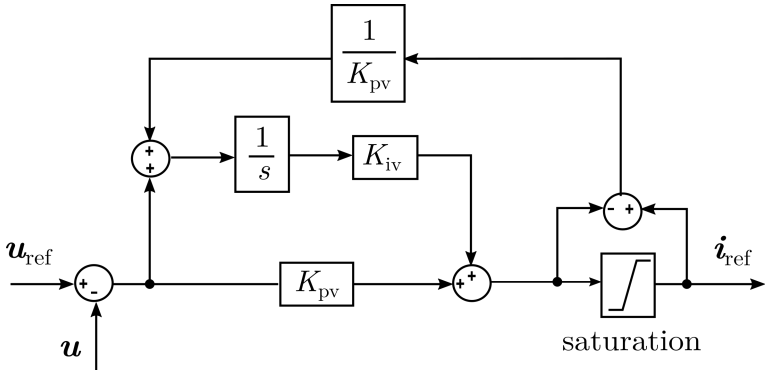

Figure 4.5: PI-controller with anti-windup loop

This voltage controller derives the current reference in *dq*-frame. The converter current should be limited within its rated design to protect the device. Thus, the current reference given to the inner current-controller should be limited within rated current. As soon as the current exceeds a threshold value the *dq*-current reference gets saturated [19, 26] based on the equations (4.37) and (4.38).

$$|i_{\mathrm{d,ref}}| = min \left\{ |i_{\mathrm{d,ref}}|,\ i_{\mathrm{c,max}} \right\} \tag{4.37}$$

$$|i_{\mathrm{q,ref}}| = min \left\{ |i_{\mathrm{q,ref}}|,\ \sqrt{i_{\mathrm{c,max}}^2 - i_{\mathrm{d,ref}}^2} \right\} \tag{4.38}$$

This current limitation technique is used with all the converters used in this work.

4.3.4 Current Controller

LCL-filter behaves like an L-filter at low frequencies. Current controller design for LCL-filter can be carried out with the L-filter approximation taken from [12, 15]. The voltage over the inductor in stationary frame can be,

$$L_{\mathrm{f}} \frac{\mathrm{d}i_{\mathrm{c}}}{\mathrm{d}t} + i_{\mathrm{c}} R_{\mathrm{f}} = u_{\mathrm{c}}^{\mathrm{s}} - u_{\mathrm{g}}^{\mathrm{s}} \tag{4.39}$$

The differential equation in synchronous coordinates be,

$$L_{\mathrm{f}} \frac{\mathrm{d}i_{\mathrm{c}}}{\mathrm{dt}} + j\omega_{\mathrm{g}} L_{\mathrm{f}} i_{\mathrm{c}} + i_{\mathrm{c}} R_{\mathrm{f}} = u_{\mathrm{c}} - u_{\mathrm{g}} \tag{4.40}$$

i_{c} is the converter current and u_{c} is the converter voltage. The corresponding *dq*-component form is

$$L_{\mathrm{f}} \frac{\mathrm{d}i_{\mathrm{cd}}}{\mathrm{dt}} = u_{\mathrm{cd}} - u_{\mathrm{gd}} - j\omega_{\mathrm{g}} L_{\mathrm{f}} i_{\mathrm{cq}} + i_{\mathrm{cd}} R_{\mathrm{f}} \tag{4.41}$$

$$L_{\mathrm{f}}\frac{\mathrm{d}i_{\mathrm{cq}}}{\mathrm{dt}} = u_{\mathrm{cq}} - u_{\mathrm{gq}} + j\omega_{\mathrm{g}}L_{\mathrm{f}}i_{\mathrm{cd}} + i_{\mathrm{cq}}R_{\mathrm{f}} \tag{4.42}$$

The cross-coupling effect in the dq-frame can be seen in equations (4.41) and (4.42). Change in current i_{cd} affects i_{cq} and vice-versa. To control the two-axis current separately the cross-coupling terms should be cancelled by adding the term $j\omega_{\mathrm{g}}L_{\mathrm{f}}i_{\mathrm{c}}$ to the current controller output as shown in the figure 4.6. The converter current is controlled with a PI-controller by controlling the voltage across inductor. By adding u_{g} as a feed-forward compensation term (with a gain term, $H_{\mathrm{f}} = 1$) to the controller output, the effect of the grid disturbance is nullified.

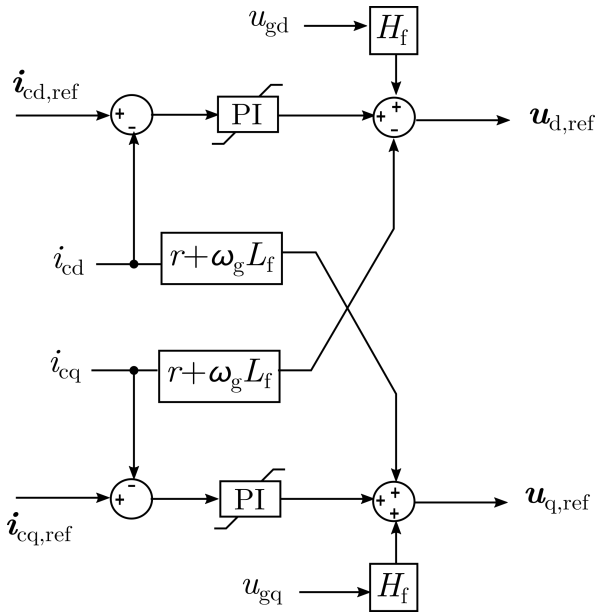

Figure 4.6: Current controller block

The transfer function of plant dynamics to be controlled is,

$$G_{\mathrm{pc}}(s) = \frac{i_{\mathrm{c}}(s)}{u_{\mathrm{c}}(s)} = \frac{1}{L_{\mathrm{f}}s + R_{\mathrm{f}}} \tag{4.43}$$

The desired first order closed-loop system be,

$$G_{\mathrm{cl,f}}(s) = \frac{\alpha_{\mathrm{c}}}{s + \alpha_{\mathrm{c}}} = \frac{\frac{\alpha_{\mathrm{c}}}{s}}{1 + \frac{\alpha_{\mathrm{c}}}{s}} \tag{4.44}$$

α_{c} is the bandwidth of the closed-loop system. The desired closed-loop transfer function from the given plant and controller be,

$$G_{\mathrm{cl,f}}(s) = \frac{G_{\mathrm{cc}}G_{\mathrm{pc}}}{1 + G_{\mathrm{cc}}G_{\mathrm{pc}}} \tag{4.45}$$

The controller is tuned by equating the closed-loop transfer function of the plant to desired closed-loop system.

$$G_{\mathrm{cc}}G_{\mathrm{pc}} = \frac{\alpha_{\mathrm{c}}}{s} \tag{4.46}$$

$$G_{\mathrm{cc}}(s) = \frac{\alpha_{\mathrm{c}}}{s}(G_{\mathrm{pc}}^{-1}) \tag{4.47}$$

$$G_{\mathrm{cc}}(s) = \frac{\alpha_{\mathrm{c}}}{s}(L_{\mathrm{f}}s + R_{\mathrm{f}}) \tag{4.48}$$

$$K_{\mathrm{pc}} = \alpha_{\mathrm{c}}L_{\mathrm{f}} \tag{4.49}$$

$$K_{\mathrm{ic}} = \alpha_{\mathrm{c}}R_{\mathrm{f}} \tag{4.50}$$

Since the control is designed with an inverse plant model, the pole of the plant is directly cancelled. This tuning method is termed as direct synthesis, a special case of internal model control (IMC). However, this pole cancellation design leads to poor disturbance rejection. This can be avoided by increasing the integral gain, by increasing the resistance value. This results in more losses. Thus, the resistance in added virtually in the control loop, which yields a controller that has two inputs: control error and current from active resistance. So, it is termed as two-degrees-of-freedom controller. This leads to the gain,

$$K_{\mathrm{ic}} = \alpha_{\mathrm{c}}(R_{\mathrm{f}} + r) \tag{4.51}$$

Regarding the value of the virtual resistance r, it is useful to make the inner loop as fast as the total closed-loop system bandwidth, α_{c}

$$\frac{r + R_{\mathrm{f}}}{L_{\mathrm{f}}} = \alpha_{\mathrm{c}} \tag{4.52}$$

This yields,

$$r = \alpha_{\mathrm{c}}L_{\mathrm{f}} - R_{\mathrm{f}} \tag{4.53}$$

Substituting, equation (4.53) in equation (4.51) gives,

$$K_{\mathrm{ic}} = \alpha_c^2 L_{\mathrm{f}} \tag{4.54}$$

The park transformation block requires voltage angle, θ which is given by the reference generation techniques. u_{abc} is the reference voltage output for the converter from the current controller block. u_{abc} is modulated with high-frequency switching pulses using the Third-Harmonic Injected Pulse Width Modulation (THPWM) unit and applied to power converter switches.

4.4 Control of Grid-feeding Converters

Power converters controlled as AC current-source for feeding power in grid-connected mode is termed as grid-feeding converter control. The control block diagram is given in the figure 4.7.

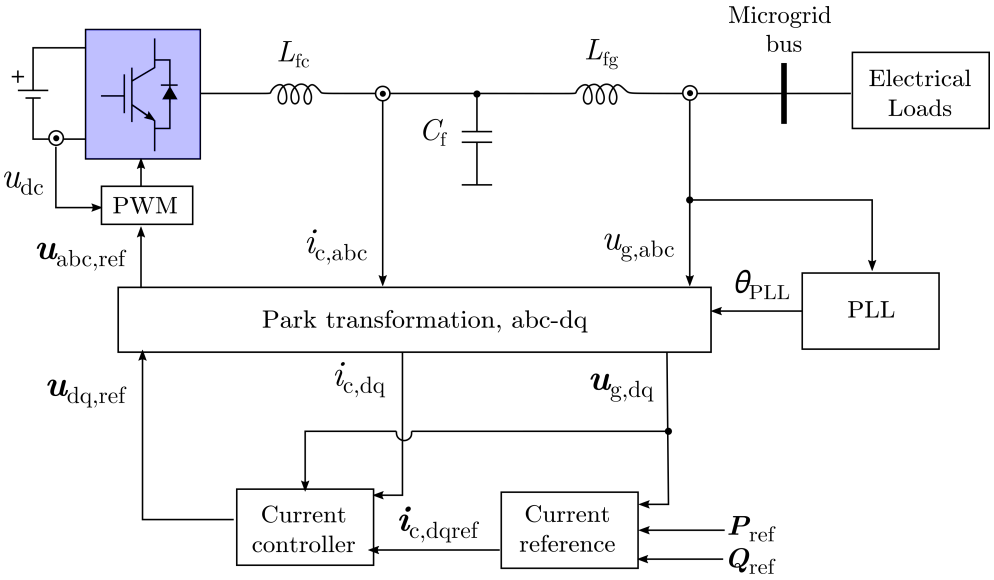

Figure 4.7: Grid-feeding converter control block diagram

It uses reference generated by the phase-locked loop to follow the voltage and frequency reference ($u_{gd}\angle\theta_{PLL}$) of the grid-forming source. PLL tracks the frequency and the voltage of the grid for the synchronized power injection. The block diagram of PLL is shown in the figure 4.8.

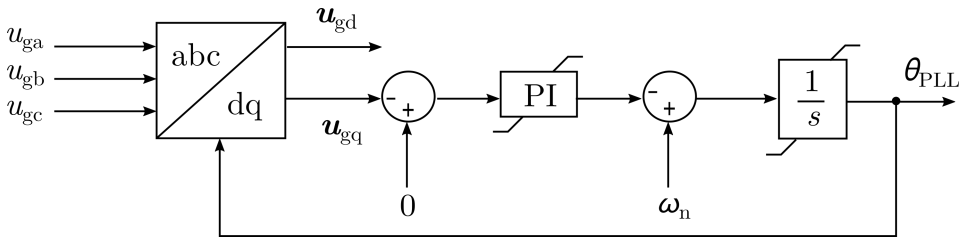

Figure 4.8: PLL control structure used in grid-feeding converter

The open-loop transfer function of the system be,

$$G_{ol,PLL}(s) = \left(\frac{K_{p,PLL}s + K_{i,PLL}}{s}\right)\left(\frac{u_g}{s}\right) \tag{4.55}$$

The closed-loop transfer function of the PLL be,

$$G_{cl,PLL}(s) = \frac{G_{ol,PLL}(s)}{1 + G_{ol,PLL}(s)} \tag{4.56}$$

$$G_{\mathrm{cl,PLL}}(s) = \frac{u_{\mathrm{g}}(K_{\mathrm{p,PLL}}s + K_{\mathrm{i,PLL}})}{s^2 + s(u_{\mathrm{g}}K_{\mathrm{p,PLL}}) + u_{\mathrm{g}}K_{\mathrm{i,PLL}}} \tag{4.57}$$

The poles of the second-order transfer function are given by,

$$s^2 + 2\zeta\omega_{\mathrm{o}}s + \omega_{\mathrm{o}}^2 \tag{4.58}$$

ζ is the damping ratio and ω_{o} is the natural frequency. The controller gains $K_{\mathrm{p,PLL}}$ and $K_{\mathrm{i,PLL}}$ are obtained by comparing the poles of the transfer function [12].

$$K_{\mathrm{p,PLL}} = \frac{2\zeta\omega_{\mathrm{o}}}{u_{\mathrm{g}}} \tag{4.59}$$

$$K_{\mathrm{i,PLL}} = \frac{\omega_{\mathrm{o}}^2}{u_{\mathrm{g}}} \tag{4.60}$$

The natural frequency ω_{o} is selected less than the grid frequency which is generally 0.2-0.4 p.u and the damping ratio is set to 1. Since the PLL is designed for p.u operation, u_{g} is 1 for gain calculation. Voltage from the PLL is used to derive the current reference from the power equations as shown in figure 4.9. The current reference is limited using current limitation block and the current is controlled using the current controller. The current injected into the grid is based on the active-reactive power set-points.

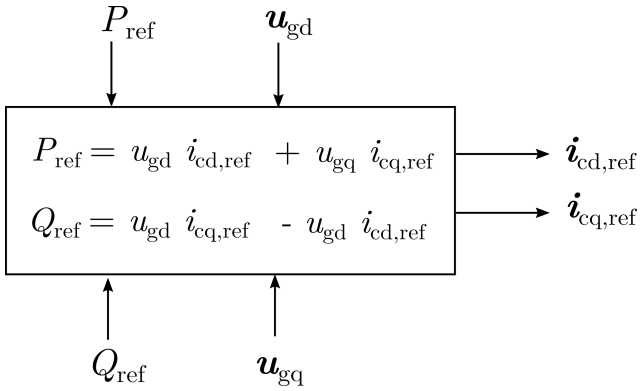

Figure 4.9: Current reference block

The design procedure for the current controller used in the grid-forming control is adopted for the grid-feeding control. The park transformation block requires a voltage angle θ which is given by the PLL. u_{abc} is the reference voltage output for the converter from the current controller block. u_{abc} is modulated with high-frequency switching pulses using the Third-Harmonic Injected Pulse Width Modulation (THPWM) unit and applied to power converter switches.

4.5 Simulation Setup

Three different scenarios are considered for the simulation. First, a single grid-forming converter with electrical load forms a microgrid as shown in figure 4.10 is simulated to understand the normal behavior of the control system and its differences.

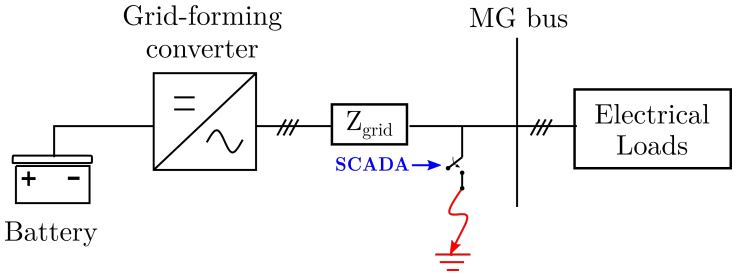

Figure 4.10: Test setup-1 – grid-forming converter and load

The next test setup includes two grid-forming converters in parallel with rated electrical loads (figure 4.11). Two converters are operated to check nominal operation and its stability problems, the importance of line impedance connecting those converters, scenario of paralleling converters with different droop gains and power ratings are simulated with this setup.

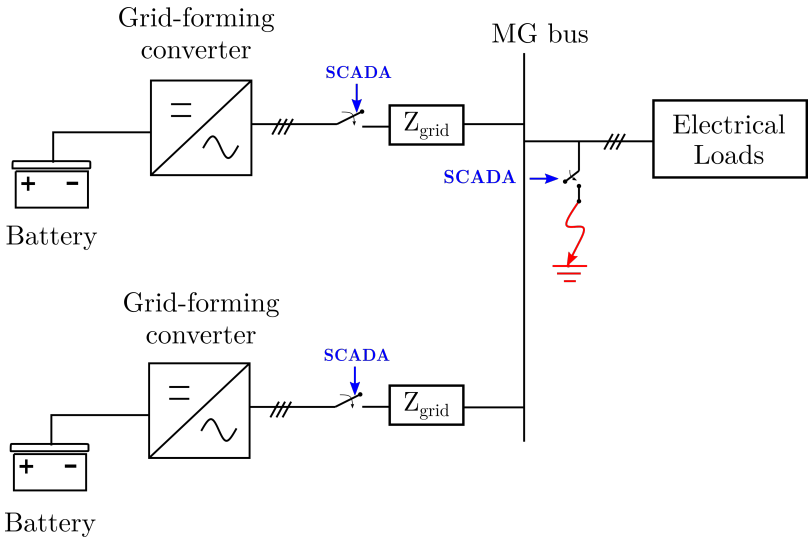

Figure 4.11: Test setup-2 – parallel-forming converters and load

The last setup has parallel operation of grid-forming converter with grid-feeding converter (figure 4.12). Operational stability, PLL operation with weak grid and strong grid and short-circuit conditions are simulated. For strong grid condition, the grid-feeding converter is connected to grid-simulator.

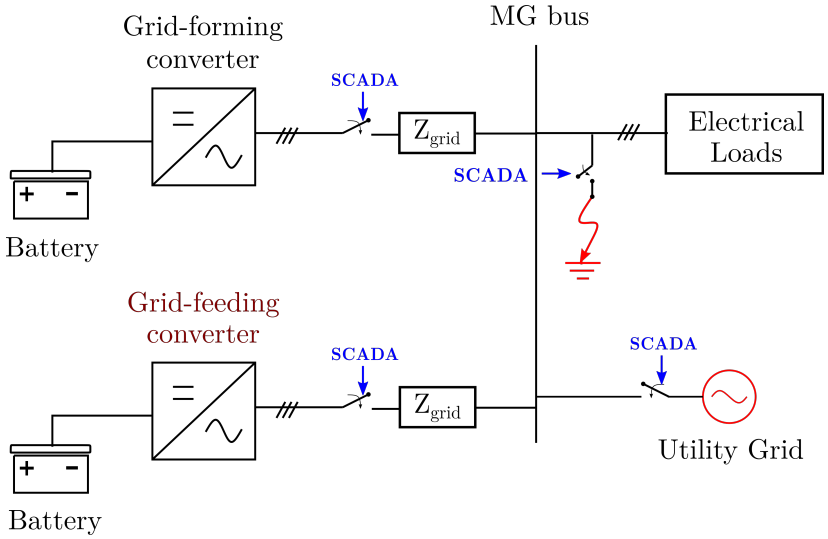

Figure 4.12: Test setup-3 – grid-forming converter, grid-feeding converter and load

Electrical loads

The electrical load used is Resistive-Inductive-Capacitive type (RLC-Load) which is varied using SCADA inputs. The pattern and magnitude of the load applied to the converter are given in figure 4.13 and Table 4.1. This pattern of load switching is used to test the system stability at different types of disturbances. Step change in load is considered as a disturbance.

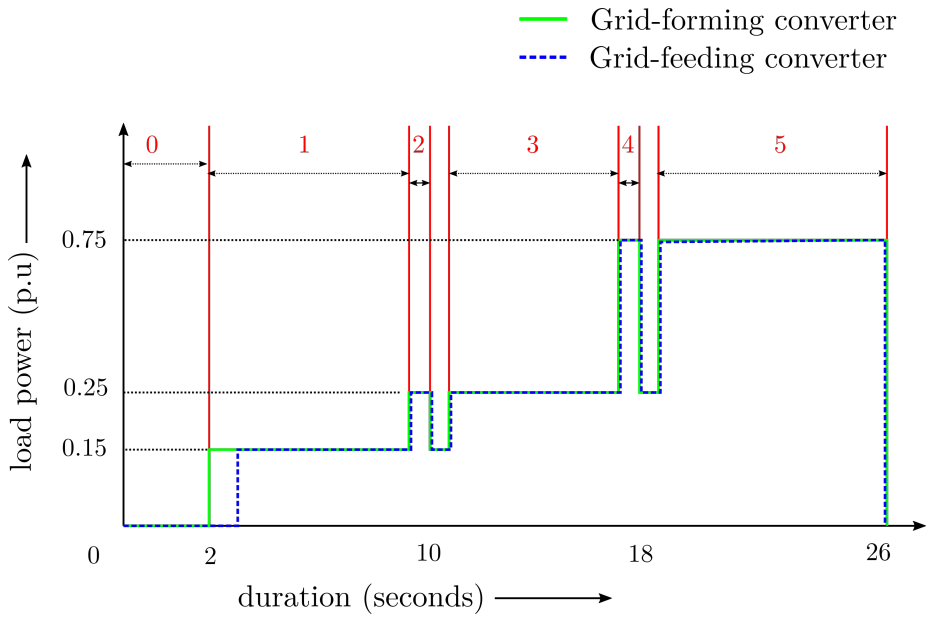

Figure 4.13: Pattern of load connected to grid-forming and grid-feeding converter

Depending upon the magnitude and duration of the load change, they are classified as small-signal/large-signal + short-time/long-time disturbances. Figure 4.13 shows

a switching pattern defining the duration and magnitude of different loads for grid-feeding and grid-forming converters. Grid-feeding converter is switched with a delay, as it should track the voltage of the grid-forming converter.

In state 0, the converter is switched on but not connected to the load. In state-1, a small load is applied to the grid-forming converter. With a short-delay in state-1, the grid-feeding converter starts to inject the power to the grid/load. Delivered power output is same for two converters. In state-2, there is a small increase in load for a short time leading to a condition of small-signal short disturbance. With a short delay, a small load step is applied again but now for a longer duration, forming the small-signal long disturbance condition in state-3. In state-4, there is a large load step for short-time leading to a condition of large-signal short disturbance for short-time. With a short delay, a large load step is applied again but now for a longer duration, forming the large-signal long disturbance condition in state-5. This switching pattern is applied for setup-3 having both grid-feeding and grid-forming converters. The switching pattern of the grid-forming converter (green line) is applied for setup-1 and setup-2 to test the different operating conditions. The types of disturbances are taken from the stability classifications mentioned in section 3.3.4. Using these disturbances, the behavior of converters are studied. The load connected to the converter at every state is shown in the figure 4.13. The value of the load impedance is given in Table 4.1.

Table 4.1: Load values connected to converter at every state

States	**Duration**	**RLC-load value**			**Test condition**
	(seconds)	$\boldsymbol{R(\Omega)}$	$\boldsymbol{L(mH)}$	$\boldsymbol{C(mF)}$	**(Disturbance)**
0	2	-	-	-	No Load
1	7.5	1.07	-	-	Base Load
2	0.5	0.61	2	6	Small-short load
3	7.5	0.61	2	6	Small-long load
4	0.5	0.22	0.4	31	Large-short load
5	7.5	0.22	0.4	31	Large-long load

To understand the switching patterns and relate with the load values in Table 4.1, state-2 is explained. At state-2, the load connected to a (single) converter changes from 1.07 Ω to (0.61- 1.25j) Ω. Now, the load power consumption increases from 0.15 p.u to 0.25 p.u. This load change lasts only for 0.5 seconds, after that load value changes back to 1.07 Ω. This load change is an example for small-signal short load disturbance. When two converters are used in the setup, two such loads are connected, and the consumed load power is 0.5 p.u. Power system stability is defined with these type of disturbances in [1], thus the load pattern derived from the combination of all these disturbances, is used as a standard test-case in this work. So, when the converter works for this load pattern, system is stable.

Stability Limits

Stable operating points of the interconnected grid is defined in the country grid-codes. These operating points are defined based on the safety of the connected equipment. So, stability and protection are two interrelated terms. Regulation of grid codes for isolated electrical systems are not standardized or evenly followed. Thus, the interconnected (central) grid-codes defined in [8] are used as the stability limits in this simulation. Standard grid-codes are defined for synchronous machine-based grids and when used in power converter-based grid, the difference could be easily identified. An aggregated protection function is used to give the trip signal when the system parameters are not within the limits. The relay function gives a trip signal only when the fault persists more than trip-delay time (0.2 seconds). The threshold values for different fault conditions used in the relay/protection function are mentioned in Table 4.2. This function is used in all the simulation models.

Table 4.2: Protection threshold and trip-delay

Fault or Abnormality type	**Actual value**	**Per-unit value**	**Trip-delay(s)**
Over-voltage (V)	440	1.1	0.2
Under-voltage (V)	360	0.9	0.2
Over-frequency (Hz)	52.5	1.05	0.2
Under-frequency (Hz)	47.5	0.95	0.2
Rate of Change of Frequency (Hz/s)	2.5	0.05	0.2
Over-current (A)	2041	1	0.2

RoCoF calculation involves 3 cycles and when 2.5 Hz/s value sustains for more than 0.2s, protection function gives a trip signal. Trip signal is used only in the plot to identify the threshold crossing and not to disable the converter/load.

4.6 Simulation Parameters

The parameters used in the design of grid-forming power converters are summarized in the Table 4.3 below. The current controller bandwidth for the grid-forming converter is selected as one-thirtieth of the sampling frequency. For grid-forming converter, the calculated value of current-controller proportional gain K_{pc} has a system pole near the right-half plane as shown in the results of (grid-forming) controller-stability analysis in [29]. Increasing the gain moves the controller towards the left-half plane and stabilizes the system. Thus, K_{pc} value used in the simulation is higher than the calculated value. The network impedance is chosen such that the R/X ratio is 8 and R value of 0.1 p.u. Battery used as DC-source is operated with a low State-of-Charge (SoC) value of 20% to check the transient instability issues.

Table 4.3: Grid-forming converter model specification

Parameters	**Actual value**	**unit**	**Per-unit value**
Base voltage	326.6	V	1
Base power	1	MVA	1
Base frequency	50	Hz	1
Base impedance	0.16	Ω	1
DC-bus voltage, u_{dc}	800	V	2.45
Battery energy rating	200	Ah	-
Battery SoC	20	%	-
Switching frequency, f_{sw}	2500	Hz	50
Sampling frequency, f_{s}	5000	Hz	100
Converter-side filter inductance,L_{fc}	108	µH	0.21
Converter-side filter inductance ESR, R_{c}	15	$m\Omega$	0.09
Grid-side filter inductance, L_{fg}	62	µH	0.12
Grid-side filter inductance ESR, R_{g}	10	$m\Omega$	0.06
Filter capacitor, C_{f}	716	µF	0.04
Filter capacitor ESR (damping), R_{d}	78	$m\Omega$	0.48
DC-bus capacitor, C_{dc}	7.5	mF	0.38
Network resistance	14.2	$m\Omega$	0.09
Network reactance	6	µH	0.01
Active power droop gain, D_{p}	17	µHz/W	-
Reactive power droop gain, D_{q}	24	µV/VAr	-
Synchronverter damper, D	182	-	-
Synchronverter inertia, J	182	-	-
Field voltage constant, $M_{\mathrm{f}}.i_{\mathrm{f}}$	1.04	-	-
Feed-forward voltage gain, K_{f}	1	-	-
Feed-forward current gain, H_{f}	1	-	-
Current-controller bandwidth, α_{c}	1047	rad/s	3.33
Current-controller proportional gain, K_{pc}	0.16	-	-
Current-controller integral gain, K_{ic}	187.2	-	-
Voltage-controller bandwidth, α_{v}	350.38	rad/s	1.12
Voltage-controller proportional gain, K_{pv}	0.25	-	-
Voltage-controller integral gain, K_{iv}	29.42	-	-

The parameters used in the design of grid-feeding power converters are summarized in Table 4.4 below. The bandwidth of the PLL is selected as $2\pi.15$ rad/s and corresponding the gain values are mentioned below. The current controller bandwidth is selected one-tenth of the sampling frequency. The calculated gains are directly used in the model.

Table 4.4: Grid-feeding converter model specification

Parameters	**Actual value**	**unit**	**Per-unit value**
PLL-controller bandwidth, α_{PLL}	94.24	rad/s	0.3
PLL-controller proportional gain, $K_{\mathrm{p,PLL}}$	188	-	-
PLL-contoller integral gain, $K_{\mathrm{i,PLL}}$	8882	-	-
Current-controller bandwidth, α_{c}	3142	rad/s	10
Current-controller proportional gain, K_{pc}	0.54	-	-
Current-controller integral gain, K_{ic}	1688	-	-

5 Simulation Results and Discussion

This chapter presents the results from the microgrid model tested under various operating conditions.

5.1 Grid-forming Converter

Setup-1 having a single grid-forming converter is tested to study the difference between droop and synchronverter control techniques and their effectiveness for the applied load transients. The step-time of the simulation is 2 µs. Model sampling time is 200 µs. Figure 5.1 shows the results of the converter and grid voltage for a larger load step (increase). This is captured from the scope with $5e^5$ samples/second.

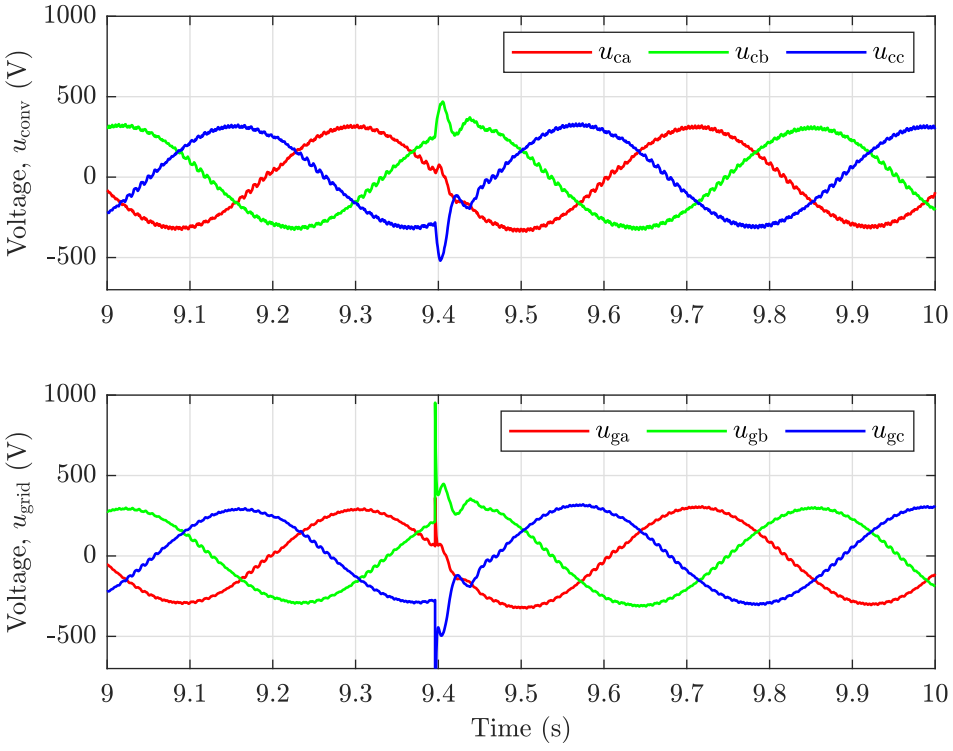

Figure 5.1: Phasor values of converter voltage and grid voltage during a large step change (decrease) in RLC-load

As the simulation run time is 26 seconds as defined in Table 4.1, capturing multiple

parameters handles very large data. Thus, data is exported using a data-logger from SCADA editor, which has its minimum sampling interval of 250ms. Hence, the ripples seen in the figure 5.1 will not be visible in the other plots. Also, the simulation results are normalized to per-unit RMS values for easing the analysis. In figure 5.1, the peak RMS value of the phase voltage is 326.6V. The transient spikes are higher in the load-side or grid due to the switching of RLC-load. The converter side voltage is measured from the LCL filter-capacitor. The subscript "conv" represents the converter-side measurement, "load" represents load-side measurement which is used in the plots. Response of a droop control-based power converter for the RLC-load transients are shown in the figures 5.2 and 5.3

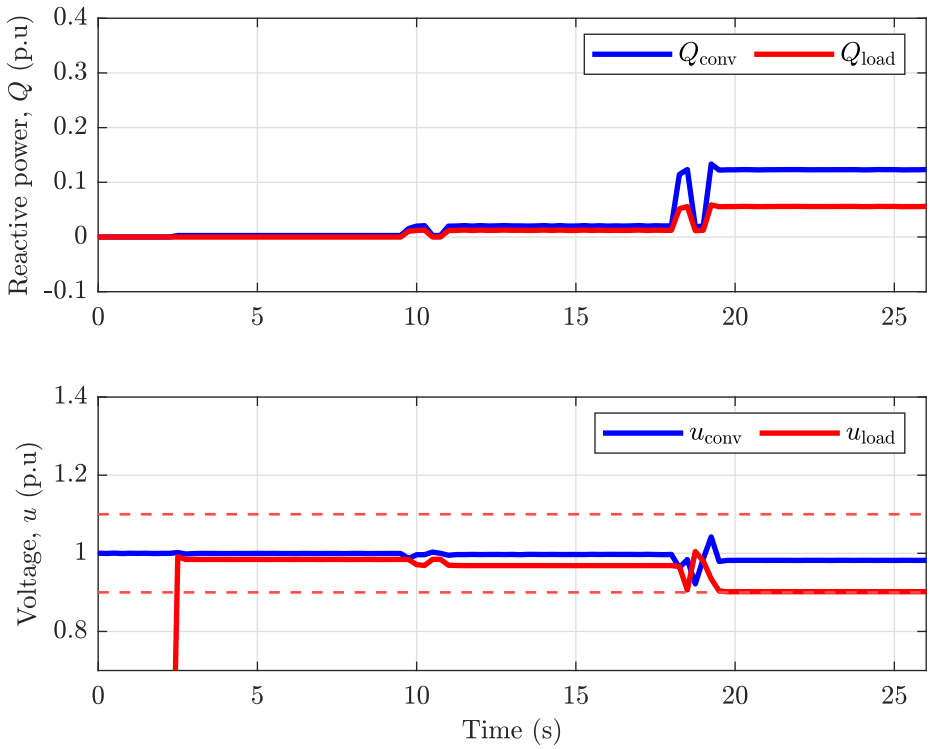

Figure 5.2: Voltage and reactive power output of droop-controlled converter for the RLC-load switching defined in Table 4.1. Red dotted-lines represent the voltage tripping limit

Figure 5.2 shows that the converter output voltage is well within the limits. The load voltage is not the same as the converter voltage, due to the drop in the series impedance between converter and load. At large load disturbance, the reactive power consumption of the network is twice the load as shown. The load voltage has reached the tripping limit 360V. As per conventional droop, voltage value must be reduced based on reactive power consumption but here voltage drop is more because of the non-negligible line-resistance. This control inaccuracy is the main issue with the droop control when used in resistance dominant network.

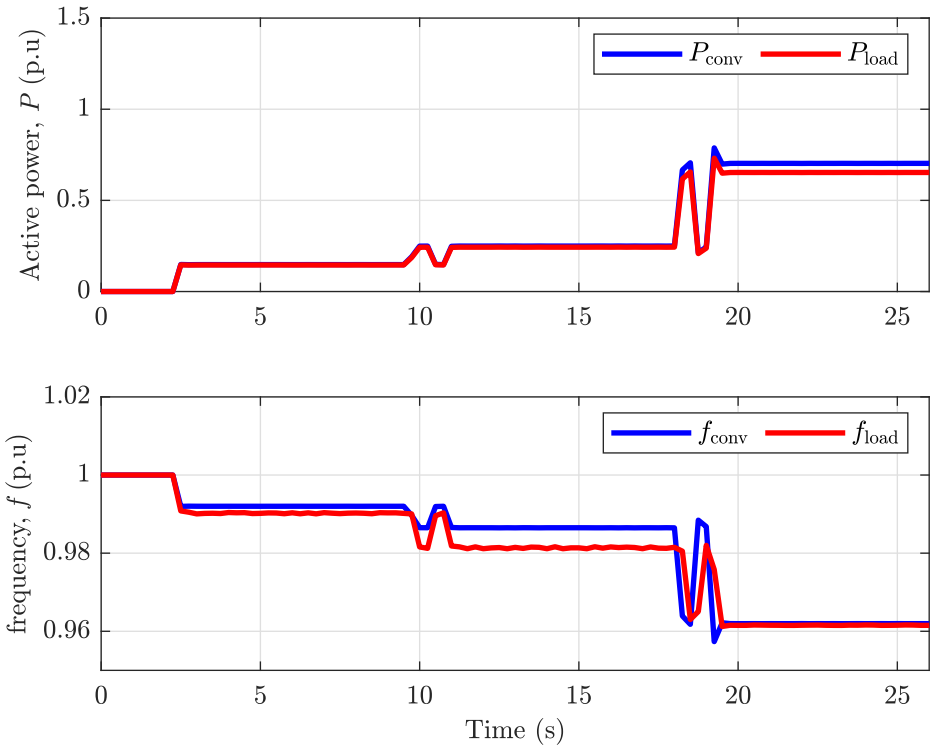

Figure 5.3: Frequency and active power output of droop-controlled converter for the RLC-load switching defined in Table 4.1

Figure 5.3 shows the frequency and the active power output measured at the converter and the load. As the change in frequency is directly coupled to the active power, the frequency changes even for a short-term load disturbance. The maximum converter loading is 0.7 p.u. The applied load power rating is maximum 0.75 p.u at nominal voltage. Power losses in the line impedance also limit the power transfer. Converter frequency is from the droop reference. The load-side measurement unit uses PLL for measuring the frequency. The steady-state difference between the converter and the grid frequency is the tracking error by the PLL. The load transients are now applied for synchronverter-controlled converter and tested.

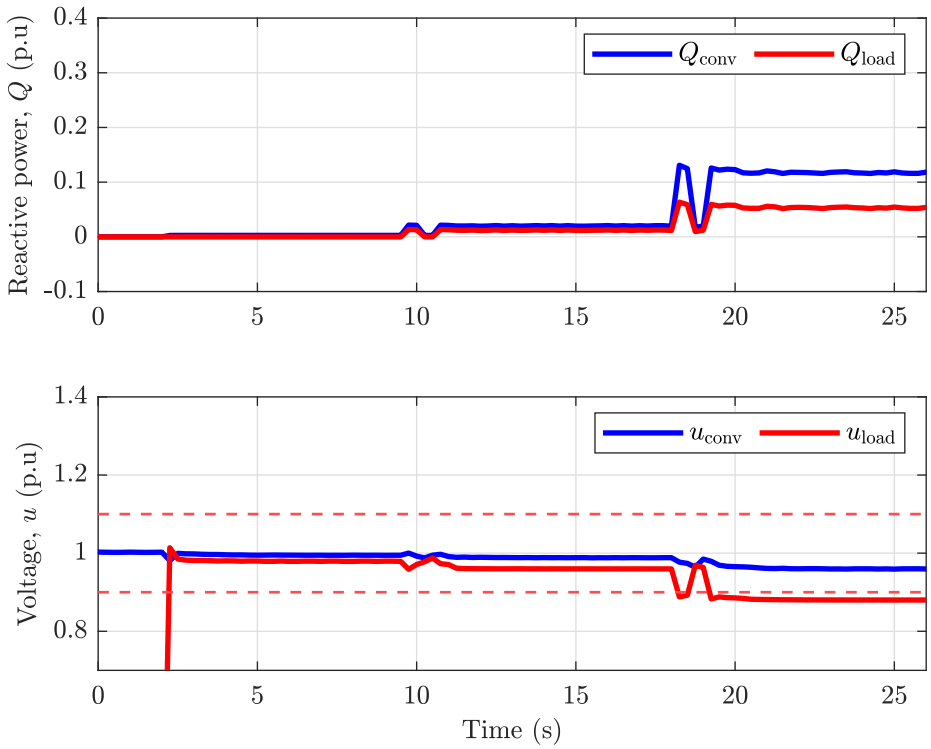

Figure 5.4: Voltage and reactive power output of synchronverter-controlled converter for the RLC-load switching defined in Table 4.1. Red dotted-lines represent the voltage tripping limit

Voltage droop and virtual angular frequency is associated with the generated voltage reference. Hence, the voltage drop is more with the synchronverter control as shown in figure 5.4. But the converter voltage reference changes slowly for the disturbance, much like SM. Inertia contributes to these slow dynamics. The $M_{\text{f}}.i_{\text{f}}$ constant must be varied to maintain the voltage at the nominal value. This will increase the active and reactive power supplied by the converter. This auto-adjustment is not added in the model.

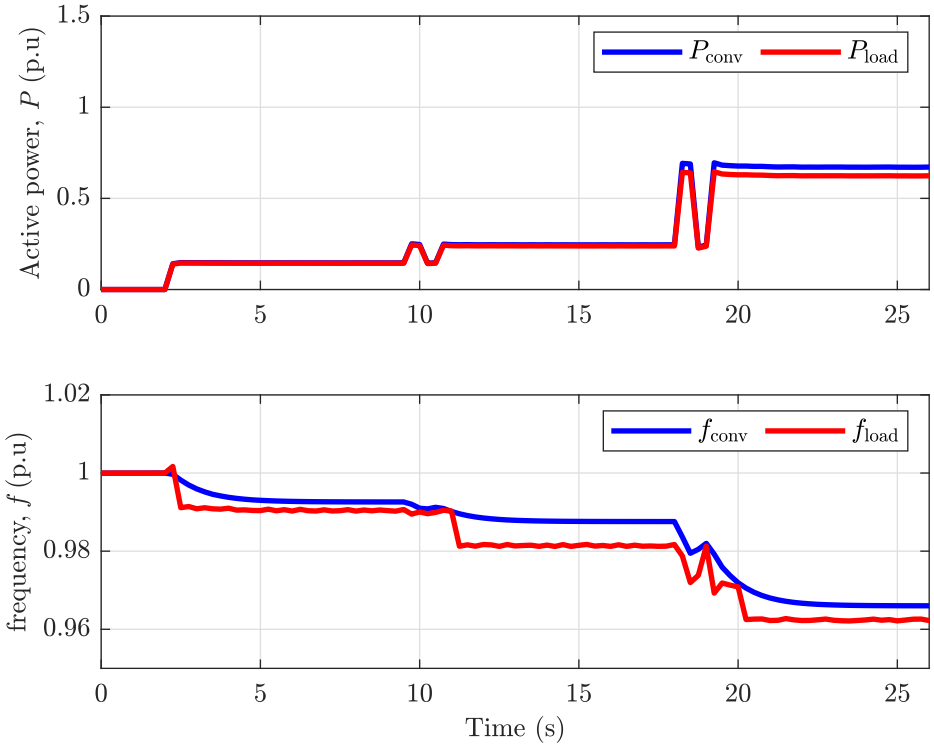

Figure 5.5: Frequency and active power output of synchronverter-controlled converter for the RLC-load switching defined in Table 4.1.

In figure 5.5, frequency and active power output of synchronverter-controlled converter is shown. The frequency change in the synchronverter is slower than the droop due to added inertia in the SM model. There is no significant change in frequency for the short-term short disturbance. For long-term short disturbance, the frequency reduction is very lower than the droop control. The maximum active power supplied is 0.68 p.u. This slow-changing frequency reference is compared with the fast-changing droop control in the figure 5.6.

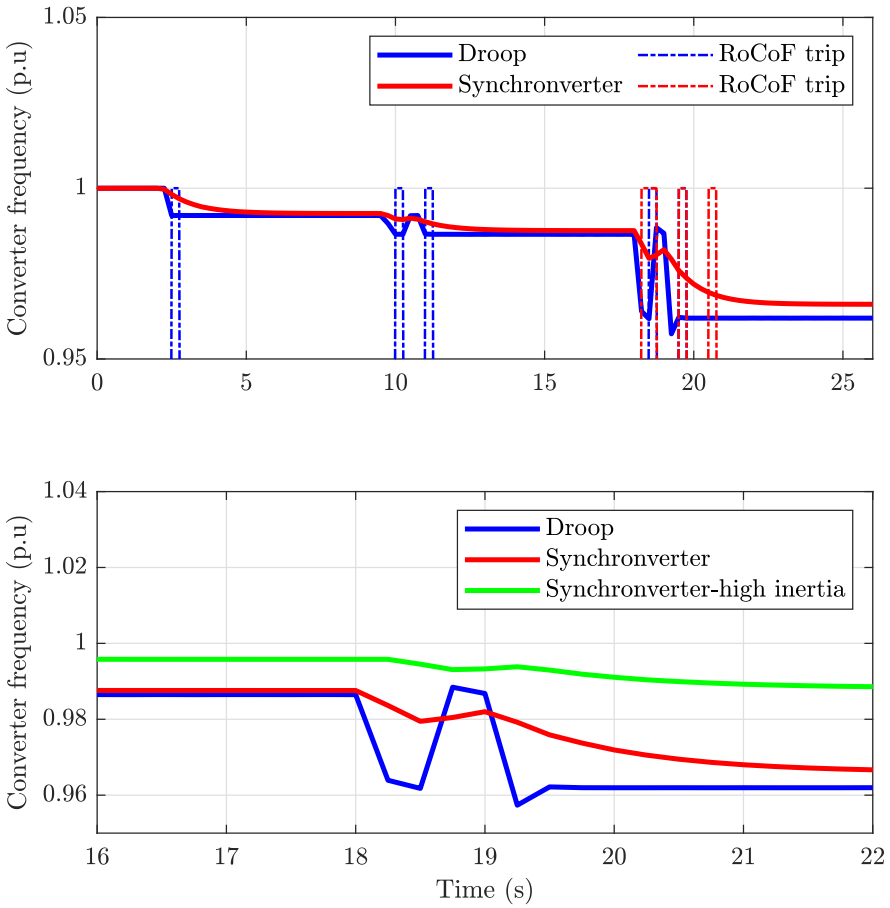

Figure 5.6: Inertial difference between droop and synchronverter frequency for the RLC-load disturbance

Figure 5.6 shows the inertial difference between the droop and synchronverter control. On a small short-term disturbance at 10.5 seconds, droop control has the fast-changing frequency reference. This change in frequency is based on active power change. As mentioned earlier, RoCoF is an important signal to maintain power imbalance and system stability on large disturbance. This fast-changing droop has a fast RoCoF detected (blue-dotted line) even for a small change in load. This leads to frequent tripping making the frequency stability critical.

Output frequency of synchronverter (red line) has slower dynamics due to the virtual inertia of SM, thus no significant change or RoCoF trip detected for smaller load disturbances. To show the effect of the inertia for a large disturbance, the synchronverter plot is presented with a zoomed view in the second subplot of figure 5.6. The change in frequency reference is slower than the droop control. Also, the response is further slowed down when higher inertia is used. Frequency change is insignificant for short-term disturbances, irrespective of disturbance magnitude. But for large long-term disturbance after 19 seconds, frequency reduces to new operating point. Synchronverter can damp down the short-term disturbance and maintain the system stability depending on the selected inertia.

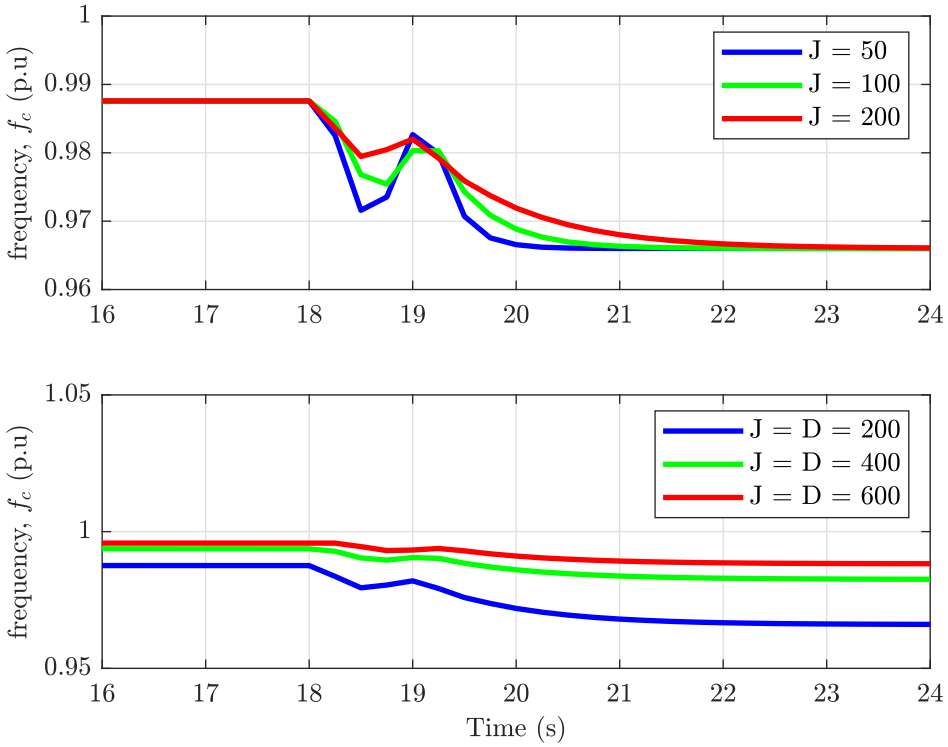

Figure 5.7: Inertial difference for the different inertia (J) and damper (D) values on large disturbance RLC-load switching

Selection of synchronverter parameters and their behavior can be seen in figure 5.7. It shows the large disturbance response of synchronverters with different values of inertia (J). As $J = D\tau$, adjusting the time-constant of the synchronous machine τ, allows the different inertia. For all the inertia values, Damper (D) = 200, calculated for 5% frequency deviation on full rated power 0.9 MW. For the inertia, $J = 50$ (blue line), the frequency reference settles to a new operating point faster than the inertia $J = 200$ (red line). As shown in the second subplot of figure 5.7, to limit the frequency deviation for applied load change, D value should be increased. For $D = 200$, the frequency deviation reaches to 4% and $D = 600$ has a frequency deviation of only 1.2%. Deviations are shown for 0.75 p.u RLC-load connected to the converter.

Thus, damper adjusts the frequency deviation and inertia adjusts the settling time for a response. Both can be selected for a given RoCoF tripping threshold limits. The virtual inertia added to the converter provides better small-signal frequency stability. To have a distinguishable (slow) dynamics when compared with the droop control and study its impact, $J = D$ is used for all the simulation models.

5.2 Parallel Grid-forming Converters

The main aim of simulating parallel converters (setup-2) is to study the voltage stability issues due to poor power-sharing. The load conditions are same as mentioned in Table 4.1. The subscript "conv1", "conv2" represents the measurement at the two grid-forming converters and "load" represents the measurement near loads, which are used in the plots.

5.2.1 Identical Converters

The condition of two identical converters operating in parallel are tested. Each converter is connected to the equal load through equal line-impedance.

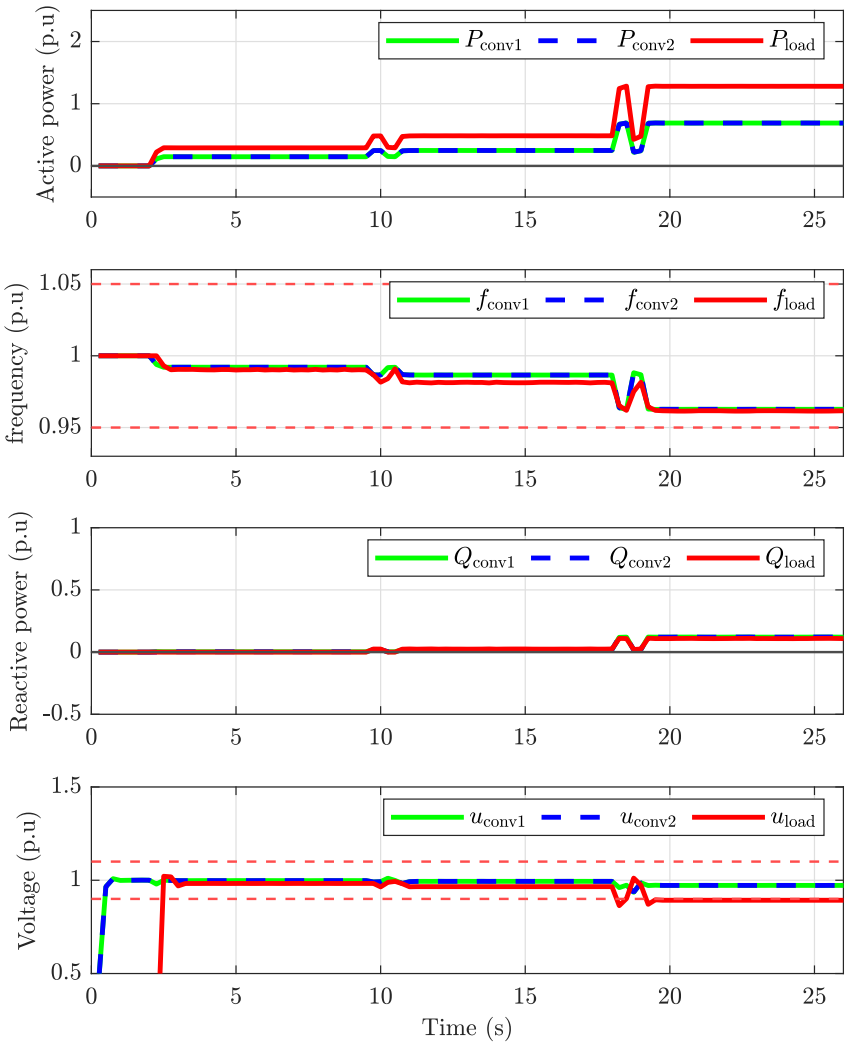

Figure 5.8: Output of droop-controlled parallel converters for the RLC-load switching defined in Table 4.1. Red dotted-lines represent the frequency and voltage tripping limit

Figure 5.8 shows the voltage and reactive power output of parallel droop-controlled identical converters. The converter voltage is within the limits and the reactive power is equally shared between the converters. Frequency stability is critical, much like the single converter case, due to the fast-changing reference. Active power is equally shared between the converters, but load voltage is equal to under-voltage limit. As the converters are connected via two line-impedance, the drop is higher than the single converter case. The maximum active power supplied is reduced to 0.65 p.u, which was 0.7 p.u in single converter case. For large short-term disturbance at 17 seconds, there is a possible under-voltage tripping as the voltage slips below the limit.

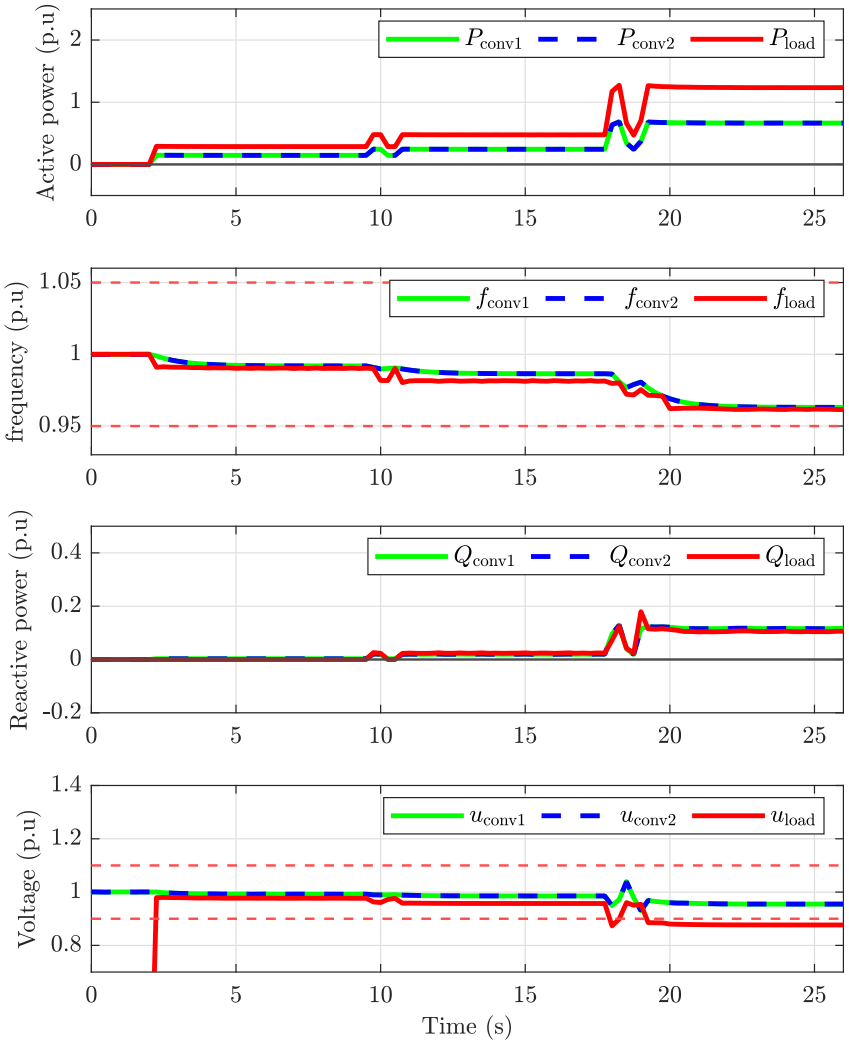

Figure 5.9: Output of synchronverter-controlled parallel converters for the RLC-load switching defined in Table 4.1. Red dotted-lines represent the frequency and voltage tripping limit

Figure 5.9 shows the output of the parallel synchronverter-based converters. Along with line voltage drop, synchronverter voltage has a frequency deviation drop as

mentioned in the single converter case. Thus, the active power loading by each of the converter (0.6 p.u) is lower than the droop control. There will be an under-voltage tripping at the large disturbances. The line impedance compensation should be considered to deliver the required power. As the stability of parallel identical converters is not critical except the line voltage drop, the behavior of non-identical converters is tested. Response of parallel identical converters in figures 5.8 and 5.9 are considered as ideal case. For a perfect synchronization voltage, frequency and phase angle should be same. Non-identical control parameters, power rating and line-impedance between the converters disturbs the power-sharing between the parallel converters (which has wireless synchronization).

5.2.2 Effect of Different Droop Gains

Droop gains sets the voltage, frequency based on the load power consumption. The effect of having droop gain mismatch between two identical converters operating in parallel are shown in the figure 5.10. The different frequency and voltage droop gains used in the converters are mentioned in Table 5.1.

Table 5.1: Different frequency and voltage droop gains for parallel converters

Droop gains	**Actual value**
Converter 1, frequency droop gain, D_{p1}	$17e^{-6}$
Converter 1, voltage droop gain, D_{q1}	$24e^{-6}$
Converter 2, frequency droop gain, D_{p2}	$9.5e^{-6}$
Converter 2, voltage droop gain, D_{q2}	$12e^{-6}$

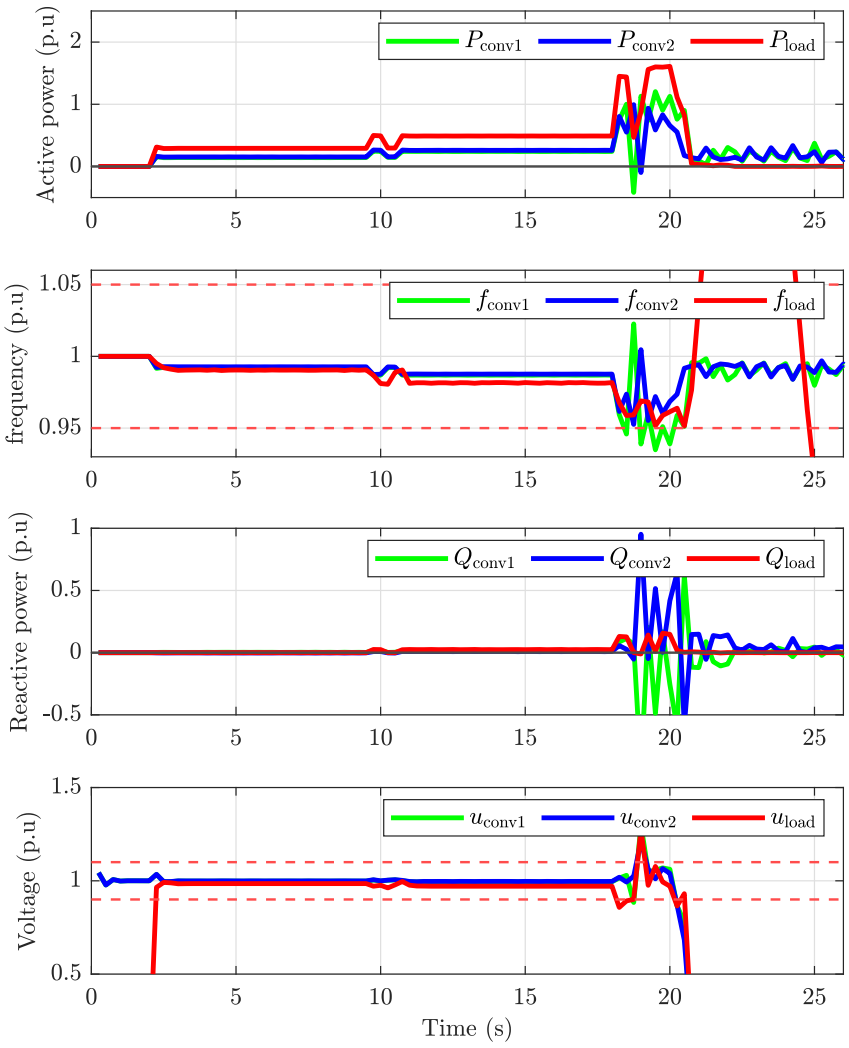

Figure 5.10: Output of droop-controlled parallel converters with droop gains of $D_{p1} = 17e^{-6}$, $D_{q1} = 24e^{-6}$, $D_{p2} = 9.5e^{-6}$, $D_{q2} = 12e^{-6}$ for the RLC-load switching defined in Table 4.1. Red dotted-lines represent the frequency and voltage tripping limit

For a large load disturbance, parallel converters operating with different droop gains, lose their synchronization leading to high reactive currents flowing between the converters, which is shown in figure 5.10. As the converter currents are limited, the system loses its voltage stability at 17 seconds. The droop gain mismatch causes different voltage and frequency based on active and reactive powers consumed. Large oscillations in active power leads to unstable frequency besides the fast RoCoF issue. Grid frequency measurement unit loses its stability for the distorted grid-voltage, thus grid frequency - red line goes out of limits.

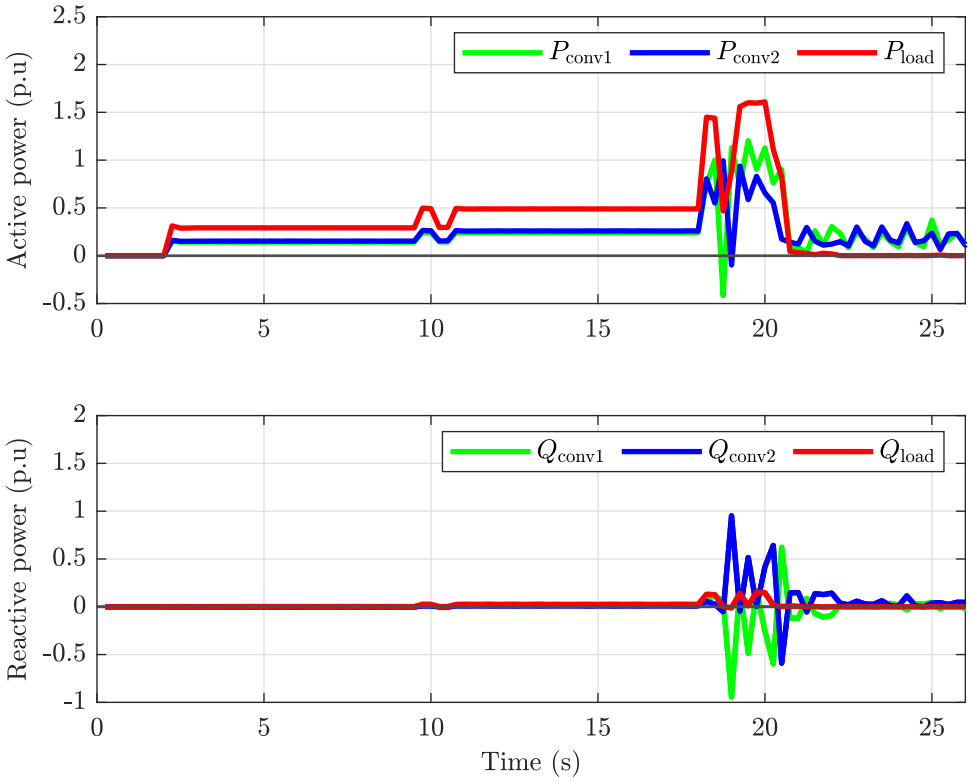

Figure 5.11: Active power and reactive power output of the parallel-forming converters and the load for different droop gain condition

The converter with higher voltage acts as a load for the other converter leading to a circulating current flowing between the converters instead of supplying the load, thereby deteriorating the voltage stability. This circulating current is explained using the different droop gain scenario in the figure 5.11. For a large load disturbance, when the synchronization is lost, output voltage of the converters is not the same. Thus, the converter-2 loads the converter-1, the reactive power is not supplied to the grid (red line is near zero) but flows between the two converters (blue and green lines). This is clearly an unstable oscillatory condition. However, even in some marginally stable conditions, one converter loads the other (seen as unequal power-sharing) which should be avoided. Since power consumption drives the voltage and frequency variables, there is a possible under-voltage/frequency tripping for the loaded converter. This will lead to large power imbalance in the microgrid resulting in complete shutdown.

5.2.3 Effect of Different Line-impedance

Line-impedance is an important factor for power-sharing between parallel converters. Generally, the wires connecting two equally rated converters could be different depending upon the distance between them and types of wires or cables used. The effect of the different line-impedance for the different load disturbance is shown in the figure 5.12.

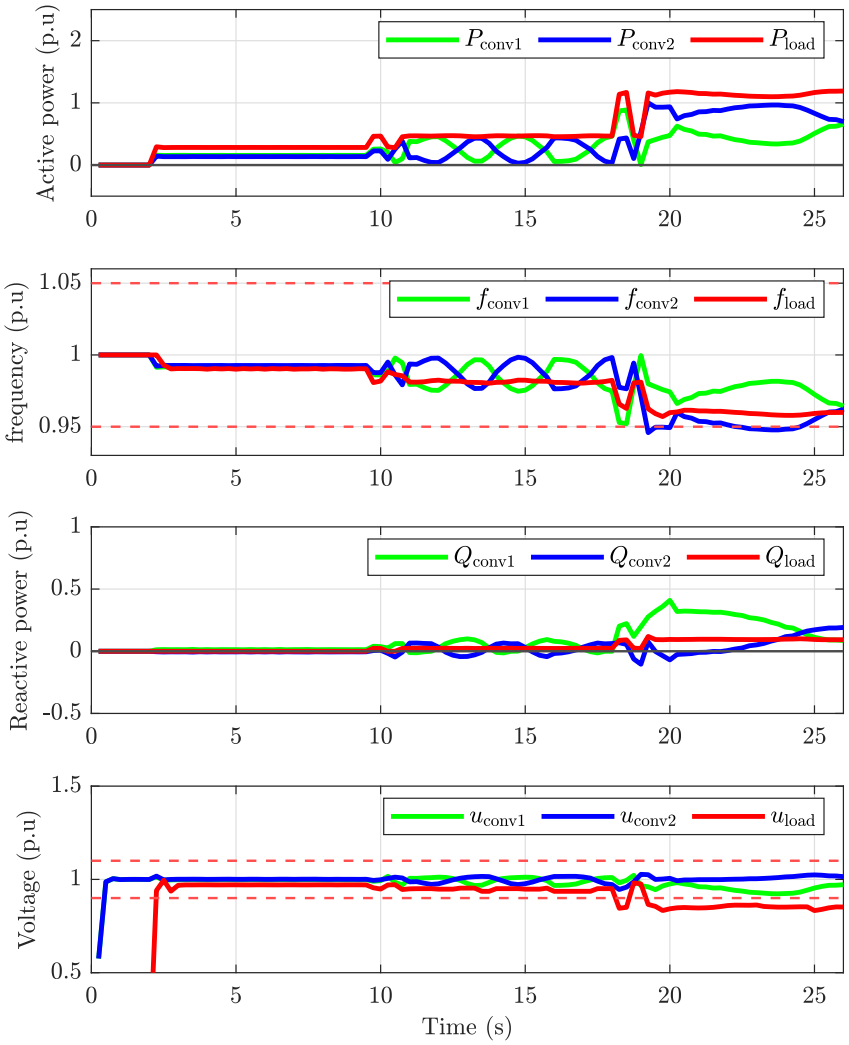

Figure 5.12: Output of droop-controlled parallel converters with different line-impedance for the RLC-load switching defined in Table 4.1. Red dotted-lines represent the frequency and voltage tripping limit

Though the droop parameters are same, there is an oscillation in the system parameters due to the difference in phase angle. Thus, the synchronization is poor and during the disturbance converter outputs starts oscillating. This poor power-sharing or reactive power oscillation can be avoided by adjusting the output impedance angle using virtual impedance as mentioned in section 3.3.3.

Table 5.2: Parameters used in different line-impedance test case

Parameters	**Actual value**	**Per-unit value**
Converter-1 Line-impedance	20+9j $(m\Omega)$	0.17+0.06j
Converter-2 Line-impedance	30+13j $(m\Omega)$	0.16+0.07j
Virtual impedance, $R_v + jX_v$	100+22j $(m\Omega)$	0.62+0.13j
Low pass filter bandwidth, ω_v	314.16 rad/s	1

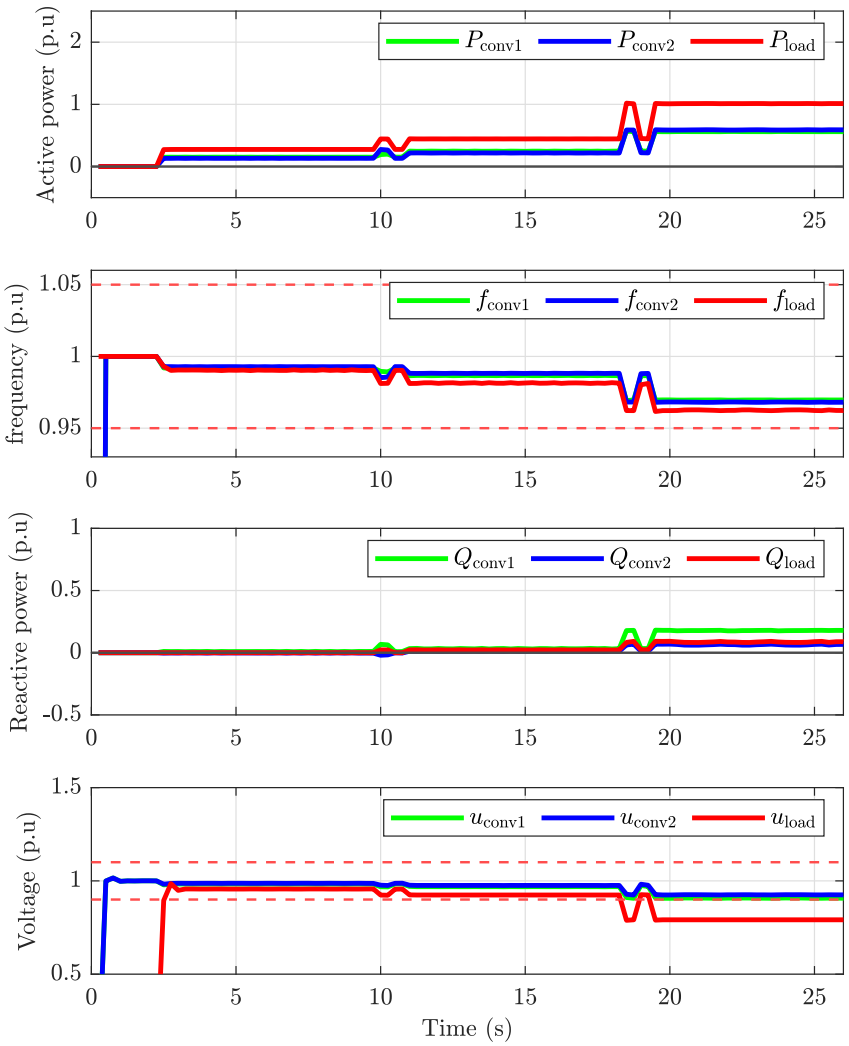

Figure 5.13: Output of droop-controlled parallel converters with different line-impedance and added virtual impedance for the RLC-load switching defined in Table 4.1. Red dotted-lines represent the frequency and voltage tripping limit

The reduced voltage reference using a virtual series impedance improves the system damping. The effect of virtual impedance can be seen in figure 5.13. It eliminates the circulating current flowing between unequal impedance thereby enhancing reactive power-sharing. Virtual impedance stabilizes the system oscillation between 10-20 seconds. The test parameter of line and virtual impedance are given in the Table 5.2. As the voltage reference is reduced, converter voltage is lower than the ideal case. The load voltage decreases below the 0.8 p.u and limits the active power supplied by each converter to 0.5 p.u. This limitation should be considered while selecting the virtual impedance. Here, virtual impedance is selected more than the output impedance as suggested in [7]. Lower values of impedance have poor stability in few load conditions.

5.2.4 Effect of Different Converter Ratings

When two converters with different power-ratings are paralleled, on a stable operation power is shared as a ratio of their ratings. Two connected converters have a power rating of 0.5 p.u and 1 p.u. The power rating of the connected load is maximum of 0.75 p.u at nominal voltage.

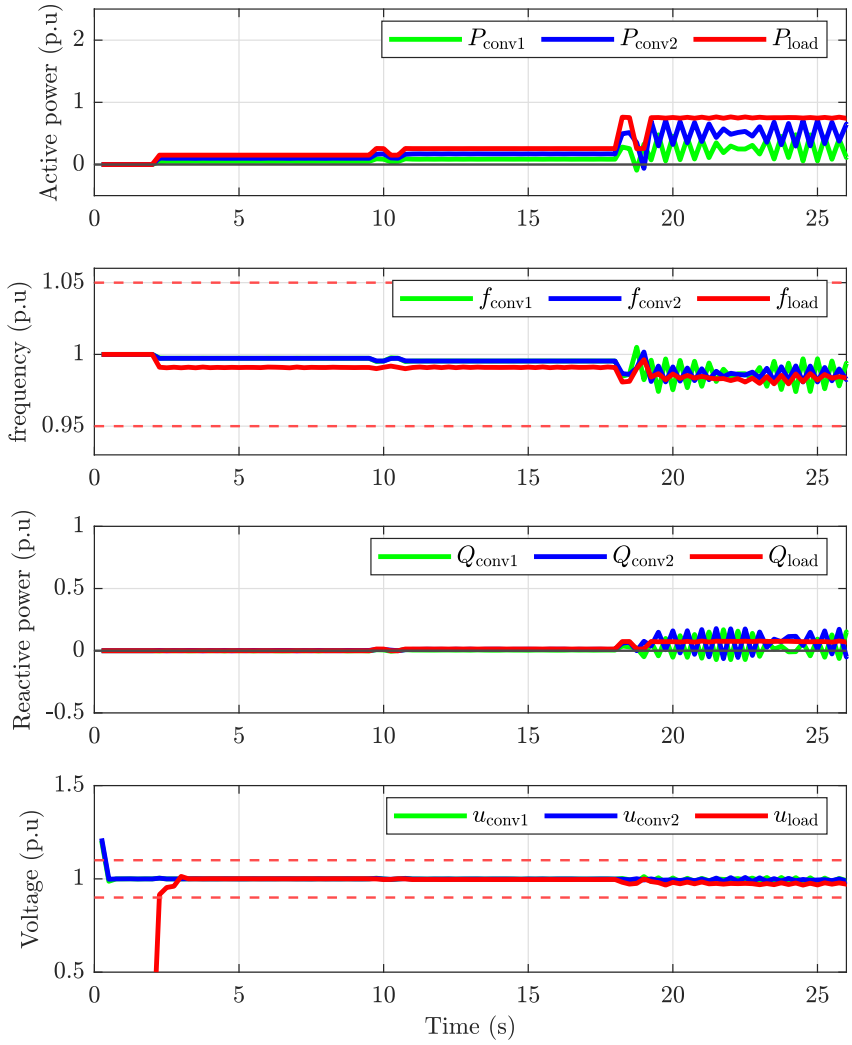

Figure 5.14: Output of droop-controlled parallel converters of different power rating for the RLC-load switching defined in Table 4.1. Red dotted-lines represent the frequency and voltage tripping limit

During the disturbances, with different filter-controller combination, response time of each converter differs leading to reactive power oscillations as shown in figure 5.14. This will be a real-time issue as the converters operating in parallel are not necessarily identical in many conditions. All the non-identical test cases were also tested with synchronverter-controlled parallel converters, but synchronverters are more sensitive to parameter variations. For example, considering the parallel operation of different

converter rating case, the system starts oscillating even for a small load disturbance. Due to slower transient state in the synchronverter control, non-identical response of parallel converters introduce a significant difference between their output voltage. Thus, the converters cannot preserve the synchronization and outputs start oscillating which is shown in figure 5.15.

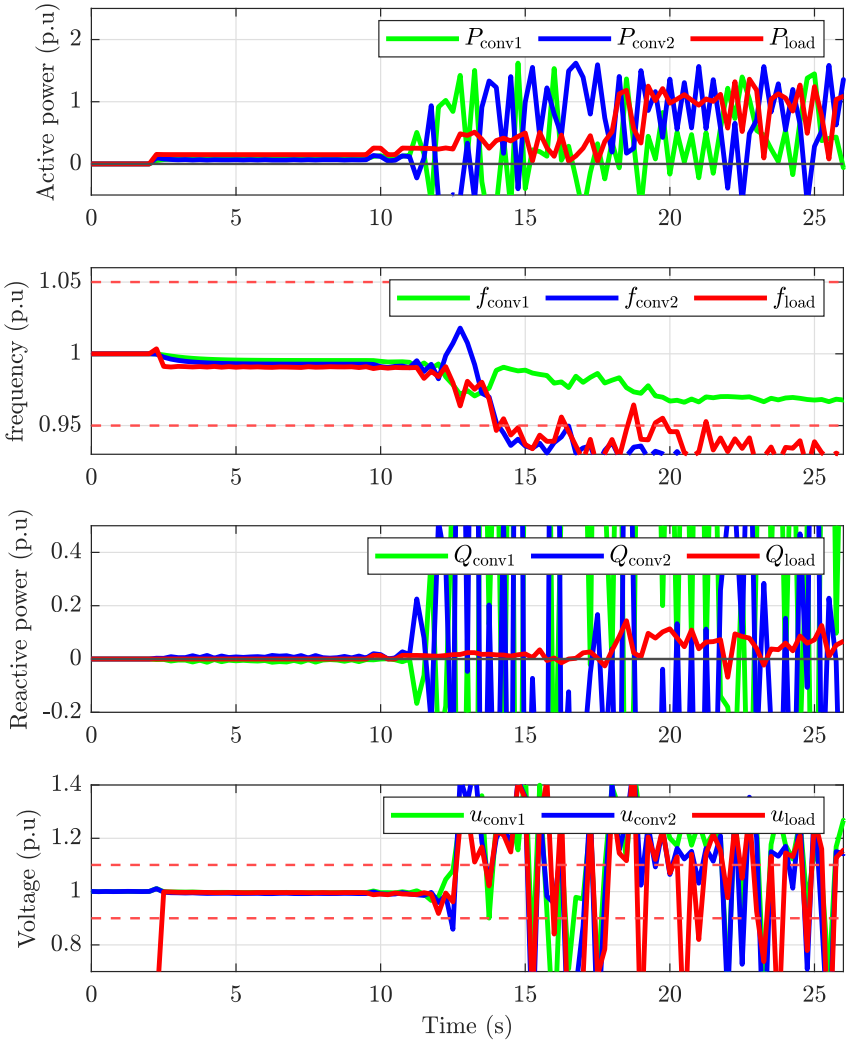

Figure 5.15: Output of synchronverter-controlled parallel converters with different power ratings for the RLC-load switching defined in Table 4.1. Red dotted-lines represent the frequency and voltage tripping limit

As synchronverter has a similar response for other test conditions, their results are not discussed further. A proper synchronization unit could increase the small-signal stability of all the above-mentioned non-identical converter issues. Large-disturbance stability highly depends on the line dynamics and the power adequacy. For a perfect synchronization in any load condition, it is good to have a synchronization unit like PLL, but PLL has its own limitation when working with weak grid condition which will be studied using different simulation setup in the next section.

5.3 Grid-forming and Grid-feeding Converters

Setup-3 having one grid-forming converter, grid-feeding converter and the RLC-load is used to study the effect of PLL with different grid conditions. The subscript "conv1" represents the measurement at the grid-forming converter, "conv2" represents the measurement at the grid-feeding converter and "load" represents the measurement near the load, which are used in the plots.

Table 5.3: Additional model parameters used in PLL test case

Parameters	**Actual value**	**unit**	**Per-unit value**
Grid short-circuit power	15	MVA	15
Power factor	0.9	-	-
Grid line-line voltage	400	V	1
Grid frequency	50	Hz	1
PLL-controller bandwidth, α_{PLL}	31.4	rad/s	0.1
PLL-controller proportional gain, $K_{\mathrm{p,PLL}}$	62.8	-	-
PLL-contoller integral gain, $K_{\mathrm{i,PLL}}$	987	-	-

5.3.1 PLL in Strong Grid

Grid-simulator with high short-circuit capacity is used as the grid-forming source (forms strong grid condition) and the grid-feeding converter follows its voltage and frequency to inject the active power.

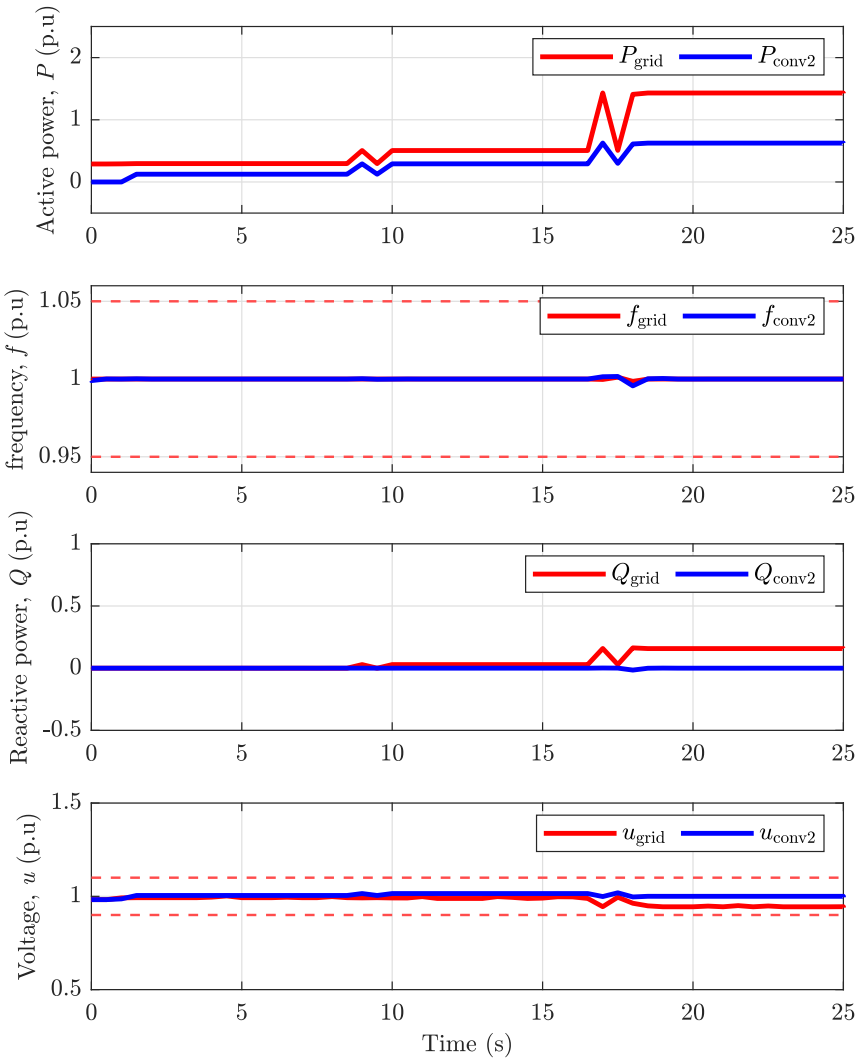

Figure 5.16: Output of grid and grid-feeding converter with PLL bandwidth = $2\pi.15$ rad/s for the RLC-load switching defined in Table 4.1. Red dotted-lines represent the frequency and voltage tripping limit

Reactive power is not supplied by the grid-feeding converter, as the adjustments based on network reactive power requirement is not added in the model. Figure 5.16 shows the output response of the grid and the grid-feeding converter for the applied RLC-loads. It can be noted that the PLL clearly tracks the grid-frequency and remains synchronized in all the load step conditions. PLL is completely stable with a bandwidth of $2\pi.15$ rad/s as the frequency deviations are not high. This is same in the real grid conditions, where the frequency stability is high due to large inertia.

Grid supplies the reactive power requirement of the microgrid. Due to low impedance angle, PLL can remain synchronized. The rated load power (1.5 p.u) apart from the grid-feeding converter contribution (0.65 p.u) is supplied by the grid (0.85 p.u) even with the voltage drop, which is not the case for converter having limited current rating.

5.3.2 PLL in Weak Grid

For operating in weak grid condition, PLL bandwidth is selected as $2\pi.15$ rad/s, same as used in the strong grid condition. Synchronverter-controlled converter having better frequency stability than the droop-controlled converter, is used as the grid-forming source.

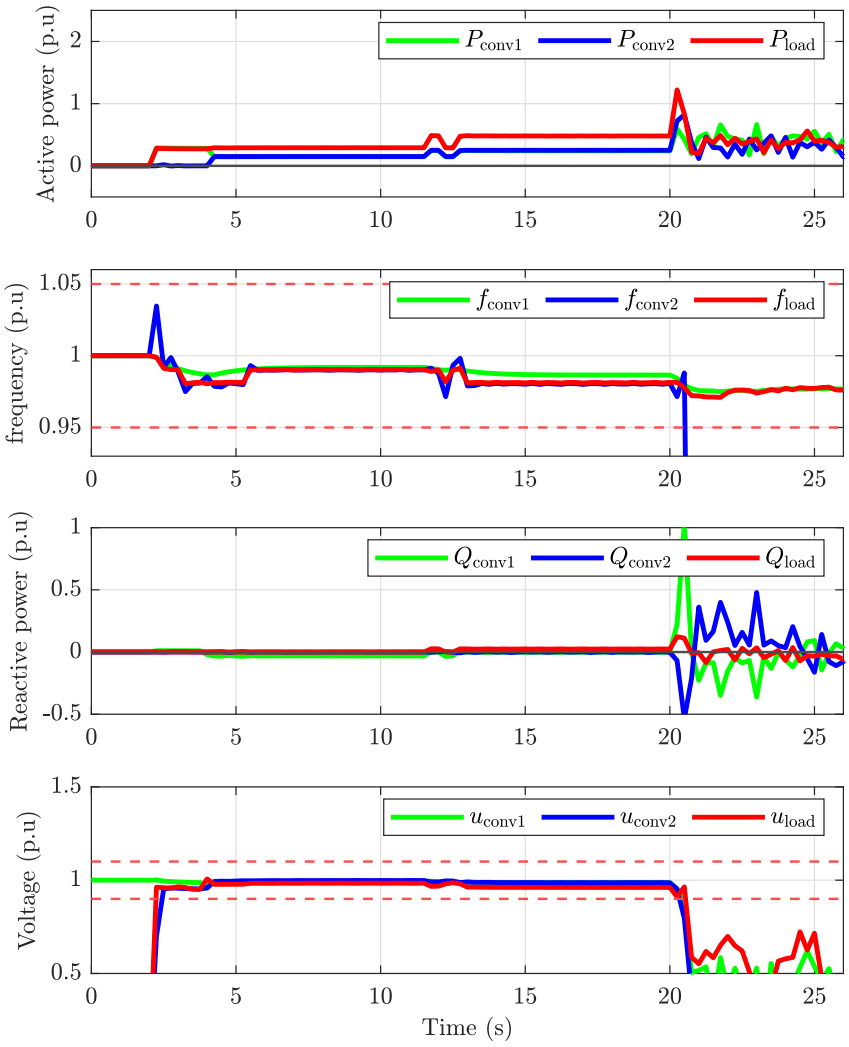

Figure 5.17: Output of synchronverter-controlled converter and grid-feeding converter (P injection) with PLL bandwidth = $2\pi.15$ rad/s for the RLC-load switching defined in Table 4.1. Red dotted-lines represent the frequency and voltage tripping limit

At small-disturbance conditions, the system is stable and PLL follows the reference. However, at large disturbance, the impedance-angle increases and when PLL tries to track the large angle difference with faster dynamics results in the loss of phase-lock, which is shown in figure 5.17.

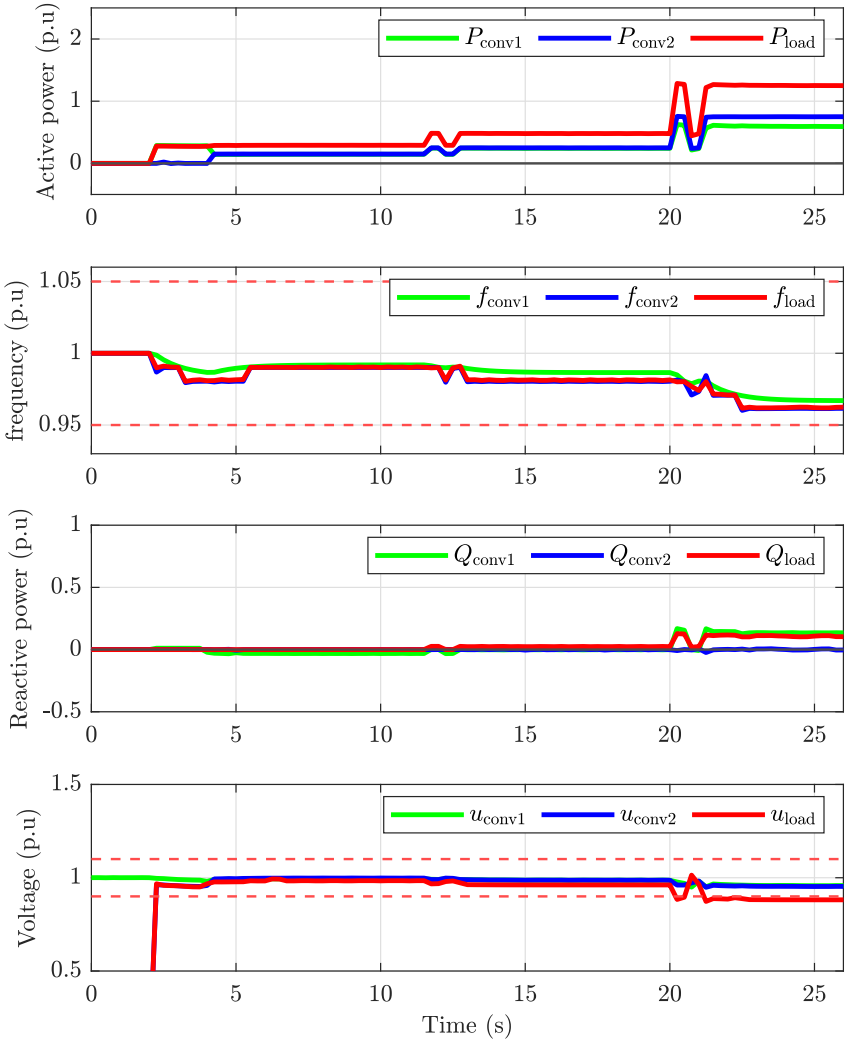

Figure 5.18: Output of synchronverter-controlled converter and grid-feeding converter (P injection) with PLL bandwidth = $2\pi.5$ rad/s for the RLC-load switching defined in Table 4.1. Red dotted-lines represent the frequency and voltage tripping limit

When the PLL bandwidth is reduced to $2\pi.5$ rad/s, the system remains stable and PLL tracks the synchronverter reference. Grid-feeding converter remains synchronized with the grid for all the load conditions. Figure 5.18 shows the working of the grid-forming and grid-feeding converter in feeding the RLC-load. Active power supplied is nearly 1.3 p.u, as there is a load voltage drop due to line-impedance. Also, in this operating condition, there is no reactive power injection from the grid-feeding converter. However, there is no problem of unequal power-sharing, unlike the parallel grid-forming converters. Microgrid reactive power requirement is supplied only by

the grid-forming converter. Thus, the output voltage reduces which affects the total active power supplied by both the converters. So, the reactive power set-point is applied for grid-feeding converters in a way that the power is equally shared between the converters. The output response is as shown in figure 5.19.

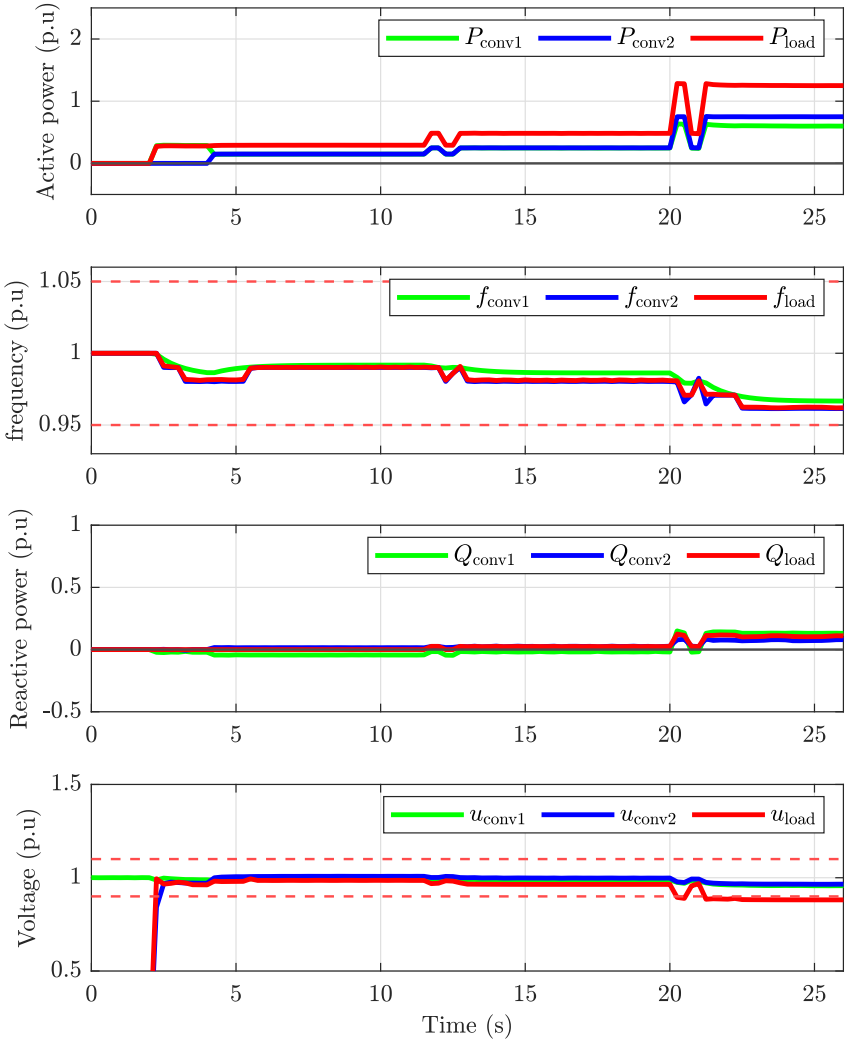

Figure 5.19: Output of synchronverter-controlled converter and grid-feeding converter (PQ injection) with PLL bandwidth = $2\pi.5$ rad/s for the RLC-load switching defined in Table 4.1. Red dotted-lines represent the frequency and voltage tripping limit

The voltage and active power supplied to the load are slightly increased due to the reactive power supplied by the grid. It can be noticed that the grid-forming converter has negative reactive power (green line) from the instance of parallel connection until large load-change. This is because at light load condition and due to the higher R/X ratio of the network, the grid impedance angle is low. When grid-feeding converter is paralleled, the impedance angle increases and becomes negative (capacitive). The grid-feeding converter voltage is higher than that of grid-forming converter, until the impedance angle becomes positive. This is not seen with strong grid condition as

the grid is inductive. Though low bandwidth PLL ensures synchronized operation, the stability and bandwidth selection depends on the SCR or the grid impedance. Higher the SCR, better is the stability.

5.3.3 Short-circuit Test

As mentioned earlier, three phase-ground faults are the most severe fault involving high short-circuit current. Thus, it is the only fault simulated to study the response. The short-circuit impedance is the sum of connected equipment impedance from source to point of fault (Table 5.4). Point of fault is located just before the load, so the load impedance is not included in the fault-impedance.

Table 5.4: Magnitude of short-circuit impedance

Connected components	$\sum$ **Impedance** (Ω)	**Per-unit**	$Z_{\mathrm{k,pu}}$
Line and fault-impedance	0.015 + 0.0018j + 0.01	0.15 + 0.01j	0.15
Line and fault-impedance	0.015 + 0.0018j + 0.1	0.7 + 0.01j	0.7

For the short-circuit test using setup-3, both the grid current and converter current is compared. Figure 5.20 shows the short-circuit response of the grid-forming and grid feeding converters in parallel without any current limitations. After applying the base-load to converters, fault occurs at 12 seconds. First the grid-forming converter immediately responds to the fault with short-circuit current of 3 p.u. Here PLL loses its stability on large impedance angle-change. The grid-feeding converter power is not properly synchronized which ends up in distorted power.

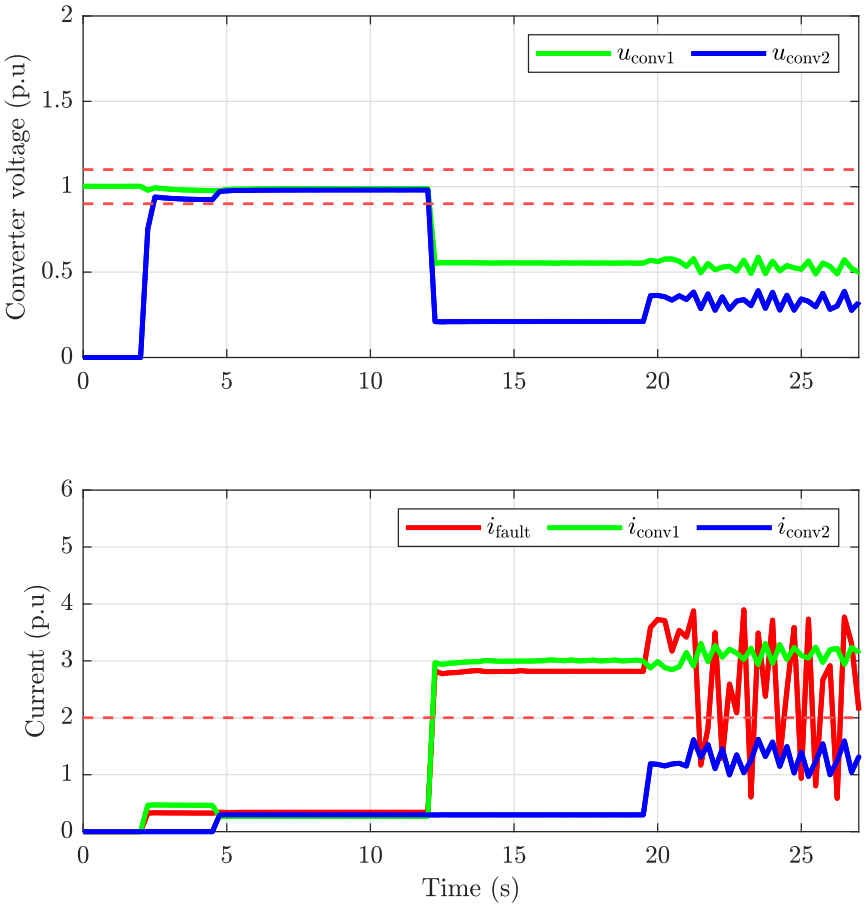

Figure 5.20: Output Voltage and current of the grid-forming and grid-feeding converters (without current limitation) for a 3-phase to ground short-circuit at 12s with $Z_k = 0.15$ p.u. Red dotted-lines represent the voltage and current tripping limit

The converter cannot withstand this high current and it increases with lower short-circuit impedance. Thus, current limitation function is applied, and fault is simulated again.

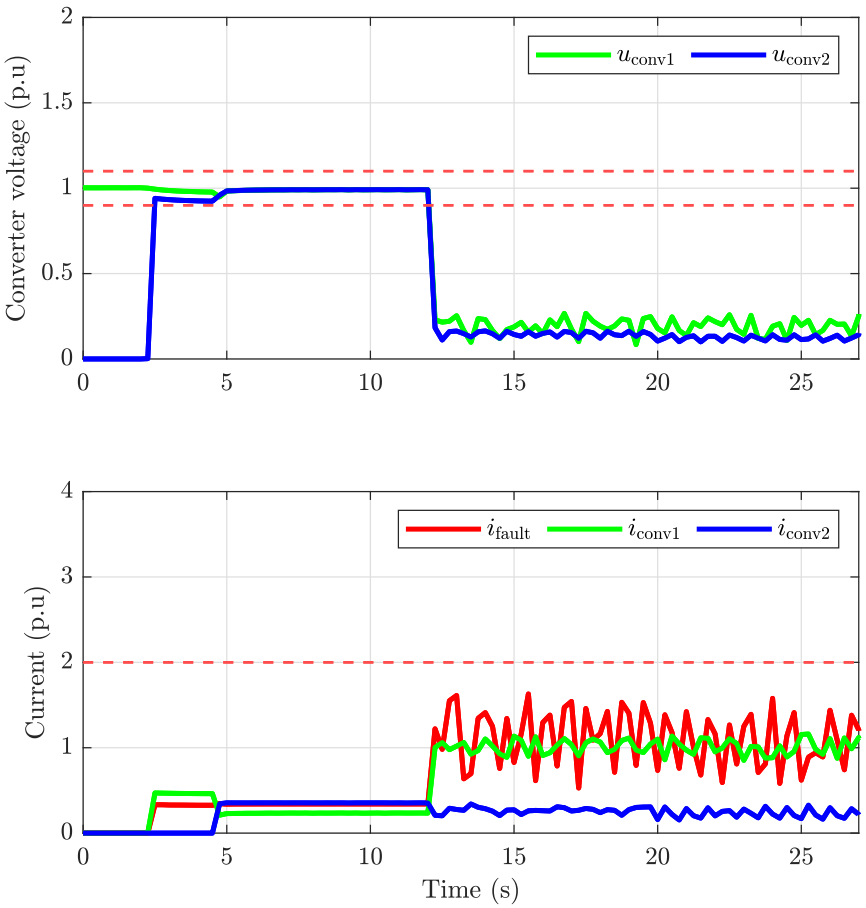

Figure 5.21: Output voltage and current of the grid-forming and grid-feeding converters (with current limitation) for a 3-phase to ground short-circuit at 12s with Z_k = 0.15 p.u. Red dotted-lines represent the voltage and current tripping limit

Figure 5.21 shows the fault current from the grid-feeding and grid-forming converters. Compared to the previous case, the fault current from the grid-feeding is very low for two reasons: PLL loses its stability due to large tracking angle, current limitation in the grid-forming converter saturates and the output is highly distorted leading to loss of phase-lock with the grid. Fault current from the grid-forming converter is limited within 1 p.u. Grid-feeding converter fault contribution is poor due to the instability of PLL.

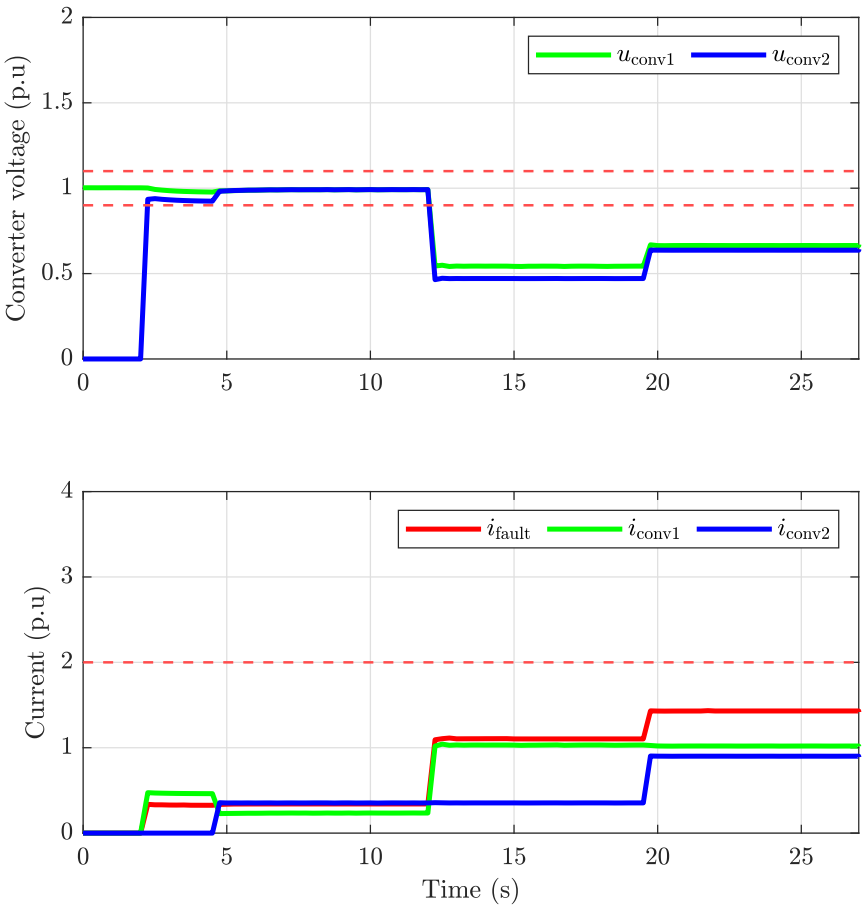

Figure 5.22: Output voltage and current of the grid-forming and grid-feeding converters (with current limitation) for a 3-phase to ground short-circuit at 12s with Z_k = 0.7 p.u. Red dotted-lines represent the voltage and current tripping limit

Figure 5.22 shows the fault characteristics of the converter with fault-impedance equal to 0.7 p.u. This high-impedance fault condition is simulated to show the proper working of the converter current-limitation function and PLL. Both the converter currents are limited within 1 p.u without any distortion. It can be noted that the converter voltage is improved, when the grid-feeding converter starts power injection at 19s.

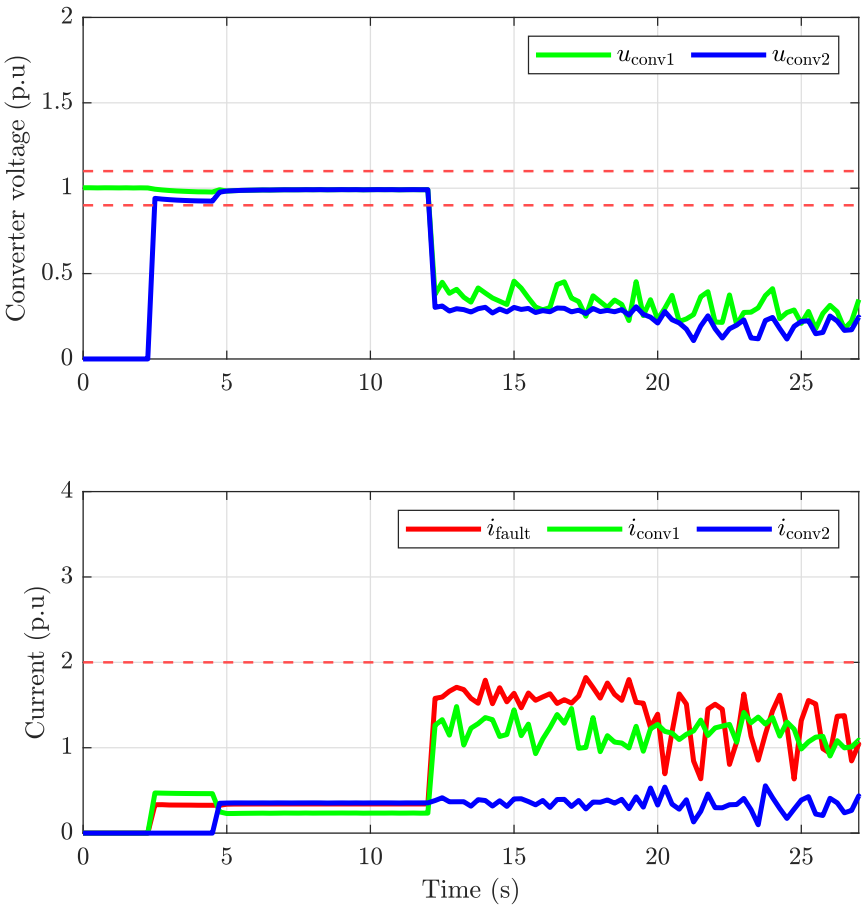

Figure 5.23: Output voltage and current of the grid-forming and grid-feeding converters (with current limitation) for a 3 phase-ground unbalanced short-circuit at 12s with $Z_k = 0.15$ p.u. Red dotted-lines represent the voltage and current tripping limit

In case of unbalanced fault condition, the current is not limited within limits using the *dq*-frame. This shown in the figure 5.23. fault-impedance of the B-phase is set to 5 times higher than the other phases (A and C). The grid-forming converter (green) current is not limited within limits of 1 p.u for the unbalanced fault. Grid-feeding converter has no power injection due to PLL instability.

6 Conclusion

In this work, the stability issues of power converter-based microgrids are studied using the typhoon real-time simulator. Three simulation setups are created to test the different scenarios based on the stability classification defined in the section 3.3. All the setups are tested with varying load conditions in a way to test the small-signal/large-signal + short/long disturbance stabilities of the voltage, frequency and control system deviations. Frequency stability is explained using the setup-1 having one grid-forming converter. Voltage stability is explained using the setup-2 having two grid-forming parallel converters. Control system stability is explained using setup-3 having grid-forming and grid-feeding converters in parallel. Short-circuit condition is tested with setup-3. All these tests are done with two types of grid-forming control techniques namely droop and synchronverter.

Grid-forming control changes the voltage and frequency reference based on the change in active and reactive power output. The two control techniques used in this work - droop and synchronverter use the same approach. Droop control uses only the voltage and frequency droops used in the synchronous machine, which gives a faster response. Synchronverter uses synchronous machine model in the control loop, thus it slowly responds to the changes with a delay due to the virtual inertia. As these converter-based microgrids do not possess inertia and enough short-circuit power, the system is prone to many abnormalities. These abnormalities are detected using a protection function in this thesis. This function detects under/over - voltage and frequency, over-current and RoCoF threshold crossings.

Voltage and frequency stabilities are critical in droop control as the fast changes lead to RoCoF detection even for a short-term load change which might lead to unnecessary tripping. But, in synchronverter due to slow change in the reference, the system is free from these abnormalities. The addition of virtual inertia introduces a time-delay in reference change, avoiding the instability due to fast dynamics. For a parallelly operated identical converter with LCL-filters the resonant frequency tends to move towards lower frequencies depending on the number of converters which should be considered for selecting the controller bandwidth.

Converters can be operated in parallel without any communication link using the droop/synchronverter control. For this, voltage, frequency and phase angle of the two

converters must be identical. Synchronverter-controlled parallel converters have a stable operating point only when their parameters and output impedance are identical. Parallel droop-controlled converters having different droop gains leads to poor power-sharing. For a large load change, droop control changes frequency and voltage references based on the droop gains. When there is a significant difference between the converter output voltages, circulating current flows between the converters. Output impedance defines the power-sharing ratio between the parallel converters. For converters with different line-impedance, the power-sharing is critical as the change in line-impedance affects the synchronization angle, resulting in instability. The virtual impedance control improves output impedance angle resulting in better synchronization and load sharing among the parallel converters. Parallel converters with different power ratings also suffer from reactive power oscillations. This is because, different filter-controller combination has different response rate which causes oscillations for unequal voltages or phase angles. A synchronization unit like PLL can be used in the converter to make the paralleling smooth and share the load power equally without the problem of different impedance/droop gains/controller gains. However, PLL is not stable for operating in weak grid conditions. The setup with grid-forming and grid-feeding converters is mainly used to study the PLL stability. With a typical PLL bandwidth (0.3 p.u) $2\pi.15$ rad/s the system is stable for grid-connected operation. But, PLL is not stable for islanded grid conditions formed with grid-forming converters. For islanded microgrid, the short-circuit capacity is low, thus termed as weak grid. At large-signal disturbance, to track the large-angle difference, PLL loses its stability and synchronization. When bandwidth is reduced to $2\pi.5$ rad/s, PLL synchronizes with the grid and remains stable for all the load conditions completing the stability test runs successfully. Low bandwidth PLL works for weak grid condition, but the slower tracking could reduce the power flow accuracy during transients. This can be addressed with a better synchronization using the virtual oscillator control [25] or with a communication link inside the microgrid. Use of power-synchronization control [31] can also be one solution for the PLL-stability issues in weak grid condition.

On a short-circuit condition in the microgrid having grid-feeding and grid-forming converters, fault current from the converters are limited within their ratings. For lower fault-impedance, voltage drops to a very low magnitude and distorted. Thus, PLL cannot track the grid voltage angle and so the grid-feeding converter contribution is poor. For higher fault-impedance, PLL is stable and the fault current is the rated contribution from both the converters. For unbalanced faults, the current limitation in dq-frame does not produce satisfactory results. The over-current protection will not be effective, as the load current and short-circuit current might be almost equal, leading to protection blinding. Voltage-based protection can be used in this case, as voltage drops to any magnitude based on the short-circuit impedance and converter current rating. Current-source operation during faults or adaptive virtual impedance control can be used to limit the fault current. Unbalanced load and fault conditions will be a huge concern for operational reliability. The stability limits used here is very general. Thus, it can be said that microgrid small-signal stability is more of

compatibility between parameter (inertia) selection and protection tuning. And large-signal stability depends on SCR and proper synchronization of parallel converters with energy adequacy. Still, the microgrid is less stiff than conventional grid having higher short-circuit capacity. In this work, DC-bus voltage is maintained stable using battery. However, when grid-feeding injection is based on wind or solar, then the microgrid is very prone to instability.

Future work may include these features and stability of the microgrid can be tested,

- Transformer energization, direct online starter-based induction motor, variable frequency drives can be tested with the microgrid to understand the effect of these load dynamics and their design requirement
- Parallel operation with Dual Second Order Generalized Integrator-Frequency Locked Loop (DSOGI-FLL) can be tested for better stability and harmonic tolerance than PLL
- Proper negative sequence controller for unbalanced loads, as this work only used balanced load
- Study of virtual oscillator control for parallel grid-forming converters
- Adaptive virtual impedance-based current limiting technique can be implemented and tested [18]
- Stochastic DG-source (solar,wind) can be used to study the stability issues, as this work used battery as the DC-source

References

[1] P.Kundur, "Power System Stability and Control," *McGraw-hill New York*, 1994.

[2] Z. Shuai, Y. Sun, J. Shen, W. Tian, C. Tu, Y. Li and X. Yin, "Microgrid Stability: Classification and a Review", *Renewable and Sustainable Energy Reviews*, vol. 58, pp. 167-179, 2016. doi: https://doi.org/10.1016/j.rser.2015.12.201

[3] M. Farrokhabadi et al.,"Microgrid Stability Definitions, Analysis, and Modeling," *IEEE Transactions on Power Systems*,June, 2019. doi: https:///doi.org/10.1109/TPWRS.2019.2925703

[4] F. Milano, F. Dörfler, G. Hug, D. J. Hill and G. Verbic, "Foundations and Challenges of Low-Inertia Systems (Invited Paper)," *Power Systems Computation Conference*, pp. 1-25, 2018. doi: https://doi.org/10.23919/PSCC.2018.8450880

[5] "IEEE Recommended Practice for the Planning and Design of the Microgrid," *IEEE Std 2030.9-2019*, no.3, pp.1-46, July 2019. doi: https://doi.org/10.1109/IEEESTD.2019.8746836

[6] "IEEE Guide for Planning DC Links Terminating at AC Locations Having Low Short-Circuit Capacities," *IEEE Std 1204-1997* , pp.1-216, 21 Jan. 1997 doi: https://doi.org/10.1109/IEEESTD.1997.85949

[7] J. Rocabert, F. Blaabjerg, P. Rodrıguez and L. Alvaro, "Control of Power Converters in AC Microgrids," *IEEE Transactions on Power Electronics*, vol. 27, no. 11, pp. 4734-4749, 2012. doi: https://doi.org/10.1109/TPEL.2012.2199334

[8] CIGRE/CIRED, "Protection of Distribution Systems with Distributed Energy Resources," *Joint Working Group B5/C6.26/CIRED*, 2015. doi: www.cired.net/files/download/182

[9] "IEC-60909 Short-circuit Currents in Three-phase AC Systems – Part 0: Calculation of Currents," *International Electrotechnical Commission* 2016. link: https://webstore.iec.ch/publication/24100

[10] B. d. Metz-Noblat, F. Dumas and C. Poulain, "Calculation of Short-circuit currents," *Cahier Technique Schneider Electric no: 158*, 2005. doi: https://www.schneider-electric.com.hk/en/download/document/ECT158/

[11] Z.-M. Qian, W. Yao, M. Chen, J. Matas and J. M. Guerrero, "Design and Analysis of the Droop Control Method for Parallel Inverters Considering the Impact of the Complex Impedance on the Power Sharing," *IEEE Transactions on Industrial Electronics*, vol. 58, no. 2, pp. 576-588, 2011. doi: https://doi.org/10.1109/TIE.2010.2046001

[12] L. Harnefors, S. Lundberg and M. Bongiorno, "Input-Admittance Calculation and Shaping for Controlled Voltage-Source Converters," *IEEE Transactions on Industrial Electronics*, vol. 54, no. 6, pp. 3323-3334, 2007. doi: https://doi.org/10.1109/TIE.2007.904022

[13] J. He, Y. W. Li, D. Bosnjak and B. Harris, "Investigation and Active Damping of Multiple Resonances in a Parallel-Inverter-Based Microgrid," *IEEE Transactions on Power Electronics*, vol. 28, no. 1, pp. 234-246, 2013. doi: https://doi.org/10.1109/TPEL.2012.2195032

[14] J. Z. Zhou and A. M. Gole, "VSC Transmission Limitations Imposed by AC System Strength and AC Impedance Characteristics," *10th IET International Conference on AC and DC Power Transmission (ACDC 2012)*, Birmingham, 2012. doi: https://doi.org/10.1049/cp.2012.1986

[15] R. Juntunen, "LCL Filter Designs for the Parallel-Connected Grid Inverters," *Doctoral Dissertation* - Lappeenranta University of Technology, Finland, 2018. doi: http://lutpub.lut.fi/handle/10024/158804

[16] P. Zhou, X. Yuan, J. Hu and Y. Huang, "Stability of DC-link voltage as affected by phase locked loop in VSC when attached to weak grid," *IEEE PES General Meeting | Conference Exposition*, 2014. doi: https://doi.org/10.1109/PESGM.2014.6939460

[17] J. Z. Zhou, H. Ding, S. Fan, Y. Zhang and A. M. Gole, "Impact of Short Circuit Ratio and Phase Locked Loop Parameters on the Small-signal Behavior of a VSC-HVDC converter," *IEEE Transactions on Power Delivery*, Boston, 2016. doi: https://doi.org/10.1109/TPWRD.2014.2330518

[18] X. Wang, Y. W. Li, F. Blaabjerg and P. C. Loh, "Virtual-Impedance-Based Control for Voltage-Source and Current-Source Converters," *IEEE Transactions on Power Electronics*, vol. 30, no. 12, pp. 7019-7037, Dec. 2015. doi: https://doi.org/10.1109/TPEL.2014.2382565

[19] A. Gkountaras, "Modeling Techniques and Control Strategies for Inverter Dominated Microgrids," *Universitätsverlag der TU Berlin*, Doctoral Dissertation, 2017. doi: http://dx.doi.org/10.14279/depositonce-5520

[20] N. Pogaku, M. Prodanovic and T. C. Green, "Modeling, Analysis and Testing of Autonomous Operation of an Inverter-Based Microgrid," *IEEE Transactions on Power Electronics*, vol. 22, no. 2, pp. 613-625, 2007. doi: https://doi.org/10.1109/TPEL.2006.890003

[21] Y. Li and L. Fan, "Stability Analysis of Two Parallel Converters with Voltage–Current Droop Control," *IEEE Transactions on Power Delivery*, vol. 32, no. 6, pp. 2389-2397, Dec. 2017. doi: https://doi.org/10.1109/TPWRD.2017.2656062

[22] U. Tamrakar, D. Shrestha and M. Maharjan, "Virtual Inertia: Current Trends and Future Directions," *Applied Sciences*, vol. 7, no. 7, pp. 654-684, 2017. doi: https://doi.org/10.3390/app7070654

[23] Q. Zhong and G. Weiss, "Synchronverters: Inverters That Mimic Synchronous Generators," *IEEE Transactions on Industrial Electronics*, vol. 58, no. 4, pp. 1259-1267, 2011. doi: https://doi.org/10.1109/TIE.2010.2048839

[24] W. Zhang and P. Rodriguez, "Comparison of different power loop controllers for synchronous power controlled grid-interactive converters," *IEEE Energy Conversion Congress and Exposition (ECCE)*, pp. 3780-3787, 2015. doi: https://doi.org/10.1109/ECCE.2015.7310194

[25] F. Dörfler, G.-S. Seo, M. Colombino, I. Subotic, B. Johnson and D. Groß, "Dispatchable Virtual Oscillator Control for Decentralized Inverter-dominated Power Systems: Analysis Experiments," *Proc. Applied Power Electronics Conference*, 2018. doi: https://arxiv.org/abs/1811.08842

[26] A. Tayyebi, D. Groß, A. Anta, F. Kupzog and D. Florian, "Interactions of Grid-Forming Power Converters and Synchronous Machines - A Comparative Study," *IEEE Transactions on Power Systems*, 2019. doi: https://arxiv.org/abs/1902.10750

[27] L. Huang et al., "A Virtual Synchronous Control for Voltage-Source Converters Utilizing Dynamics of DC-Link Capacitor to Realize Self-Synchronization," *IEEE Journal of Emerging and Selected Topics in Power Electronics*, vol. 5, no. 4, pp. 1565-1577, Dec. 2017. doi: https://doi.org/10.1109/JESTPE.2017.2740424

[28] M. Liserre, F. Blaabjerg and S. Hansen, "Design and control of an LCL-filter-based three-phase active rectifier," *IEEE Transactions on Industry Applications*, vol. 41, no. 5, pp. 1281-1291, Sept.-Oct. 2005. doi: https://doi.org/10.1109/TIA.2005.853373

[29] J. Wang, N. C. P. Chang, X. Feng and A. Monti, "Design of a Generalized Control Algorithm for Parallel Inverters for Smooth Microgrid Transition Operation," *IEEE Transactions on Industrial Electronics*, vol. 62, no. 8, pp. 4900-4914, Aug. 2015. doi: https://doi.org/10.1109/TIE.2015.2404317

[30] A. Yazdani, R. Iravani, "Voltage-Sourced Converters in Power Systems: Modeling Control and Applications," *Wiley Publications*, USA, 2010. doi: https://doi.org/10.1002/9780470551578

[31] L. Zhang, L. Harnefors and H. Nee, "Power-Synchronization Control of Grid-Connected Voltage-Source Converters," *IEEE Transactions on Power Systems*, vol. 25, no. 2, pp. 809-820, May 2010. doi: https://doi.org/10.1109/TPWRS.2009.2032231